Atrial mitochondrial calcium handling in patients with atrial fibrillation

Doctoral Thesis

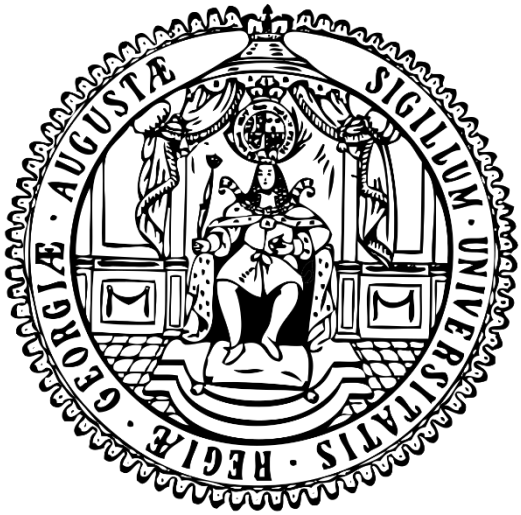

In partial fulfilment of the requirements for the degree

"Doctor rerum naturalium (Dr. rer. nat.)"

within the Molecular Medicine Study Program

of the Georg-August University School of Science (GAUSS)

at the Georg-August University Göttingen

Submitted by

Julius Ryan Duran Pronto

Born in

Manila, Philippines

Göttingen, 2022

Members of thesis committee

Prof. Dr. med. Niels Voigt (1st Reviewer)
Professor, Institute of Pharmacology and Toxicology
University Medical Center Göttingen
Robert Koch Straße 40
37075 Göttingen, Germany

Prof. Dr. Peter Rehling (2nd Reviewer)
Director, Department of Cellular Biochemistry
University Medical Center Göttingen
Humboldtallee 23
37073 Göttingen, Germany

Prof. Dr. Silvio O. Rizzoli
Director, Department of Neuro- and Sensory Physiology
University Medical Center Göttingen
Humboldtallee 23
37073 Göttingen, Germany

Extended members of thesis committee

Prof. Dr. Stefan Jakobs
Professor, High Resolution Microscopy of the Cell
Department of Neurology
University Medical Center Göttingen
Robert Koch Straße 40
37075 Göttingen, Germany
and
Group Leader, Structure and Dynamics of Mitochondria
Max Planck Institute for Multidisciplinary Sciences
Department of NanoBiophotonics
Am Fassberg 11
37077 Goettingen, Germany

Prof. Dr. mult. Thomas Meyer
Department of Psychosomatic Medicine and Psychotherapy
University Medical Centre Göttingen
Waldweg 33
37073 Göttingen, Germany

Prof. Dr. Katrin Streckfuß-Bömeke
Professor, Institute for Pharmacology and Toxicology
University of Würzburg
Versbacher Straße 9
97078 Würzburg, Germany

Date of Disputation: January 25, 2023

Affidavit

I hereby declare that the work presented in this thesis titled "*Atrial mitochondrial calcium handling in patients with atrial fibrillation*" has been written independently with no other source and aids than quoted.

_____

Julius Ryan D. Pronto
Göttingen, 2022

Acknowledgements

The fulfillment of this thesis would not be possible without the help and support of many people, but an unspeakable amount of gratitude goes to my adviser, **Prof. Niels Voigt**. By taking a chance on me, working in Prof. Voigt's group has changed in ways I have never even imagined. The amount of trust and independence I was given, and his respect on my decisions on the project gave me the confidence to know what I am capable of, and the wisdom that I can always still improve. Most importantly, to have such a supportive adviser, even beyond the walls of the lab, gives me a lot of comfort despite being away from home. I would also like to express my gratitude to **Fleur**, who is working with me on this project and who was also instrumental in matching me with this project. I also want to take my labmates, who really made a friendly work environment: **Steffi, Maren** and **Ines** for keeping the lab running (and for helping me improve me German); **Funsho** for being a really good friend and expert electrophysiologist whom I can always turn to; Tony, Will, Vanessa S., Judith, Luisa, Robin, Philipp, Marie, Lea, Paulina, Lena, Melanie, Fiona, Catriona, Yannic, Dominic, Vanessa M., Yara, and Ricky – you all are awesome. I appreciate everyone's help and support throughout the years, especially when I have self-doubts and experience frustrations. I am really blessed to be a part of this group.

I am also very grateful to have a "powerhouse" examination board including **Prof. Peter Rehling** and **Prof. Silvio Rizzoli** (who kindly shared with me his time and expertise in image analysis) and for their contributions via the past thesis committee meetings. Additionally, I thank **Prof. Stefan Jakobs, Prof. Thomas Meyer,** and **Prof. Katrin Streckfuß-Bömeke** for agreeing to be a part of my examination board. I trust that their expertise in their respective fields will bring about an interesting discussion on the day of the defense.

Some parts of this project would not have been possible without the help of some people:

First, our amazing medical students, for obtaining patient consent (on top of their own MD theses), and the cardiac surgeons at UMG, led by **Prof. Ingo Kutschka**, for their support on this project by providing us with human atrial samples. I also thank **Dr. Aschraf El-Essawi** for his interest on our project and our collaboration that started even when he was still in Braunschweig; **Dr. Sören Brandenburg** and **Prof. Stephan Lehnart**, as well as their lab members who allowed me to use their STED facility freely and guided me through optimising my experiments; **Dr. Eva Rog-Zielinska**, who kindly performed the electron tomography experiments and analyses; **Ms. Regina Waldmann-Beushausen**, who helped a lot with immunohistochemistry experiments (and with my German); **Steffi Kestel**, for all of the western blots, **Igor Khassanov**, a lab rotation student who did the COX-SDH enzymatic staining, and **Aiste Liutkute** and **Izzatulo Sobitov** for the Ca^{2+} sparks measurements; The IRTG1816 coordinators **Dr. Christina Würtz** and **Ms. Fulya M. Ören**, who assisted us IRTG students towards a smooth-sailing PhD journey;

I thank all of my friends all of my friends that I have met in Göttingen and in Germany. You made the best 4 years of my life even better. My best friends **Gerald, Sarah, Joy**, **Yannick**, and **Aiste** – for letting me be my authentic self around you; my Filipino community in Göttingen; my friends from the IRTG – for all the scientific exchanges, chats, commiserations and the laughs; my flatmates, who make me look forward to going home; and everyone else in between.

And last but not least, I thank my family for their constant support despite the great distance. I dedicate this thesis to you.

List of publications

Voigt N, Maack C, **Pronto JRD**. Targeting mitochondrial calcium handling to treat atrial fibrillation? J Am Coll Cardiol 2022. *In press*

Kim N, **Pronto JRD**, Nickerson, DP, Taberner AJ, Hunter PJ. A novel modular modeling approach for understanding different electromechanics between left and right heart in rat. Front Physiol 2022;13:965054. doi: 10.3389/fphys.2022.965054

Seibertz F, Sutanto H, Dülk R, **Pronto JRD**, Springer R, Rapedius M, Kestel S, Ritter M, Hüsgen L, Steltzer L, Jung P, Klopp M, Rubio T, Fakuade FE, Mason FE, Hartmann N, Pabel S, Sosalla S, Streckfuß-Bömeke K, Cyganek L, Heijman J, Voigt N. Electrophysiological and calcium-handling maturation during long-term culture of human induced pluripotent stem cell-derived cardiomyocytes. Basic Res Cardiol 2022. *In review*

Fakuade FE, Steckmeister V, Seibertz F, Gronwald J, Kestel S, Menzel J, **Pronto JRD**, Taha K, Haghighi F, Kensah G, Pearman CM, Wiedmann F, Teske AJ, Schmidt C, Dibb KM, El-Essawi A, Danner BC, Baraki H, Schwappach B, Kutschka I, Mason FE and Voigt N. Altered atrial cytosolic calcium handling contributes to the development of postoperative atrial fibrillation. Cardiovasc Res. 2021;117:1790-1801 DOI: 10.1093/cvr/cvaa162.

Peper J, Kownatzki-Danger D, Weninger G, Seibertz F, **Pronto JRD**, Sutanto H, Pacheu-Grau D, Hindmarsh R, Brandenburg S, Kohl T, Hasenfuss G, Gotthardt M, Rog-Zielinska EA, Wollnik B, Rehling P, Urlaub H, Wegener J, Heijman J, Voigt N, Cyganek L, Lenz C and Lehnart SE. Caveolin3 stabilizes McT1-mediated lactate/proton transport in cardiomyocytes. Circ Res. 2021;128:e102-e120 DOI: 10.1161/circresaha.119.316547.

Mason FE*, **Pronto JRD*,** Alhussini K, Maack C and Voigt N. Cellular and mitochondrial mechanisms of atrial fibrillation. Basic Res Cardiol. 2020;115:72 DOI: 10.1007/s00395-020-00827-7. (*contributed equally)

Lee SR, **Pronto JR**, Sarankhuu BE, Ko KS, Rhee BD, Kim N, Mishchenko NP, Fedoreyev SA, Stonik VA, Han J. Acetylcholinesterase inhibitory activity of pigment echinochrome A from sea urchin Scaphechinus mirabilis. Mar Drugs. 2014;12(6):3560-73. doi: 10.3390/md12063560.

Kim HK, Youm JB, Jeong SH, Lee SR, Song IS, Ko TH, **Pronto JR**, Ko KS, Rhee BD, Kim N, Nilius B, Mischchenko NP, Fedoreyev SA, Stonik VA, Han J. Echinochrome A regulates phosphorylation of phospholamban Ser16 and Thr17 suppressing cardiac SERCA2A Ca^{2+} reuptake. Pflugers Arch. 2015;467(10):2151-63. doi: 10.1007/s00424-014-1648-2. Epub 2014 Nov 21.

Lee SR, Kwak JH, Noh SJ, **Pronto JR**, Ko KS, Rhee BD, Xu Z, Kim N, Han J. Kobophenol A inhibits sodium nitroprusside-induced cardiac H9c2 cell death through suppressing activation of JNK and preserving mitochondrial anti-apoptotic Bcl-2 and Mcl-1. Chem Pharm Bull (Tokyo). 2014;62(7):713-8. doi: 10.1248/cpb.c13-00995. Epub 2014 Apr 24.

List of conference abstracts

Pronto JRD, Mason FE, Kohlhaas M, Fakuade FE, Maack C, Voigt N. Impaired redox response to increased workload in atrial mitochondria from patients with atrial fibrillation. Heart Rhythm. 2022;19(5), S70. doi: doi.org/10.1016/j.hrthm.2022.03.718

Pronto JRD, Kim J, Han J, Kim N.. Proteomic Profiling and Functional Study Between the Left and Right Ventricles in Rat Heart. Atherosclerosis Supplements. 2018;32. doi: 10.1016/j.atherosclerosissup.2018.04.102

Table of contents

Members of thesis committee ..... *ii*
Extended members of thesis committee ..... *iii*
Affidavit ..... *iv*
Acknowledgements ..... *v*
List of publications ..... *vi*
List of conference abstracts ..... *vii*
List of figures ..... *xi*
List of supplementary figures ..... *xii*
List of tables ..... *xiii*
List of abbreviations ..... *xiv*
Abstract ..... *xv*
1 Introduction *1*
1.1 Atrial Fibrillation 1
1.1.1 Epidemiology 1
1.1.2 Clinical manifestation 2
1.1.3 Pathophysiology 2
1.2 Calcium handling 3
1.2.1 Calcium 3
1.2.2 Excitation-contraction coupling 3
1.2.3 Ca^{2+} handling in AF 5
1.3 Mitochondrial function in the heart 5
1.3.1 Cardiac mitochondria 5
1.3.2 Cardiac bioenergetics 6
1.3.3 Mitochondrial ROS production and elimination 7
1.3.4 Mitochondrial Ca^{2+} 8
1.4 AF and mitochondrial function 15
1.4.1 Mitochondrial ultrastructure in AF 15
1.4.2 Mitochondrial ATP synthesis in AF 16
1.4.3 ROS in AF 17
1.5 Aims 18
2 Methods 19
2.1 Patients 19
2.3 Patch-clamp experiments 21
2.3.1 Microscope and camera 21
2.3.2 Patch-clamp rig 21
2.3.3 Fluorescence 22
2.4 NAD(P)H and FAD^+ autofluorescence recording 24
2.5 Mitochondrial and cytosolic transient recording 27
2.6 Imaging of human atrial tissue sections 30

2.6.1 Immunohistochemistry of paraffin sections of human atrial tissue 30
2.6.2 Stimulated Emission Depletion (STED) microscopy..... 31
2.6.3 Spatial analysis with colocalization 33
2.7 Electron tomography and 3D segmentation..... 33
2.8 Spontaneous Ca^{2+} release events and Ca^{2+} sparks recording 33
2.9 COX-SDH staining..... 36
2.10 Protein biochemistry 37
2.10.1 Total protein isolation and quantification 37
2.10.2 Protein detection and visualisation 37
2.11 Statistical analysis 39
3 Results 40
3.1 Patient characteristics..... 40
3.2 Redox response of human atrial myocytes to workload transitions 41
3.3 Phosphorylation status of pyruvate dehydrogenase complex..... 45
3.4 L-type Ca^{2+} currents during workload transitions in human atrial myocytes 46
3.5 Cytosolic and mitochondrial Ca^{2+} handling in human atrial myocytes.... 48
3.5.1 Mitochondrial Ca^{2+} kinetics in human atrial myocytes 48
3.5.2 Cytosolic and mitochondrial Ca^{2+} handling in atrial myocytes..... 50
3.6 Calcium handling proteins in the mitochondria 55
3.7 Structural differences in the mitochondria of human atrial appendages 58
3.8 Ultrastructural changes in the mitochondria in human atrial appendages 61
3.9 Accumulation of defective OXPHOS components as pro-arrhythmic substrate 65
3.10 Ezetimibe and its effects on spontaneous Ca^{2+}-release events in human atrial myocytes 66
3.11 Ezetimibe and its effects on Ca^{2+} sparks in atrial human induced stem cell-derives cardiac myocytes 68
4 Discussion 70
4.1 Summary of results..... 70
4.2 Impaired redox response during increased workload in AF 71
4.3 Contribution of L-Type Ca^{2+} currents in the redox response of atrial myocytes during increased workload and β-adrenergic stimulation 72
4.4 Oscillatory Ca^{2+} kinetics in human atrial myocytes 72
4.5 Impaired mitochondrial Ca^{2+} handling in AF atrial myocytes 74
4.6 Impaired interaction of mitochondria and SR in AF..... 77
4.7 Normalisation of mitochondrial Ca^{2+} uptake as a potential therapeutic for AF..... 79

5 Limitations 81
6 Conclusion and Outlook 82
7 Bibliography 83
8 Supplementary figures 104

List of figures

Figure 1. Ca^{2+}-handling mechanisms in the cardiac myocyte. 4
Figure 2. Kinetics of mitochondria Ca^{2+} transients in atrial myocytes. 9
Figure 3. Mitochondrial Ca^{2+} uniporter complex and its regulators. 11
Figure 4. Ca^{2+} sensitive proteins in the mitochondria..... 13
Figure 5. SR/ER-mitochondria crosstalk. 14
Figure 6. Optical filtering for autofluorescence recording. 25
Figure 7. NAD(P)H and FAD^+ autofluorescence recording protocol and analysis. 26
Figure 8. Optical filtering for Ca^{2+} transient recording. 28
Figure 9. Mitochondrial and cytosolic Ca^{2+} labelling and transient recording protocol. 29
Figure 10. Validation of VDAC1 as mitochondrial marker. 32
Figure 11. Optical filtering for recording spontaneous Ca^{2+}-release events. 35
Figure 12. Autofluorescence of NAD(P)H and FAD^+ as an estimate of cellular redox index in atrial myocytes from CTL and AF patients. 43
Figure 13. Efficiency of sarcoplasmic reticulum-dependent cytosolic Ca^{2+} increase by caffeine on NADH and FADH2 recovery in atrial myocytes from CTL and AF patients. 44
Figure 14. Protein expression pyruvate dehydrogenase regulators detected by immunoblotting of RAAs from CTL and AF patients. 45
Figure 15. L-type Ca^{2+} current ($I_{Ca,L}$) densities in atrial myocytes from CTL and AF patients. 47
Figure 16. Validation of distinct cytosolic and mitochondrial transients recorded from atrial myocytes isolated from CTL patients. 49
Figure 17. Ca^{2+} accumulation in cytosol and mitochondria during workload transitions..... 51
Figure 18. Cytosolic and mitochondrial Ca^{2+} transients recorded from atrial myocytes from CTL and AF patients at 0.5 Hz. 52
Figure 19. Cytosolic and mitochondrial Ca^{2+} transients recorded from atrial myocytes from CTL and AF patients at 3 Hz..... 53
Figure 20. Cytosolic and mitochondrial Ca^{2+} transients recorded from atrial myocytes from CTL and AF patients at 3 Hz + ISO. 54

Figure 21. Protein expression of proteins involved Ca^{2+} handling between SR and mitochondria detected by immunoblotting of RAAs from CTL and AF patients.... 56
Figure 22. Protein expression of mitochondrial Ca^{2+} uniporter (MCU) complex detected by immunoblotting of RAAs from CTL and AF patients. 57
Figure 23. Stimulated Emission Depletion (STED) images of paraffin sections of RAAs from CTL and AF patients showing mitochondrial and SR localisation. 59
Figure 24. Colocalisation of RyR2 and VDAC1 in paraffin sections of RAAs from CTL and AF patients. 60
Figure 25. Ultrastructural changes of the RAA from CTL and AF patients observed by transmission electron microscopy (TEM). 62
Figure 26. Sarcoplasmic reticulum and mitochondria interaction in RAAs from CTL and AF patients visualised by electron tomography (ET). 63
Figure 27. Protein expression of structural proteins detected by immunoblotting of RAAs from CTL and AF patients. 64
Figure 28. COX-deficient myocytes in RAAs from CTL and AF patients. 65
Figure 29. Spontaneous Ca^{2+}-release events (SCaEs) in atrial myocytes from CTL patients and AF patients with or without Ezetimibe. 67
Figure 30. Ca^{2+} spark measurements in human induced pluripotent stem cell-derived atrial myocytes (hiPSC-AMs). 69

List of supplementary figures

Supplementary Figure 1. Revert™ Total Stain labelled membranes used for normalization of target protein. 104

List of tables

Table 1. Cardioplegic solution 20
Table 2. Ca^{2+}-free isolation solution 20
Table 3. Isolated myocyte storage solution 20
Table 5. Bath solution for patch clamp experiments 23
Table 6. Bath solution for Ca^{2+} sparks and current clamp experiments 23
Table 7. Pipette solution for patch clamp experiments 23
Table 8. Antibodies used for immunostaining 31
Table 9. Solutions used for immunostaining. 31
Table 10. Solutions for COX-SDH staining. 36
Table 11. Solutions used for protein biochemistry. 38
Table 12. Antibodies used for protein biochemistry 38
Table 13. Cumulative table showing patient characteristcs of the samples used in the project. 40

List of abbreviations

$[Ca^{2+}]_c$	cytosolic calcium concentration
$[Ca^{2+}]_m$	mitochondrial calcium concentration
AF	atrial fibrillation
AM	acetoxymethyl
AP	action potential
APD	action potential duration
ATP	adenosine triphosphate
Ca^{2+}	calcium
CaSps	calcium sparks
COX	cytochrome oxidase *c*
CTL	control; sinus rhythm
DAD	delayed afterdepolarisation
ΔΨm	mitochondrial membrane potential
EAD	early depolarisations
Eze	Ezetimibe
FADH2	flavin adenine nucleotide, reduced
hiPSC-CM	human induced pluripotent stem cell-derived cardiac myocytes
ICDH	isocitrate dehydrogenase
IMM	inner mitochondrial membrane
IMS	intermembrane space
K^+	potassium
MCU	mitochondrial calcium unipoter
MCUB	double-dominant regulator of MCU
MICU	mitochondrial calcium uptake
mPTP	mitochondrial permeability transition pore
Na^+	sodium
NADH	nicotinamide adenine nucloeotide, reduced
NADPH	nicotinamide adenine dinucleotide phosphatem, reduced
NCX	sodium-calcium exchanger
NNT	nictotinamide nucleotide translocator
OMM	outer mitochondrial membrane
RAA	right atrial appendage
RyR2	ryanodine receptor
SAN	sinoatrial node
SCaEs	spontaneous calcium events
SDH	succinade dehydrogenase
SERCA	serca/endoplasmic reticulum calcium ATPase
SR	sarcoplasmic reticulum
TCA	tricarboxylic acid
VDAC	voltage dependent anion channel
αKGDH	α-ketoglutarate dehydrogenase

Abstract

Atrial fibrillation (AF) is the most common form of arrhythmia however, due to the incomplete understanding of its molecular mechanisms, there are several limitations of the currently available therapeutic strategies. Impaired cytosolic calcium (Ca^{2+}) handling is a well-described mechanism in the persistent form of AF. Mitochondria comprise up to a third of the volume of cardiac myocytes and are able to take up Ca^{2+} from the cytosol. One function of mitochondrial Ca^{2+} accumulation is to increase cellular energy production, matching bioenergetic supply with demand. A disturbance in this process in the ventricle has already been observed in cardiovascular diseases. Mitochondrial Ca^{2+} handling, however, is not well-studied in the atria and in AF. Here, we show a disturbance in the interaction between the sarcoplasmic reticulum and mitochondria in the right atrial appendage from patients with *long-standing persistent atrial fibrillation* (AF). The close apposition of these "kissing cousins" generates Ca^{2+} microdomains which facilitate efficient Ca^{2+} uptake by mitochondria. This appears to be altered in AF, as Mitochondrial Ca^{2+} transient amplitude and diastolic Ca^{2+} accumulation are reduced, compared to non-AF myocytes, particularly in conditions of increased workload. As a consequence, Ca^{2+}-activated mitochondrial processes are impaired, such as the regeneration of electron donors necessary for ATP production and, potentially also, mitochondrial mechanisms protecting against cellular oxidation. We have, however, found a possible compensatory mechanism involving the mitochondria Ca^{2+} uniporter (MCU) complex, whereby a decrease in MICU2/MCU ratio could prevent detrimental Mitochondrial Ca^{2+} loss. We also provide new evidence in human atrial myocytes and human induced-pluripotent stem cell derived cardiac myocytes (hiPSC-CMs) for the antiarrhythmic potential of ezetimibe, a lipid-lowering drug, recently shown to enhance Mitochondrial Ca^{2+} uptake. Overall, the findings of this project highlight the significance of altered Mitochondrial Ca^{2+} handling, particularly in the face of increased bioenergetic demands, in AF. Furthermore, evidence is shown that enhancing mitochondrial Ca^{2+} uptake can protect against potentially arrhythmogenic mechanisms underlying AF.

1 Introduction

1.1 Atrial Fibrillation

Atrial fibrillation (AF) is the most common form of supraventricular arrhythmia, where the pacemaking activity of the sinoatrial node (SAN) is overridden by impulses originating elsewhere in the atrial tissue. These ectopic impulses occur at high rates and can result in a conceivable bioenergetic alteration. Impaired calcium (Ca^{2+}) handling is well-described in the cytosol of cardiac mayocytes, involving both sarcolemmal and sarcoplasmic reticulum (SR) membrane proteins. The mitochondria, being the major energy supplier in cardiac myocytes, are able to decode Ca^{2+} oscillations as metabolic signals during stress, but this has not been characterised in AF. Therefore the aim of this thesis was to investigate mitochondrial Ca^{2+} handling in AF and its potential role in the disease process.

1.1.1 Epidemiology

AF is considered as a progressively worsening cardiovascular epidemic due to the fact that life is expectancy is increasing and the ageing population are the group most vulnerable to AF (Kornej et al., 2020; Schnabel et al., 2015). Combined with atrial flutter, AF was estimated to affect more than 37 million individuals worldwide, according to the 2017 Global Burden of Disease Study (James et al., 2018), and AF burden is projected to increase further (Krijthe et al., 2013; Rahman et al., 2014). This is particularly concerning in the United States and Europe, where prevalence of AF and AF-related mortality are the highest (Benjamin et al., 1994). However, these estimations are complicated by the asymptomatic or mild nature of AF (Rienstra et al., 2012; Staerk et al., 2017). This also results in late detection of this condition, where it is more likely to contribute to major cardiovascular events such as stroke and myocardial infarction (Kirchhof et al., 2016). However, with the advent of portable AF detection modalities, such as smartwatches and wearable devices, early detection of AF is now possible but remains in its nascent stages of development (Abu-Alrub et al., 2022; Hermans et al., 2022). Moreover, this offers minimal benefit to patients with advanced stages of AF. Thus, a better understanding of the molecular mechanisms of AF pathophysiology could contribute to the improvement of therapies for AF.

1.1.2 Clinical manifestation

The use of a 12-lead electrocardiogram (ECG), first popularised by Einthoven (Einthoven, 1997), is useful for locating the source of arrhythmia, and thus, its management (Wellens & Gorgels, 2004). In a typical ECG readout from a patient with AF, RR intervals, denoting rhythmicity, are irregular in duration, and P waves, denoting atrial activation, are indistinct (Kirchhof et al., 2016). Ectopic paroxysms have been found to originate from the muscle sleeves of the atrial tissue surrounding the pulmonary veins (Haïssaguerre et al., 1998), and the ablation of these focal points can reduce, but not eliminate, the reoccurrence of these impulses (Kottkamp et al., 2004). AF can be classified as paroxysmal, when it self-terminates within 1 week, otherwise it is known as persistent (>1 week), long-standing persistent AF (>1 year) or permanent AF, depending on the patient's response to antiarrhythmic regimen. The aetiology of human AF is also varied. These factors contribute to the complex nature of AF and can complicate its management and treatment (Brundel et al., 2022; Iwasaki et al., 2011). Therefore, discerning novel druggable targets in AF requires a deeper knowledge of the governing mechanisms, based on disease duration and aetiology.

1.1.3 Pathophysiology

Ectopic activity outside of the SAN, as previously mentioned, is one of the accepted trigger mechanisms in AF (Haïssaguerre et al., 1998). This occurs as premature action potentials (AP) during or after the repolarization phase, termed as early- or delayed afterdepolarisations (EADs and DADs), respectively. EADs are related to AP duration (APD) prolongation while DADs are due to SR Ca^{2+} releases after AP repolarization which activate the Na^{+}/Ca^{2+} exchanger (NCX), resulting in an electrogenic current that prematurely depolarizes the membrane. These events have been observed both in paroxysmal and chronic AF (Voigt et al., 2012, 2014). Reentry is a mechanism proposed for the maintenance of AF, where rotor activity or multiple wavelets result from slow conduction velocity and shortened effective refractory period (Staerk et al., 2017). Reentry requires the presence of both a trigger and a substrate, that can either be structural, for example fibrosis (Nattel, 2017), or functional, such as remodeling of ionic currents (Heijman, Voigt, Nattel, et al., 2014; Wijesurendra & Casadei, 2019; Zipes et al., 2017). Considering the

importance of Ca^{2+} in these processes, we will take a deeper look into the Ca^{2+} handling of atrial myocytes and how it is altered during AF.

1.2 Calcium handling

1.2.1 Calcium

Ca^{2+} is a ubiquitous and versatile second messenger in cellular physiology. Calcium can exert its effect either by causing a conformational change in a protein upon binding to it, or by binding to a Ca^{2+} sensor to initiate signal transduction (Newton et al., 2016). In cardiac myocytes, changes in global concentrations of Ca^{2+} determines contractility (D. A. Eisner et al., 2017). These changes in Ca^{2+} levels are facilitated by ion channels and transporters on the sarcolemma and on Ca^{2+} stores and sinks in the subcellular organization of a myocyte. Subcellular compartmentalization also generates Ca^{2+} concentration gradients that drive the movement of Ca^{2+}. Normally, cytosolic Ca^{2+} levels $[Ca^{2+}]_c$ are maintained at 100 nM when at rest, but can reach up to 1 µM during contraction. However, these represent only unbound Ca^{2+} as the majority of Ca^{2+} in the cytosol is bound to buffers (D. A. Eisner et al., 2017). Impairment of Ca^{2+} handling is evident in AF and will be discussed in the next sections.

1.2.2 Excitation-contraction coupling

The contraction of the heart is initiated by APs generated by the SAN, which is the starting point of an electrical conduction system that terminates at the ventricles. On the cellular level, membrane depolarization is mainly due to the fast-activation of sodium (Na^+) channels. Membrane depolarization activates the opening of voltage-dependent L-type Ca^{2+} channels. This Ca^{2+} entry into the cytosol activates a greater release of Ca^{2+} from the SR via the ryanodine receptors (RyR2), in a phenomenon known as "Ca^{2+}-induced Ca^{2+}-release", which raises $[Ca^{2+}]_c$ levels, increasing the amount of available Ca^{2+} for binding to the myofilaments. The efficiency of this process is due to the existence of dyadic clefts (around 15 nm) between L-Type Ca^{2+} channels and RyR2 (D. A. Eisner et al., 2017). When Ca^{2+} binds to cardiac troponin C on the actin filament, this results in a conformational change which allows the myosin head to bind to actin, initiating contraction. This is followed by a relaxation phase, where cytosolic Ca^{2+} returns to basal level,

predominantly being taken back up in to the SR via SERCA, but also via extrusion to the extracellular space by NCX. In comparison to SERCA and NCX, the plasma membrane Ca^{2+} ATPase (PMCA) only plays a minor role in Ca^{2+} removal and, although mitochondria can take up Ca^{2+}, their contribution to the relaxation phase is deemed negligible (Bers, 2008; D. A. Eisner et al., 2017)

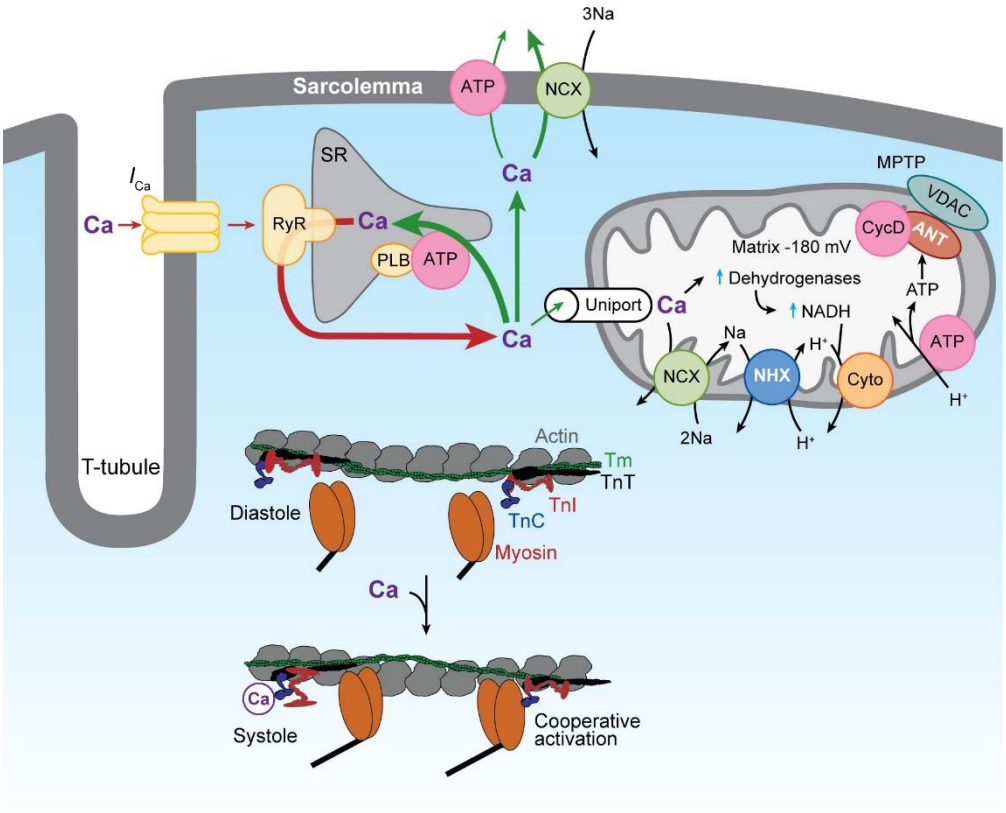

Figure 1. Ca^{2+}-handling mechanisms in the cardiac myocyte. See Sections 1.2.2 and 1.3.4 for a detailed description. Obtained with permission (Bers, 2008)

While excitation-contraction coupling is generally similar between cardiac myocytes of the ventricles and atria, there are key structural differences that can influence Ca^{2+} handling. First, the presence of an extensive t-tubular network in ventricular cells. There is also a clear separation between junctional and non-junctional SR, where SR and mitochondria take up Ca^{2+} in the subsarcolemmal space, thus preventing centripetal Ca^{2+} movement (Mackenzie et al., 2004). Considering the differences between atrial and ventricular Ca^{2+} handling, it is therefore important to consider that observations on ventricular myocytes will reflect that of atrial myocytes.

1.2.3 Ca^{2+} handling in AF

In AF, reduced Ca^{2+} entry via the L-type Ca^{2+} channel is a known hallmark of atrial cellular remodeling, and is proposed as a compensatory mechanism in chronic forms of AF, known as "Ca^{2+} silencing" (Greiser, 2017; Greiser & Schotten, 2013). The occurrence of triggered activity, such as DADs, is due to SR Ca^{2+} leak via dysregulation (i.e. CAMKII-mediated hyperphosphorylation) of the RyR2 channels (Chiang et al., 2014; Hove-Madsen, Llach, Bayes-Genís, et al., 2004; Neef et al., 2010; Voigt et al., 2012). (Heijman, Voigt, Wehrens, et al., 2014; Voigt et al., 2012). Increased NCX1 function has a compounded effect, where electrogenic Na^{+} entry promotes DADs (Voigt et al., 2012).

A further phenomenon observed in malignant arrhythmias is that of alternans, which have been observed clinically in ECGs (Armoundas et al., 2002) and occur as oscillations in Ca^{2+} and/or AP morphology, as observed in cardiac myocytes (Edwards & Blatter, 2014; Fakuade et al., 2021). Interestingly, redox and metabolic underpinnings have been ascribed to the occurrence of alternans (Akar et al., 2005; Aon et al., 2003; Belevych et al., 2009; Cortassa et al., 2004; Hüser et al., 2000; Stary et al., 2016), and antioxidative targeting of the reactive oxygen species-producer xanthine oxidase (XO) in myocardial infarction has been shown to prevent the occurrence of repolarisation alternans (Plummer et al., 2015). Since the mitochondria clearly has a capacity to modulate cardiac function, alterations in mitochondrial function may undergo alterations to accommodate the increased atrial activation rate. However, there is limited literature available on human AF (Mason et al., 2020).

1.3 Mitochondrial function in the heart

1.3.1 Cardiac mitochondria

Mitochondria are key players in metabolism and their role is not limited to energy production by catabolism of nutrients. Mitochondria are also involved in biosynthetic processes, management of metabolic by-products, and modulation of the redox environment to maintain homeostasis (Spinelli & Haigis, 2018). Mitochondrial role in signal transduction has recently been highlighted. In cardiac muscle, mitochondria are abundant, occupying up to 30% of the cellular fractional volume

second to myofilaments (~60%) (Brown et al., 2017). Indeed, the abundance of mitochondria positively correlates to heart rate. Mitochondria are present in three different subpopulations: subsarcolemmal (SSM), intramyofibrillar (IFM), and perinuclear (PNM), which perform similar functions in a location-specific manner. In mature cardiac myocytes, mitochondria appear to be in a rigid organisation in between sarcomeres, at least in the IFM subpopulation. However, fusion-fission events also persist among cardiac mitochondria (V. Eisner et al., 2017), as well as more minute mitochondrial communications such as “kissing” and nanotunneling (Cao et al., 2019; Huang et al., 2013), which are thought to preserve mitochondrial quality.

1.3.2 Cardiac bioenergetics

The contraction of the cardiac muscle is an energy-consuming mechanism, where ATP hydrolysis is required by ATPases such as SERCA, N^+/K^+-ATPase, and the myosin ATPase of the myofilaments. Up to 95% of the bioenergetic demand of the heart is supplied by the mitochondria by oxidative phosphorylation (OXPHOS) (Bertero & Maack, 2018; Kohlhaas et al., 2017). Contraction of the heart is powered by nutrient sources and oxygen supply. Nutrients such as glucose and fatty acids are catabolised to produce acetyl CoA (Lopaschuk et al., 2021), the initial step in the tricarboxylic acid (TCA) cycle. The TCA cycle is a series of redox processes, transferring electrons to cofactors NAD^+ and FAD^+. These become NADH and $FADH_2$, which in turn supply electrons to the electron transport chain (ETC). OXPHOS is achieved by the coordinated electron transfer from NADH and $FADH_2$ through four IMM protein complexes. The pumping H^+
from the matrix into the IMs generates a proton gradient that fuels a fifth complex, the F_1/F_o ATP-synthase, which ultimately generates ATP.

The high turnover rate of ATP in the heart requires the tight regulation of ATP production during changes in workload (Stanley et al., 2005). The idea of parallel activation of mitochondrial bioenergetics by Ca^{2+} was introduced by Balaban (Balaban, 2002) to rationalise the “metabolic homeostasis” observed during increased cardiac workload: on the one hand, increased time-averaged cytosolic Ca^{2+} during increased workload increases contractility, and thus ATP hydrolysis. The rise in ADP/ATP ratio will oxidise available electron donors to supply

appropriate amounts of ATP, the so-called “pull” condition. On the other hand, cardiac inotropy or chronotropy causes increased cytosolic Ca^{2+}, as well as mitochondrial Ca^{2+}, potentiating electron donor regeneration by Ca^{2+} sensitive dehydrogenases in the TCA cycle, the so-called “push” condition (Bhosale et al., 2015; Kohlhaas & Maack, 2013). When pull and push are in balance, this is how the heart meets energy supply to demand. During the process, however, the presence of O_2 and electron transfer via the ETC also leads to the formation of toxic by-products: reactive oxygen species (ROS).

1.3.3 Mitochondrial ROS production and elimination

ROS are products of the step-wise monovalent reduction of oxygen (O_2). These intermediates are involved in signal transduction when tightly controlled, but in excess, they can result in modifications of various targets (D’Autréaux & Toledano, 2007). Major sources of ROS include xanthine oxidases (XO), NADPH oxidases (NOX), and mitochondrial ETC (Bedard & Krause, 2007; M. P. Murphy, 2009), although many other sources have been identified (Sies & Jones, 2020). Mitochondria produce both superoxide ($^{\cdot}O_2^-$) and hydrogen peroxide (H_2O_2). In the ETC, O_2 is the last electron receptor and is converted to H_2O by Complex IV. However, its monovalent reduction due to electron slippage gives rise to $^{\cdot}O_2^-$ (M. P. Murphy, 2009). This can occur when electron flow is disturbed by reduced redox components of the ETC complexes or reverse electron transport, where both processes increase the likelihood of electron slippage to O_2 (M. P. Murphy, 2009; Turrens et al., 1985). α-ketoglutarate dehydrogenase (αKGDH) and pyruvate dehydrogenase (PDH), via the dihidrolipoamide dehydrogenase, have also been reported to produce ROS in a $NADH/NAD^+$-dependent manner (Ambrus, 2019; M. P. Murphy, 2009; Quinlan et al., 2014). Recently, however, α-KGDH was disputed to be a source of ROS under physiological conditions in working cardiac myocytes, but instead contributes to reduced nicotinamide adenine dinucleotide phosphate (NADPH) regeneration through nicotinamide nucleotide transhydrogenase (NNT) (Wagner et al., 2020).

The importance of ROS in mitochondrial function is underscored by the presence of antioxidative mechanisms in the mitochondria. For example, dismutation of $^{\cdot}O_2^-$

to H_2O_2 by mitochondrially-localised manganese superoxide dismutase (MnSOD) keeps $^{\cdot}O_2^-$ levels in the picomolar range (Krumova & Cosa, 2016; M. P. Murphy, 2009). However, this results in a more stable H_2O_2, the main ROS signal, and can diffuse throughout the mitochondria and beyond. NADPH oxidases (NOX) can also produce H_2O_2. Once in the cytosol, it can indeterminately bind to other macromolecules. H_2O_2 is eliminated by mitochondrial catalase (mCAT), peroxiredoxin, and glutathione peroxidase. PRx and GPx convert H_2O_2 to water, and is coupled to the electron transfer from NADPH to glutathione by glutaredoxin and thioredoxin by thioredoxin reductase (Bertero & Maack, 2018). Besides the pentose phosphate pathway, NADPH can be regenerated by repurposing NADH produced by α-KGDH means of nicotinamide nucleotide transhydrogenase (NNT) (A. G. Nickel et al., 2015; Wagner et al., 2020). Since TCA cycle substrates ICDH and malic enzyme produce NADH that can be converted to NADPH, TCA cycle turnover rate can determine the net ROS emission (Bertero & Maack, 2018; Kohlhaas et al., 2017). Some of these mechanisms can be activated by Ca^{2+} during the parallel activation with increased workload (Balaban, 2002; Kohlhaas et al., 2017) and will be discussed in the next sections. Therefore, an intermediate redox state, as opposed to a reduced one, is favourable over an oxidised state. This has been previously proposed by O'Rourke's group (Aon et al., 2010; Cortassa et al., 2014), who describe a scenario where either extreme of cellular environment – reduced or oxidised - results in ROS accumulation: ROS production due to increased electron slippage from the ETC during the mitochondrial reduced state vs. compromised ROS-scavenging capacity of the mitochondria in the oxidised state (A. G. Nickel et al., 2015).

1.3.4 Mitochondrial Ca^{2+}

Mitochondrial Ca^{2+} is an important regulator of metabolism, cell death, autophagy, signal transduction and, more controversially, cytosolic Ca^{2+} dynamics (Garbincius & Elrod, 2022). At rest, mitochondrial Ca^{2+} levels have been reported to be similar to that in the cytosol (100-200 nM) (Giorgi et al., 2018). With a highly electronegative membrane potential ($\Delta\Psi_m \approx$ -180 mV) of the inner mitochondrial membrane (IMM), mitochondria are excellent candidates for Ca^{2+} buffering. However, their

contribution to shaping cytosolic Ca^{2+} dynamics is trivialized by the major Ca^{2+} efflux mechanisms SERCA and NCX (Bers et al., 1996). A greater contribution by mitochondria and would require large and prolonged increases in cytosolic Ca^{2+} (Williams et al., 2013). These will be discussed further in the following sections.

1.3.4.1. Kinetics of mitochondrial Ca^{2+} uptake

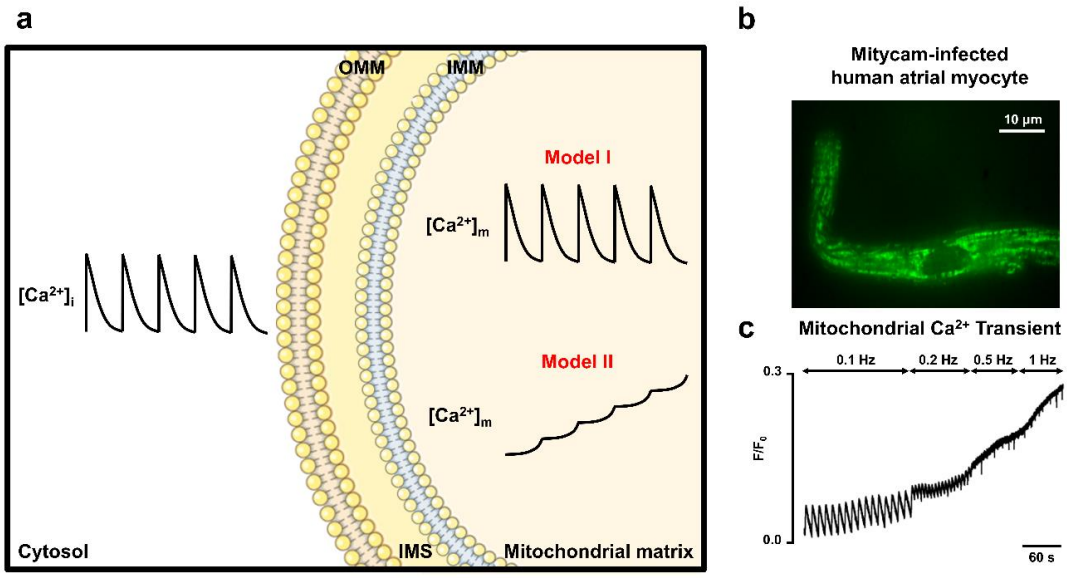

Figure 2. Kinetics of mitochondria Ca^{2+} uptake in atrial myocytes. A, a diagram of the debated kinetics of mitochondrial Ca^{2+} influx: Model I – oscillatory and Model II – integrator. **B,** a confocal image of a Mitycam-infected human atrial myocyte. Scale bar=10µm. **C.** Representative trace of Ca^{2+} transients recorded from a Mitycam-infected myocyte demonstrating the occurrence of both models mentioned in **A.** IMM=inner mitochondrial membrane; IMS=intermembrane space; OMM=outer mitochondrial membrane. Obtained with permission (Mason et al. 2020)

The kinetics of mitochondrial Ca^{2+} uptake has been controversial, but two models have previously been proposed (Mason et al., 2020, **Figure 2**). First is the intergrator mode, where Ca^{2+} is slowly taken up by the mitochondria and Ca^{2+} extrusion is even slower, allowing for Ca^{2+} accumulation until a new steady-state is reached. The other model is the oscillator mode, where Ca^{2+} uptake occurs in a beat-to-beat fashion. Recent advances for measuring mitochondrial Ca^{2+} allow for better temporal resolution of Ca^{2+} kinetics and there is evidence for both models of mitochondrial Ca^{2+} handling, occurring in combination, depending on stimulation frequency (Andrienko et al., 2009; Lu et al., 2013; Maack et al., 2006). Ca^{2+} accumulation in the mitochondria at higher stimulation frequencies can have bioenergetic consequences. To gain a better understanding as to why Ca^{2+}

accumulation occurs, an overview of Ca^{2+} influx and efflux mechanisms will be discussed in the next section.

1.3.4.2. Mitochondrial Ca^{2+}-influx and -efflux pathways

The kinetics of mitochondrial Ca^{2+} handling are distinct from those of the cytosol due to the efficiency of Ca^{2+} influx and efflux mechanisms. The highly electronegative membrane potential ($\Delta\Psi_m \approx$ -180 mV) on the matrix side of the inner mitochondrial membrane (IMM) must be maintained, thus cationic entry must be tightly regulated. Indeed, the mitochondrion has two membranes through which ions and metabolites must pass through. On the outer membrane, a voltage-dependent anion channel (VDAC) is present (Rapizzi et al., 2002; Wilting et al., 2020). In the heart, there are three isoforms of VDAC, with VDAC1 being most abundant. It allows small passage of molecules up to 6 kDa, which includes metabolites and ions. VDAC has Ca^{2+} sensing capabilities and allows Ca2+ entry both in its open and closed states (Najbauer et al., 2021), at voltages >40 mV, VDAC conductance and anion selectivity reduces, potentially by intrinsic gating or by occlusion by an interacting protein (Sander, Gudermann, et al., 2021).

On the inner membrane, a low-affinity ($K_d \approx$ 10-30 µM) transmembrane Ca^{2+} channel was identified as being the mitochondrial Ca^{2+} uniporter (MCU) (De Stefani et al., 2011; Kwong et al., 2015). This channel relies on localized Ca^{2+} rises in microdomains, which bathe the mitochondria with Ca^{2+} levels higher than the global cytosolic Ca^{2+} level. Indeed, mitochondria Ca^{2+} levels near the z-lines of sarcomeres where SR is enriched are higher than that in between the z-lines (Lu et al., 2013). Moreover, SR-independent mitochondrial Ca^{2+} increase is less efficient for driving mitochondrial Ca^{2+} uptake (Kohlhaas & Maack, 2010). MCU was later found out to form a supercomplex with regulators that mediate assembly and Ca^{2+} threshold setting (Pallafacchina et al., 2021, **Figure 3**). Ca^{2+} sensing of the MCU is mediated by mitochondrial Ca^{2+} uptake 1 and 2 (MICU1/2) in the intermembrane space (IMS) of mitochondria. MICU1 and MICU2 cooperatively activate MCU, while MICU2 sets the threshold for mitochondrial Ca^{2+} uptake (Kamer & Mootha, 2014; Patron et al., 2014), and these MICU isoforms form disulfide-linked heterodimers that promote Ca^{2+} entry when disengaged (Kamer et al., 2017; Petrungaro et al., 2015). A third

isoform, MICU3, has subsequently also been identified. The MICU1 can form either homodimers or heterodimers (with MICU2 and MIUC3) to fine-tune mitochondrial Ca^{2+} sensing (Patron et al., 2014, 2019). These Ca^{2+} sensing constructs are integrated into the MCU complex by the scaffolding protein, EMRE (essential MCU regulator) (J. C. Liu et al., 2020; Sancak et al., 2013) and via a scaffolding factor, MCU regulator 1 (MCUR1). A dominant-negative regulator of the MCU, MCUB has also been identified (Raffaello et al., 2013), and has been shown to exert beneficial effects during I/R injury (Lambert et al., 2019).

Interestingly, isolated mitochondria that obviously lack Ca^{2+} microdomain provided by their membrane association with SR in intact cells are able to uptake submicromolar levels of Ca^{2+} (De Stefani et al., 2016). Rapid-mode mitochondrial Ca^{2+} uptake (RaM) transporters are highly conductive even at nanomolar Ca^{2+}

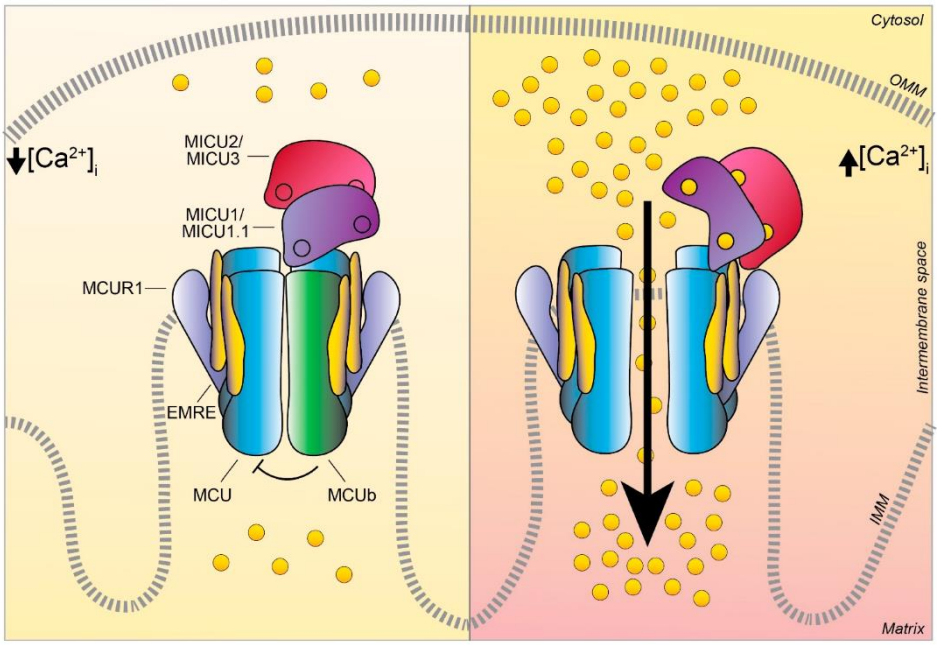

Figure 3. Mitochondrial Ca^{2+} uniporter complex and its regulators. Diagram showing the MCU complex and its regulators: the Ca^{2+}-sensing MICU1/2 (MICU1.1/3 for skeletal muscle); the essential MCU regulator, EMRE; the dominant-negative regulator, MCUb; and the scaffolding factor, MCUR1. (Left) At low cytosolic Ca2+, no Ca^{2+} binding to the MICU isoforms occur, thus limiting Ca^{2+} entry into the matrix. However, at high cytosolic Ca2+ (right), the binding of Ca^{2+} to both MICU1 and MICU2 promotes cooperative activation of the MCU complex, thus allowing Ca^{2+} entry. Obtained from (Pallafacchina et al., 2021).

levels (Buntinas et al., 2001). However, the reactivation of these transporters take up to 90 seconds and this mechanism also inactivates beyond 150 nM Ca^{2+}, minimising its role in beat-to-beat mitochondrial Ca^{2+} changes. Another mode of Ca^{2+} entry is provided by mitochondrial RyR1 (mRyR1), which was shown to be

physically linked to of inositol 1,4,5-triphosphate receptor (IP_3R) (Seidlmayer et al., 2016, 2019). Ca^{2+} sequestration occurs even at low $[Ca^{2+}]_c$ and poses a potential role in the beat-to-beat mitochondrial Ca^{2+} uptake (Beutner et al., 2005).

The predominant mitochondrial Ca^{2+} extrusion mechanism is the mitochondrial $Na^+/Ca^{2+}/Li^+$ exchanger (mNCLX), which is Na^+-dependent (Carafoli et al., 1974; Palty et al., 2010). Deletion of mNCLX has been shown to result in cardiac remodeling and dysfunction, due to mitochondrial Ca^{2+} overload (Luongo et al., 2017). Mitochondrial NCLX generates an electrogenic current by allowing entry of 3 Na^+ ions per extruded Ca^{2+} (E. Murphy & Eisner, 2009). The mitochondrial Na^+-H^+ exchanger (mNHE) maintains mitochondrial Na^+ concentration. The mNCLX has been shown to be sensitive to changes of cytosolic $[Na^+]$ in the physiological range (Bay et al., 2013; Bertero & Maack, 2018; E. Murphy & Eisner, 2009; Williams et al., 2015).

1.3.4.3. Mitochondrial Ca^{2+} overload

Mitochondria-mediated cell death is initiated by the sensitisation of the mitochondrial permeability transition pore (mPTP) to excessive Ca^{2+} entry, increasing osmotic pressure. This can cause the mitochondrial matrix to swell and eventually rupture, releasing its contents into the IMS (Halestrap et al., 2004). However, transient and low conductance openings of the pore have been observed, exhibiting the same properties and respond to same modulators as the mPTP, but are rare and proposed to be protective against excess mitochondrial Ca^{2+} (Lu et al., 2016).

1.3.4.4. Metabolism and Ca^{2+}

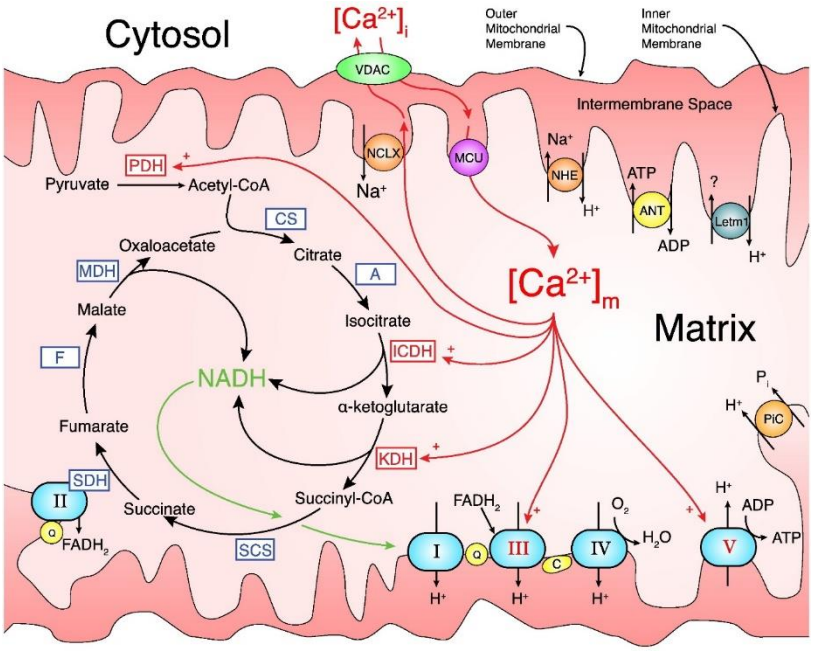

Figure 4. Ca^{2+} sensitive proteins in the mitochondria. Obtained with permission from (Williams, Boyman and Lederer, 2014)

Ca^{2+} has been reported to increase the metabolic substrate flow by activating Ca^{2+} sensitive dehydrogenases in the TCA cycle (Williams et al., 2015, **Figure 4**). Pyruvate dehydrogenase (PDH) converts pyruvate into acetyl coenzyme A (CoA) and is regulated via phosphorylation by PDK and dephosphorylation by PDP. Phosphorylation of the PDH on the E1 subunit occurs at Ser292, Ser232, and Ser300, although this may vary in different species. Interestingly, PDP isoform 1 (PDP1) can be activated by Ca^{2+}, which increases the association of the E1 subunit of the PDH complex with its E2 subunit by phosphorylation (Denton et al., 1972).

Other Ca^{2+} sensitive targets have been identified in the TCA cycle, for example Ca^{2+} increases substrate affinity of α-ketoglutarate dehydrogenase (α-KGDH) (McCormack & Denton, 1979). While Ca^{2+} alone only modestly activates ICDH, the presence of ADP potentiates its effect (Denton et al., 1978). The mechanisms underlying both Ca^{2+} mediated activations remain unknown (Glancy & Balaban, 2012). Ca^{2+} has also been shown to activate the ATP synthase and the ETC, but this has recently been contested (Wescott et al., 2019).

1.3.4.5. Mitochondria-SR crosstalk

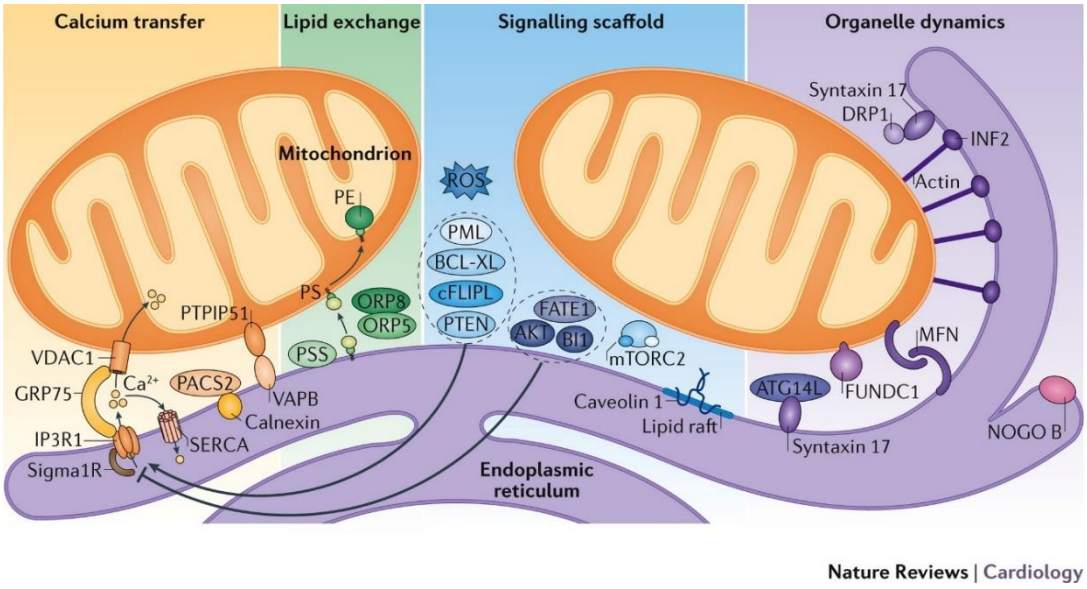

Figure 5. SR/ER-mitochondria crosstalk. Besides their close positioning, SR/ER and mitochondria interaction is enhanced by tethering proteins that facilitate specific functions such as Ca^{2+} transfer, lipid exchange, signal transduction, and organelle dynamics. Obtained with permission (Lopez-Crisostomo, et al., 2017)

The close apposition between the two organelles results in a high-Ca^{2+} environment called Ca^{2+} microdomains (Rizzuto et al., 1998). Ca^{2+} microdomains are necessary for mitochondrial Ca^{2+} uptake due to the high K_d value of the MCU (Bragadin et al., 1979; Csordás et al., 2010; Giacomello et al., 2010), as microdomains surpass the Ca^{2+} levels during bulk cytosolic Ca^{2+} increase. The network formed by the SR surrounding sarcomeres and the abundance of mitochondria in between the sarcomeres increase the chances of their interaction. The SR makes Ca^{2+} available to the sarcomeres while mitochondria provide the energy for contraction. Therefore, both close interaction of SR and mitochondria and the distinct localisation of mitochondrial Ca^{2+} influx and efflux pathways ensure an efficient excitation-energetics coupling (De La Fuente et al., 2018). However, a more direct interaction in reinforced by tethering proteins that ensure efficient material transfer between the organelles. The distance between SR and mitochondria can be between 40 and 300 nm, and during SR Ca^{2+} release, localised Ca^{2+} rises in between these organelles can reach up to 20 uM, thus overcoming the low Ca^{2+} affinity of the MCU channel (V. K. Sharma et al., 2000). Molecular tethers maintain the close structural and functional association between SR and mitochondria (Lopez-Crisosto et al., 2017, **Figure 5**). One of the well-studied tethers are mitofusins (Mfn) (de Brito &

Scorrano, 2008; Naon et al., 2016). There are two isoforms of Mfn: Mfn1 and Mfn2, and only Mfn2 tethers SR to the mitochondria (Dorn & Maack, 2013; Rossini & Filadi, 2020). Mfn1 is more involved in intermitochondria dynamics, and its loss does has not been attributed to any human disease (Dorn & Maack, 2013). Indeed, ventricular myocytes from Mfn2-deficient mice showed decreased mitochondrial Ca^{2+} uptake (Chen et al., 2012; Seidlmayer et al., 2019), and can engender metabolic consequences (Kohlhaas et al., 2017). The role of SR-mitochondria tethering has been well-studied in ischemia/reperfusion (I/R), as reperfusion results in a Ca^{2+} surge that results in organelle Ca^{2+} overload (Dorn, 2009; Paillard et al., 2013). The endoplasmic reticulum (ER) protein PDZD8 tethers the ER to the mitochondria and its modulation in neurons affects mitochondrial Ca^{2+} transfer (Hirabayashi et al., 2017), and its role in cardiac myocytes has been speculated (Ljubojevic-Holzer, 2018). PTPIP51 (protein tyrosine phosphatase interacting protein 51) is a mitochondrial outer membrane protein that interacts with VAPB (vesicle-associated membrane protein-associated protein-B) on the SR-mitochondrion interface (De vos et al., 2012), and their downregulation resulted in Ca^{2+} overload, and thus their downregulation was shown to be beneficial in I/R injury (Qiao et al., 2017). IP3R physically associates with VDAC1 (Paillard et al., 2013), which is facilitated by GRP75 (glucose-regulated protein 75), and the resulting supercomplex is involved in mitochondrial Ca^{2+} uptake (Szabadkai, Bianchi, et al., 2006). Further, the enzyme TGM2 (transglutaminase type 2) was found to regulate this complex formation, where its downregulation was found to alter the MAM protein makeup to maintain the physical interaction of mitochondria and SR, albeit with a wider distance, impairing Ca^{2+} dynamics (D'Eletto et al., 2018). This increase in the formation of this complex was also involved in atrial remodeling in diabetes (Yuan et al., 2022). Therefore, a myriad of potential regulators of Ca^{2+} communication between SR and mitochondria can be examined if their expressions and interactions are disturbed in AF.

1.4 AF and mitochondrial function

1.4.1 Mitochondrial ultrastructure in AF

Fibrillating atria from patients undergo severe ultrastructural remodelling, where mitochondrial fragmentation, sarcomeric myolysis, cellular dissociation and

interstitial fibrosis have been consistently observed (Mary-Rabine et al., 1983; S. Sharma et al., 2014; Thiedemann & Ferrans, 1977; Wiersma et al., 2019). Furthermore, free SR have been observed in left atrial tissue with AF, and (Bukowska et al., 2008) the mitochondria around these regions are either small or absent (Thiedemann & Ferrans, 1976, 1977). It is plausible that these ultrastructural changes of the mitochondria can affect potential intraorganellar interactions that can contribute to electrical conduction abnormalities in AF (Mason et al., 2020). Therefore, these findings can be further reinforced by identifying molecular determinants of mitochondrial interactions with other organelles, such as the SR.

Animal models of AF also exhibit mitochondrial structural changes. Mice with leaky RyR2 have more abnormal mitochondria (cited as reduction in electron density). Crossing this mouse with a mouse expressing human mitochondrial catalase (mCAT) to increase ROS neutralization reduces the amount of abnormal mitochondria. This excessive ROS emission from due to leaky SR, and indeed treatment of a RyR2-stabiliser, S107, mimics the effect of mCaT. Another mechanism was shown in mice expressing an incompletely-inactivating human NaV1.5 channel resulting in persistent Na^+ currents show swollen mitochondria and OMM rupture, which can be reversed by human mCAT expression (Avula et al., 2021). Increased expression of fission proteins, Opa1 and Mfn2, in this mouse model, resulting in larger mitochondria. Recently, a reduced Mfn2 expression has been found in patients with AF, and is further exacerbated by diabetes, which can be reversed by microtubule stabilization in tachypaced HL-1 cells (J. Li et al., 2022). However, several other channels and physical tethers are found in the SR-mitochondrion interface and have only been described in animal models and non-cardiac sources.

1.4.2 Mitochondrial ATP synthesis in AF

A reduced activity of ETC Complexes I and II have been observed in patients with AF, with or without diabetes (Emelyanova, Ashary, Cosic, Negmadjanov, Ross, Rizvi, Olet, Kress, Sra, Jamil Tajik, et al., 2016; Kanaan et al., 2019), despite unaffected protein expression of the complexes (Kanaan et al., 2019; Wiersma et al., 2019). Reduced Complex II and III have been observed in postoperative AF patients (Montaigne et al., 2013). However, in diabetic patients with AF the reduced activity of the ETC complexes were attributed to the impaired supercomplex

formation. Interestingly, these was accompanied by increased ATP synthesis (Emelyanova, Ashary, Cosic, Negmadjanov, Ross, Rizvi, Olet, Kress, Sra, Jamil Tajik, et al., 2016; Wiersma et al., 2019), which is feasible given the phosphocreatine systems present in muscles. However, a decreased expression of myofilament creatine kinase which was associated to an isoform change of alpha-myosin to a less ATP-expensive isoform, ß-myosin (Mihm et al., 2001). Transcriptomic analyses showed decreased fatty acid oxidation in AF (Barth et al., 2005) and metabolic adaptations in AF such as increased glycolytic activity (Barth et al., 2005; Harada et al., 2017) and the activation of ketone body metabolism (Mayr et al., 2008). These might be beneficial as an unfavorable increased fatty acid uptake has been observed in left atrial tissue of AF patients (Lenski et al., 2015).

1.4.3 ROS in AF

An altered redox environment by increased ROS production is evident in tachypaced atria in animal models (Avula et al., 2021; Dudley et al., 2005; Reilly et al., 2011; Xie et al., 2015) and in patients (Carnes et al., 2001; Dudley et al., 2005; Emelyanova, Ashary, Cosic, Negmadjanov, Ross, Rizvi, Olet, Kress, Sra, Tajik, et al., 2016; Y. M. Kim et al., 2005, 2008; Mihm et al., 2001; Wiersma et al., 2019). It is important to point out that the main source of ROS depends on the duration of AF (Anderson et al., 2014; Dudley et al., 2005; Sovari & Dudley, 2012), where atrial appendages from patients with chronic AF are more responsive to inhibition of ROS generation by Complex I by rotenone, pointing to the significance of mitochondrial ROS (Reilly et al., 2011). In pulmonary vein myocytes, H_2O_2 triggered abnormal impulse generation (Youn et al., 2013)

However, the redox environment of the heart is dictated not only by ROS production, but also by its antioxidative capacity (A. Nickel et al., 2014; Wagner et al., 2020). Therefore, it warrants further investigation on other redox-sensitive processes in the mitochondria. Central to these processes is the regeneration of electron donors, NADH and $FADH_2$, necessary for fueling the ETC and preventing ROS imbalance. Patients with poAF showed increased superoxide dismutation to H_2O_2, without a corresponding increase in catalase activity, resulting in excess ROS (Montaigne et al., 2013).

Oxidation of RyR2 resulting in a leaky SR can impair mitochondrial function, leading to even more ROS release, further triggering SR Ca^{2+} leak, and this vicious cycle is consistently observed in AF models (Cooper et al., 2013; Xie et al., 2015). Mitochondrial dysfunction and oxidative stress have been associated with increased contraction rates, as in tachycardia (Bukowska et al., 2008). ROS and Ca^{2+} closely regulate each other, resulting in a vicious cycle, wherein ROS-induced SR Ca^{2+} leak contributes to mitochondrial dysfunction. This, then, generates more ROS, that aggravates Ca^{2+} leak (Xie et al., 2015). ROS sources are also believed to vary depending on AF duration and aetiology (Anderson et al., 2014; Montaigne et al., 2013; Reilly et al., 2011). Moreover, antioxdiative mechanisms may be decreased in patients with permanent AF (Y. H. Kim et al., 2003). Therefore, several mitochondrial properties can be potential substrates for AF maintenance and must be examined more closely.

1.5 Aims

To address the gaps in knowledge about the role of mitochondria and its Ca^{2+} handling in patients with AF, we employed electrophysiological techniques coupled with fluorescence microscopy to monitor mitochondrial parameters in human atrial myocytes during transitions in workload. To relate structure to function, superresolution imaging and protein biochemistry of right atrial appendage biopsies from patients were also performed. These methods were selected to address the following aims:

Aim 1: To monitor the redox index of human atrial myocytes during workload transitions;
Aim 2: To describe the mitochondrial Ca^{2+} handling in human atrial myocytes and the changes that occur in AF; and
Aim 3: To compare structural differences relevant to mitochondrial Ca^{2+} transfer from the SR.

2 Methods

2.1 Patients

Patient consent was kindly obtained either by our medical students or surgeons from prior to the surgery day. Experimental protocols were approved by the ethics committee of the University Medical Center Göttingen (Ethics Approval No.4/11/18). Patients with sinus rhythm (CTL) and long-term persistent AF (AF) qualified for this project.

2.2 Human atrial myocyte preparations

2.2.1 Atrial myocyte isolation from patient biopsies

Right atrial appendages (RAA) were collected during open-heart surgery and transported in cardioplegic solution **Table 1**. After fat trimming, tissue samples were weighed (150-900 mg) and any excess tissue was frozen in liquid nitrogen (LN_2) for biochemical experiments. Fresh tissue was then transferred to cold Ca^{2+}-free solution, and was cut into smaller 1 mm^3 chunks before be transferred to a temperature-regulated water-jacketed chamber maintained at 37 °C. Tissue chunks were washed in Ca^{2+}-free solution **Table 2** 1-2x for 3 minutes while bubbling with 100% O_2. The solution was decanted through a mesh strainer and the tissue was transferred back to the chamber for collagenase digestion; 5750 units collagenase Type I (Worthington Biochemical, NJ, USA) and 9.6 mg protease XXIV (Sigma-Aldrich, MO, USA) were used per 20 mL Ca^{2+}-free solution and was stirred for 10 minutes. Ca^{2+} concentration was raised to 20 µM and was stirred for another 35 minutes. For the second digestion step, 20 mL collagenase solution without protease, supplemented with 20 µM $CaCl_2$ was used and was stirred for approximately 4 minutes until a single myocyte could be observed in a drop of solution under a light microscope (100x magnification). The digestion was then stopped by decanting and filtering the suspension, transferring the tissue chunks to a storage solution. To dissociate single atrial myocytes from the tissue chunks, the suspension was pipetted gently and repeatedly for 2-3 minutes, avoiding bubble formation. The suspension was filtered and the filtrate was centrifuged at 90 x g for 7 minutes. The supernatant was discarded and the atrial myocytes were resuspended in 1.5 mL of fresh storage solution. Ca^{2+} reintroduction was initiated with an initial addition of 7.5 µL of 10 mM $CaCl_2$ and was allowed to equilibrate for

8 minutes. This was followed by another 7.5 µL and a final addition of 15 µL. The cell suspension was viewed under a light microscope for the presence of rod-shaped atrial myocytes with clear striations. Atrial myocytes were kept in myocyte storage solution (**Table 3**) until further use.

Table 1. Cardioplegic solution

Component	Concentration (mM)	MW
5x Ca^{2+}-free stock solution	100 mL	
D-Glucose	20	180.16
2,3-Butanedione monoxime	30	101.1
ddH2O	To 500 mL	
pH 7.0 with 1 M NaOH		

Table 2. Ca^{2+}-free isolation solution

Component	mM	MW
KCl	10	74.56
NaCl	100	74.56
KH_2PO_4	1.2	58.44
$MgSO_4$ x 7·H_2O	5	136.09
Taurin	50	246.48
MOPS	5	125.2
D-Glucose	20	209.26
ddH_2O	To 500 mL	180.16
pH 7.0 with 1 M NaOH		

Table 3. Isolated myocyte storage solution

Component	Concentration (mM)	MW
KCl	20 mM	74.56
KH_2PO_4	10 mM	136.09
D-Glucose	10 mM	180.16
Taurin	10 mM	125.2
DL-β-Hydroxybutyric acid sodium salt	10 mM	126.09
Albumin	1%	
L-Glutamic acid	70 mM	147.13
pH 7.4 with 1 M KOH		

2.2.2 Human-derived induced pluripotent stem cell-derived atrial myocytes

Atrial human induced pluripotent stem cell-derived cardiac myocytes (hiPSC-CMs; Ethics Approval No.4/11/18) were generated according to an established protocol (Kleinsorge & Cyganek, 2020; Seibertz et al., 2020). Briefly, reprogrammed dermal fibroblasts from patients underwent mesodermal induction and cardiac induction by modulating the WNT signaling pathway using small molecules, CHIR99021 and IWP2. Atrial subtype initiation was achieved by retinoid acid treatment.

2.3 Patch-clamp experiments

2.3.1 Microscope and camera

All simultaneous patch-clamp and fluorescence recordings were done on an inverted fluorescence microscope (Olympus IX73, Olympus, Japan). For brightfield imaging, light emitting diodes (LEDs) were used (850 nm and white light via TwinLED, powered by OptoLED Lite, Cairn Research, UK). Myocytes were visualised through a monochrome industrial camera (DMK 72BUC02) via IC Capture software (Version 2.4, The Imaging Source, Germany). Myocytes were magnified with either 10x (UPlanSAPo) for ocular inspection or 40x (UApo/340) with Type-F immersion oil (Immoil-F30CC, all from Olympus, Japan) for recording.

2.3.2 Patch-clamp rig

Atrial myocytes were transferred by pipetting onto a bath perfusion chamber (RC-24E, Warner Instruments, USA), with a 22 x 22 mm coverslip sealed with glisseal N (Borer Chemie AG, Switzerland), mounted on a P1/PH1 platform, which is secured via a stage adaptor fit for an Olympus microscope (both from Warner Instruments, USA). Solutions were kept at 37°C.

A 1-HL-U pipette holder with chlorided silver wire was used on a CV 203BU headstage, connected to an Axopatch 200B amplifier. All acquired signals from the photon multiplier tubes (PMT) and the headstage were digitised via Digidata 1550B and visualised on Clampex 10.7 software (all from Axon Instruments, Molecular Devices, CA, USA). Digitised data were acquired at a sampling rate of 10 kHz.
Bath solution exchange was achieved using an 8-channel fast focal perfusion system (VM-8) controlled by valve control system and software (Octaflow II). To maintain the level of the bath chamber during perfusion, a vacuum pump system

(VWK) was connected to the chamber. The Quartz MicroManifold™ (ALA Scientific Instruments, NY, USA) was maintained at 37 °C via a temperature controller (TC-20-W1, NPI Electronic, Germany).

Pipettes were generated from 3" thin-wall borosilicate glass capillaries (TW150F-3, World Precision Instruments, FL, USA), pulled using a DMZ Universal electrode puller (Zeitz Instruments, Germany). Before pulling, glass capillaries were shortened with a glass cutter and then fire polished. Pipette resistances were between 2.5 and 4 MΩ. Series resistance and cell capacitance were compensated for in the voltage-clamp experiments but not for current clamp-experiments.

2.3.3 Fluorescence

LEDs were connected to a Dual OptoLED power supply and alternating LED excitation was done either by on automatic switching based on the program set on the Optoscan (autofluorescence recording) or via an external trigger from the digital output from Digidata 1550B (Ca^{2+} transient recording).

For the autofluorescence recordings (**Figure 6**): Using a set wavelength program on the OptoScan, myocytes were alternately excited with LEDs: 365 nm for NAD(P)H and 470 nm FAD^{+} with their respective clean up filters (365/10x and 500sp). The duration was 150 ms at each position, with a transition time of 100 µs. Emitted light passed through filters ET445/30x for NAD(P)H (435 nm) and ET535/70m for FAD^{+} (545 nm) before collection by PMTs. Emissions were collected every 4 seconds.

For the Ca^{2+} transient recordings (**Figure 8**): Using an external trigger from Clampex, myocytes were alternately excited with LEDs: 340 nm for cytosolic Ca^{2+} (Indo-1) and white light (WL) for mitochondrial Ca^{2+} (Rhod-2) with their respective clean up filters (340x and 545/25x). For the 0.5 Hz measurements, myocytes were illuminated for 2 seconds at each wavelength, followed by the same pulse protocol without illumination for 6 seconds. For the 3 Hz measurements, myocytes were illuminated for 2 seconds at each wavelength followed by the same pulse protocol without illumination for 16 seconds. Emissions passed through filters ET420/50m for Ca^{2+}-bound Indo-1 (405 nm), ET485/25m for Ca^{2+}-unbound Indo-1 (480 nm), and ET605/70m for Rhod-2 (605 nm), before collection by the PMTs. To visualise the cell via the camera, a 850 nm LED was used for brightfield illumination.

For the spontaneous Ca^{2+} event recordings (**Figure 11**): A monochromator (488 nm) generated light to excite the myocytes and the excitation light was filtered by a ET470/40x filter. Emissions passed through an emission filter ET535/50m before collection by the PMT. The excitation light was on for the entire duration of the measurements.

Table 4. Bath solution for patch clamp experiments

Component	Concentration (mM)	MW
NaCl	140	58.44
HEPES	10	238.30
Glucose	10	180.16
KCl	4	1 M stock
$MgCl_2$	1	1 M stock
$CaCl_2$	2	1 M stock
Probenecid	2	285.40
pH 7.34 with 1 M NaOH		

Table 5. Bath solution for Ca^{2+} sparks and current clamp experiments

Component	Concentration (mM)	MW
NaCl	140	58.44
HEPES	10	238.30
KCl	4	74.55
$MgCl_2$	1	1 M stock
Na-Pyruvate	2	110.04
Ascorbic acid	0.3	176.12
Glucose	10	180.16
$CaCl_2$	2	1 M stock
pH 7.34 with 1 M NaOH		

Table 6. Pipette solution for patch clamp experiments

Component	Concentration (mM)	MW
K-Glutamate	130	203.23
KCl	19	74.55
$MgCl_2$	0.5	203.3
Na-HEPES	5	260.29
Mg-ATP	5	507.2
HEPES	10	238.3
pH 7.2 with 1 M KOH		

2.4 NAD(P)H and FAD^+ autofluorescence recording

Cellular autofluorescence is predominantly attributed to reduced NAD(P)H and oxidised FAD (Abramov & Bartolomé, 2015; Blacker & Duchen, 2016; Kolenc & Quinn, 2019). FAD fluorescence predominantly comes from lipoamide dehydrogenases found in the E3 subunits of pyruvate dehydrogenase complex and αKGDH, and electron transfer flavoprotein (Kolenc & Quinn, 2019), with the contribution of Complex II regarded as negligible.

Myocytes were patched in a ruptured whole-cell configuration to simultaneously measure L-type Ca^{2+} currents with NAD(P)H and FAD autofluorescence signals. Here, the pulse protocol (**Figure 7A**) had a pulse to inactivate peak Na^+ currents and the bath solution had 4-AP and $BaCl_2$ to inhibit K^+ currents, thus isolating Ca^{2+} currents to be quantified. After a baseline measurement of autofluorescence at 0.5 Hz, atrial myocytes were subjected to a stress protocol by initially increasing stimulation frequency from 0.5 Hz to 3 Hz, and then additionally with β-adrenergic stimulation by 100 nM isoprenaline (ISO). ISO was washed out and signals were calibrated using 5 µM carbonyl cyanide-p-trifluoromethoxyphenylhydrazone (FCCP) and 4 mM sodium cynanide (Na-CN) to stimulate maximum oxidation and reduction, respectively (**Figure 7B**). Independent cell recordings for signal rundown was also performed, where only illumination and emission capture were applied. These were subtracted from the raw NAD(P)H and FAD^+ signals and ultimately used in the NAD(P)H/FAD^+ ratio calculations. The signals occur as mirror images of each other, and their ratio can minimize the influence of motion artifacts. On an independent set of myocytes, signal rundown experiments were performed, where only fluorescence excitation and emission were recorded. This was used for rundown subtraction and calculations of NAD(P)H and FAD^+ ratio (**Figure 7C**).

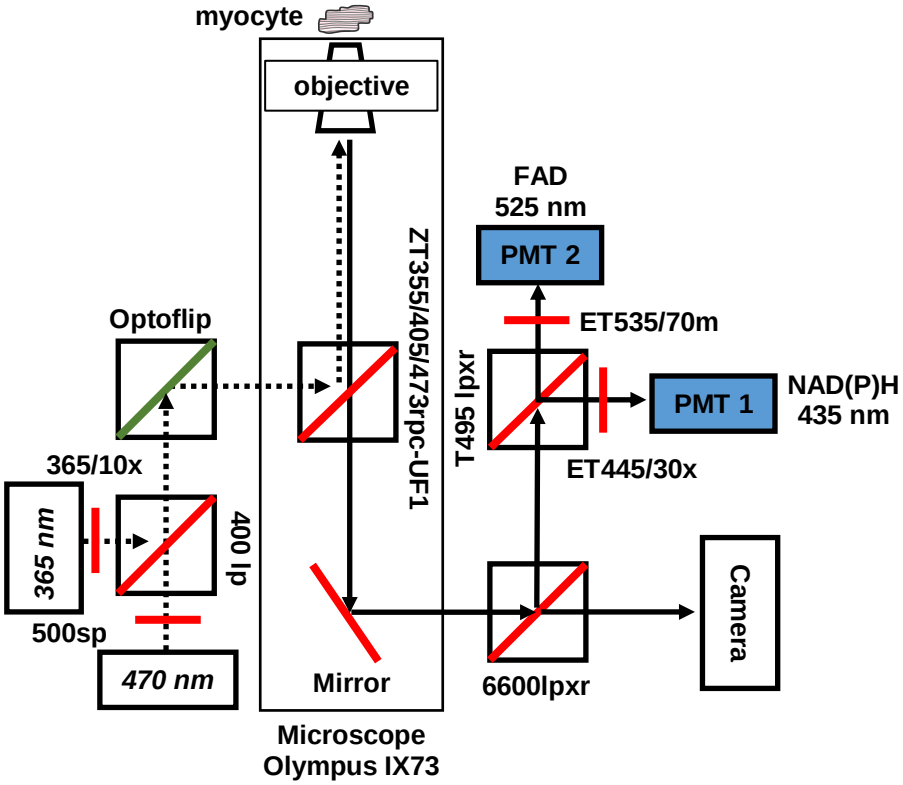

Figure 6. Optical filtering for autofluorescence recording. LEDs 365 nm and 470 nm were used to excite NAD(P)H and FAD^{+}, respectively. The excitation lights go through their respective clean-up filters before they reach the myocyte. The light emissions from the myocytes then go through beamsplitters that direct them to their respective emission filters and collect Ca^{2+}-bound Indo-1 at 405 nm, Ca^{2+}-unbound Indo-1 at 480 nm, and Rhod-2 at 605 nm.

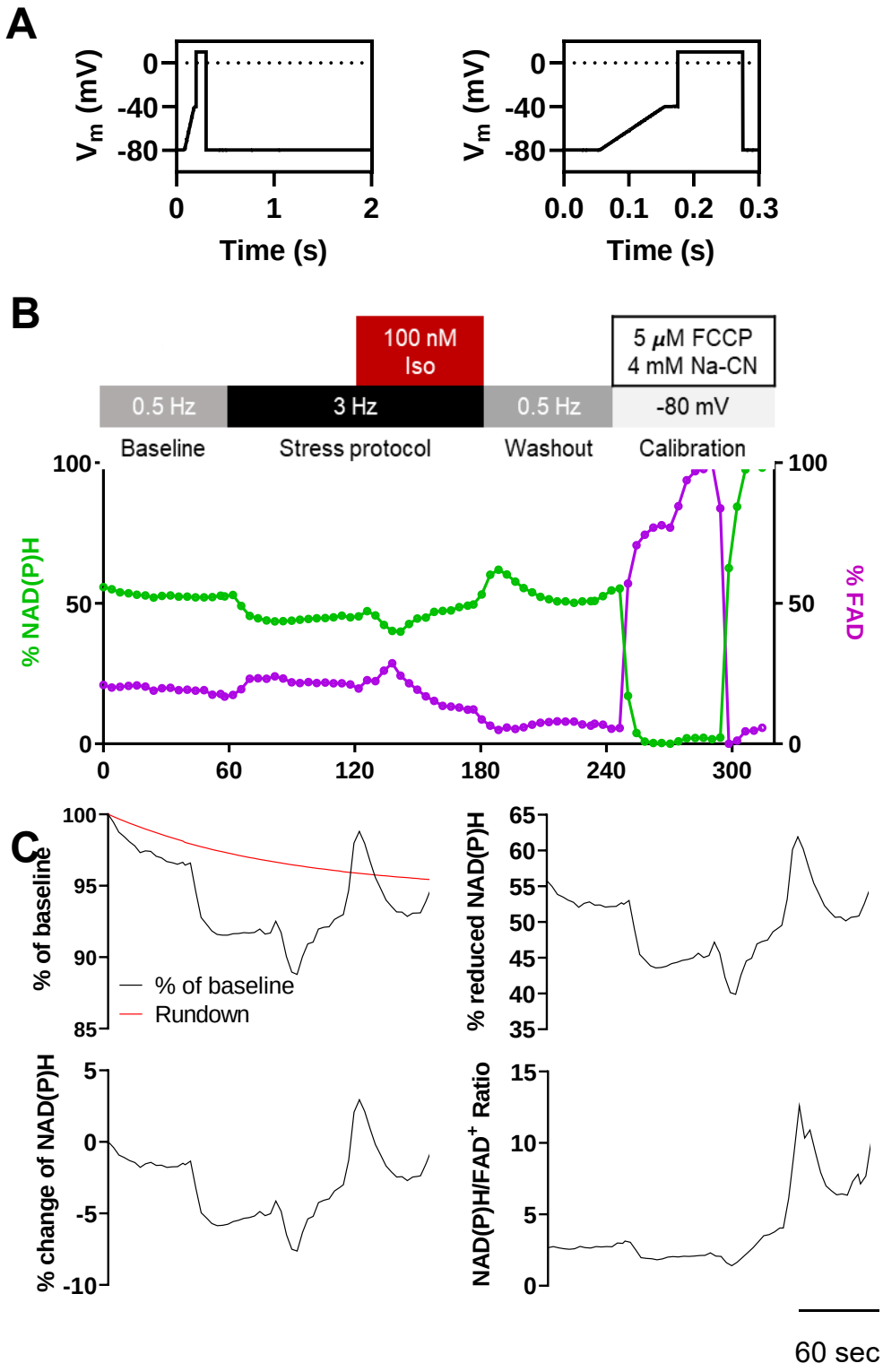

Figure 7. NAD(P)H and FAD^+ autofluorescence recording protocol and analysis. A, Diagrams of the pulse protocol for the 0.5 Hz (left) and 3 Hz (right) stimulation. **B,** (top) recording protocol showing stimulation and solution perfusion: with or without 100 nM isoprenaline (ISO) for the stress protocol, and FCCP followed by Na-CN for signal calibration. (bottom) Representative normalised % of reduced NAD(P)H and oxidised FAD signals**. C,** A rundown signal (red) was recorded on an independent set of cells per experiment day and then averaged. Fluorescence signals were corrected for rundown and % change of signal was used as basis for the calculation of NAD(P)H/FAD^+ ratio. FCCP=for maximum oxidation, Na-CN=for maximum reduction.

2.5 Mitochondrial and cytosolic transient recording

To label mitochondrial Ca^{2+}, atrial myocytes were incubated with 5 µM Rhod-2 AM for 1 hour at 37°C, followed by a 1 hour de-esterification step by replacing the staining medium with indicator-free medium. The positive charge of the indicator should facilitate the accumulation of the indicator in the electronegative mitochondrial matrix. The cytosolic Ca^{2+} indicator, a cell-impermeant variant of Indo-1 pentapotassium salt (75 uM, dissolved in dH_2O), was added to the internal solution, which will be introduced into the cell via a patch pipette. For the Ca^{2+} transient measurements, 4-AP and $BaCl_2$, as well as Na^+ channel inactivation by a ramp pulse were not applied. Myocytes were held at -80 mV, followed by a depolarising step to +10 mV for 100 ms. At 0.5 Hz, illumination was applied via an external trigger every 10 seconds at 0.5 Hz, and every 20 seconds at 3 Hz.

Cellular autofluorescence and Rhod-2 signal pre-dialysis were recorded prior to establishing a whole-cell configuration. Pipette solution with Indo-1 was transferred into borosilicate pipettes (**Figure 9A**). After rupture, a 6-minute dialysis of Indo-1 infused internal solution was done to minimise cytosolic traces of Rhod-2 (**Figure 9B and D**). During this protocol, only Indo-1 emissions were collected every 4 seconds. Rhod-2 baseline signal post-dialysis was also recorded as F_{load} (**Figure 9D**). During 0.5 Hz protocol (**Figure 9E,** left panel), alternating excitation with 340 and 540 nm was applied and emissions were collected every 10 seconds. During 3 Hz protocol (**Figure 9E**, right panel), the same principle was applied, but emissions were collected every 20 seconds. Illumination was on for 2 seconds at each position, followed by a non-illuminated stimulation protocol. Lastly, a washout step was done similar to the 0.5 Hz protocol.

Autofluorescence signals for F_{405} and F_{480} were subtracted to their respective fluorescence signals during the stimulation protocols. Reported cytosolic Ca^{2+} signals were a ratio of F_{405}/F_{480}. Rhod-2 signal was normalised to F_{load}.

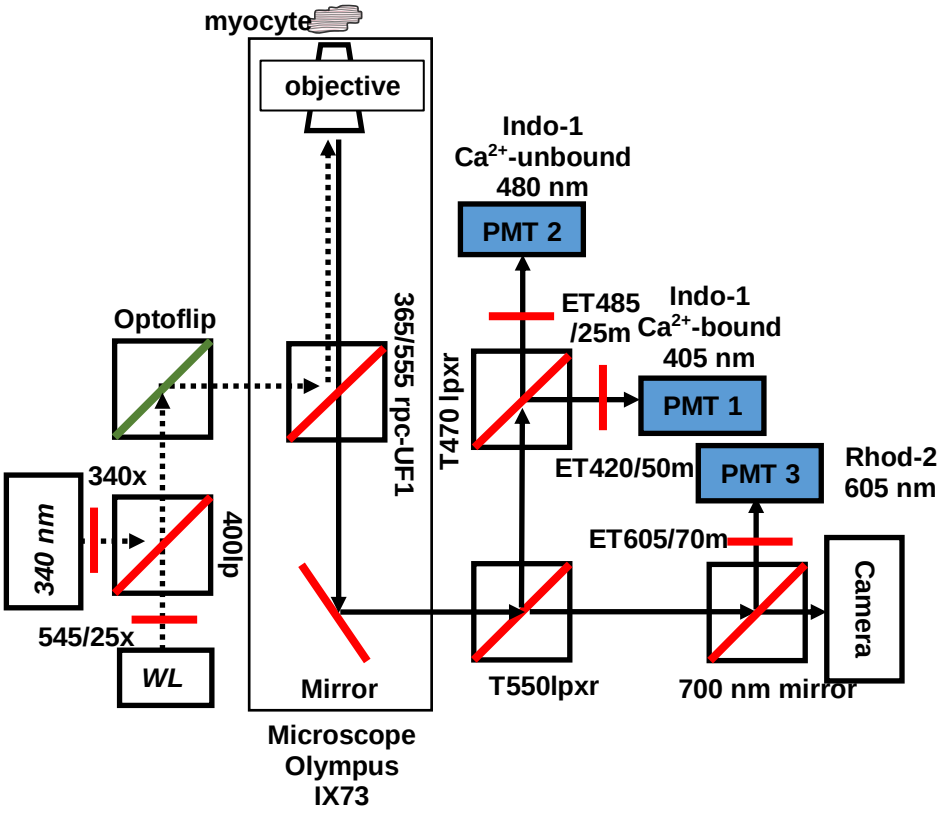

Figure 8. Optical filtering for Ca^{2+} transient recording. LEDs 340 nm and white light [WL]) were used to excite Indo-1 (cytosolic Ca^{2+}) and Rhod-2 (mitochondrial Ca^{2+}), respectively. The excitation lights go through their respective clean-up filters before they reach the myocyte. The light emissions from the myocytes then go through beamsplitters that direct them to their respective emission filters and collect Ca^{2+}-bound Indo-1 at 405 nm, Ca^{2+}-unbound Indo-1 at 480 nm, and Rhod-2 at 605 nm.

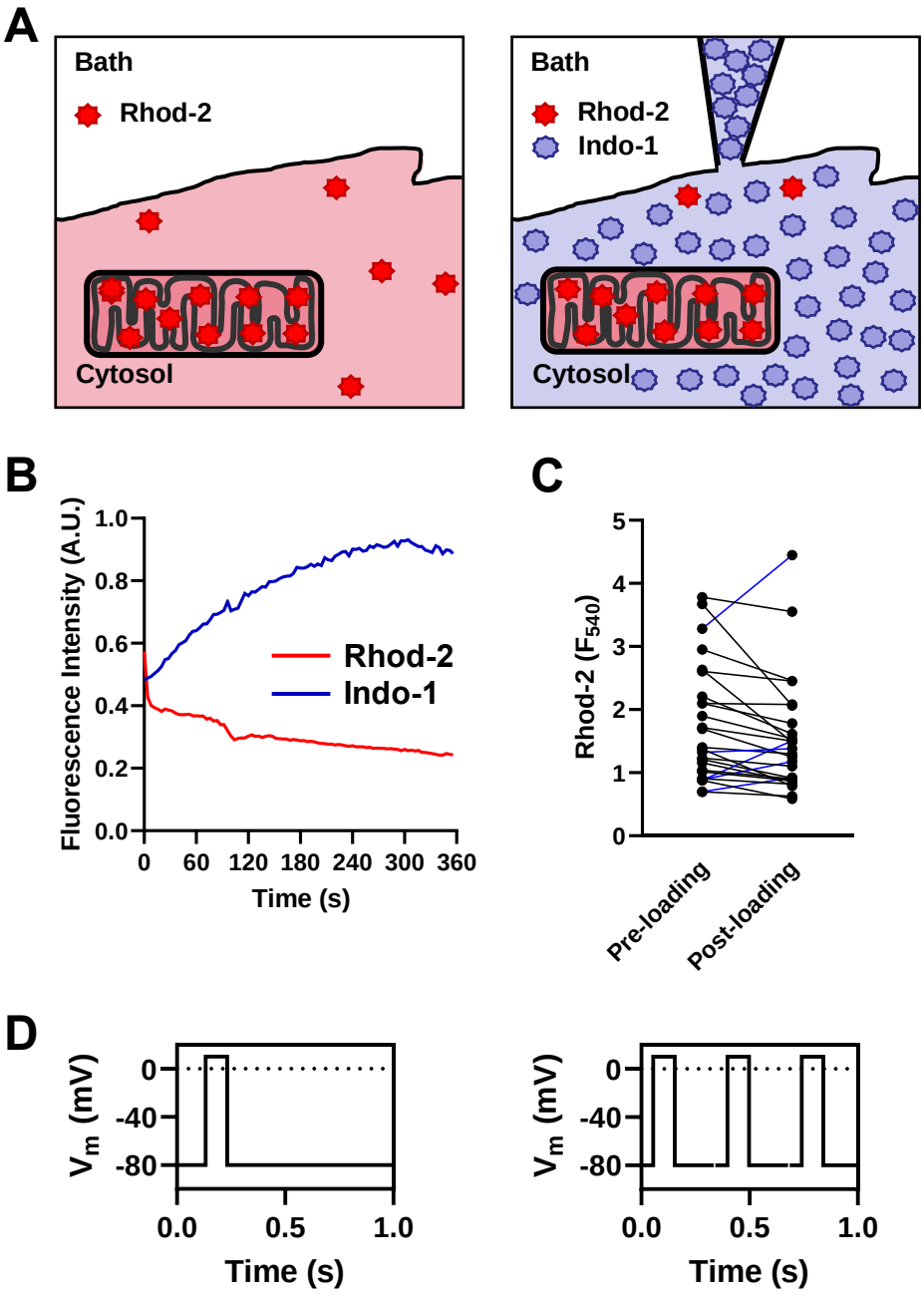

Figure 9. Mitochondrial and cytosolic Ca^{2+} labelling and transient recording protocol. **A,** Cartoon of compartment-specific Ca^{2+} indicator labelling. Myocytes were initially loaded with 5 µM Rhod-2 (left), and removal of its cytosolic remnants was done by pipette-loading of a membrane-impermeable Indo-1 pentapotassium salt (right). **B,** The pipette solution was allowed to dialyse the into the cytosol for 6 minutes, with pulses of +10 mV and simultaneous Indo-1 excitation and emission collection every 4 seconds, which increased Indo-1 fluorescence overtime. **C,** Conversely, Rhod-2 baseline fluorescence before and after pipette loading showed decreased fluorescence after 6 minutes of dialysis. Note that some cells showed increase fluorescence and must be excluded. **D,** Pulse protocols for the cell stimulation at 0.5 Hz (left) and 3 Hz (right).

2.6 Imaging of human atrial tissue sections

2.6.1 Immunohistochemistry of paraffin sections of human atrial tissue

RAAs were transferred from the transport solution to 4% PFA for 24-48 hours. Depending on fixation time, tissues were soaked in water for 3-4 hours and were then embedded on paraffin with an automated embedding machine (Leica Biosystems, Germany) with the following steps: 50% ethanol (EtOH), 70%, 80%, 2x 96%, 2x 100%, 2x chloroform and 3x paraffin. Hot paraffin (60°C) was poured into standard blocks with the tissue, and was allowed to cool down to 20°C on a cooling plate (Leica Biosystems, Germany). Tissue sections of 1 µm to 0.5 µm thickness were done with a S35 blade mounted to a sliding microtome (Leica SM 2000R, Leica Biosystems, Germany). Sections were then transferred onto cold water and then allowed to expand on 45°C water before mounting onto glass slides.

After preparing the slides, the slides were subjected to a deparaffinisation step with xylol (3x, 5 minutes) and rehydration step (100% EtOH 2x, 96%, 70%, 50%, 30% and deionised water, 5 minutes each step). An antigen retrieval step was performed using citrate buffer (pH 9) for 20 minutes at 90°C and the slides were transferred to a staining jar with TBST buffer followed by as washing step with TBST buffer (4x for 5 minutes). The surrounding of the tissue section was dried and an oval perimeter around the tissue was drawn using a hydrophobic pen. The sections were blocked with TBS+ buffer in a damp chamber for 1 hour at room temperature and then washed. Primary antibodies were diluted with FB1 buffer, vortexed and spun down. The antibody solution was then pipetted onto the slides and were incubated overnight at 4°C. The slides were washed and the secondary antibody solution was prepared. The secondary antibody was incubated on the slides for 2 hours at room temperature in the dark. The succeeding washing step was also done in the dark. After drying the surroundings of the tissue sections, a drop of Mowiol was carefully pipetted onto #1.5 cover slips (160-190 µm), and the slides were carefully placed against the coverslips with the section side facing down. The slides were secured with a nail polish the following day and were kept at 4°C in the dark until STED microscopy.

VDAC1 antibody was validated using: 1) independent antibody strategy (**Figure 10A and B**), where antibodies with non-overlapping epitopes were used; and 2) immunoblotting (**Figure 10**C) (Edfors et al., 2018).

Table 7. Antibodies used for immunostaining

Primary Antibody	Host	Catalogue Number	Company	Dilution
VDAC1	anti-mouse	75-204	NeuroMab	1:2000
	anti-rabbit	LS-C312926	LSBio	1:500
RyR2	anti-rabbit	HPA009975	Sigma	1:2000
Secondary Antibody				
IRDye 800CW	anti-rabbit	926-32213	Li-Cor	1:10000
IRDye 800CW	anti-goat	926-32214	Li-Cor	1:10000

Table 8. Solutions used for immunostaining.

TRIS-buffered saline (TBS)	
Reagent	**Amount**
TRIS	121.14 g
NaCl	3175.32 g
Deionised H_2O	Up to 2 L
pH 7.6	
TBST (Washing buffer)	
Reagent	**Amount**
TBS	10 ml
Tween®20	500 µL
Deionised H_2O	Up to 1 L
TBS+ (Blocking solution)	
Reagent	**Amount**
TritonX-100	100 µL
TBS	38 mL
Goat serum	2 mL
FB1 (Antibody diluent)	
Reagent	**Amount**
PBS	50 mL
Bovine serum albumin	1%
Mowiol (Mounting media)	
Reagent	**Amount**
Mowiol	20 g
0.2 M Tris buffer, pH 8.0	80 mL
Glycerol	40 mL

2.6.2 Stimulated Emission Depletion (STED) microscopy

Leica TCS SP8 system with a HC PL APO C2S 100x/1.40 oil objective was used for dual-color STED imaging. Type-F immersion liquid (all from Leica Microsystems, Germany) was used during experiments. Using the Leica Application Software (LAS-X), the following parameters were assigned: pixel size 16.23 x 16.23 nm, 1024 x 1024 pixel image, 200 Hz sampling rate, 32x line averaging. Regions to be imaged were selected using the transmitted light differential interference contrast (TL-DIC) setting of the microscope. Once a region was selected, a zoom factor was set to 7 and the imaging was initiated. A sequential line scanning mode was chosen to alternately scan confocal and STED images of RyR2 and VDAC1. STAR 580 (VDAC1) was excited at 580 nm and emissions were collected at 600-630 nm and

STAR 635P (RyR2) was excited at 635 nm and emissions were collected at 650-700 nm. Depletion of both fluorophores was achieved via a 775 nm laser beam. STED images were acquired at 200 Hz. Raw images were processed in Fiji (https://imagej.net/Fiji).

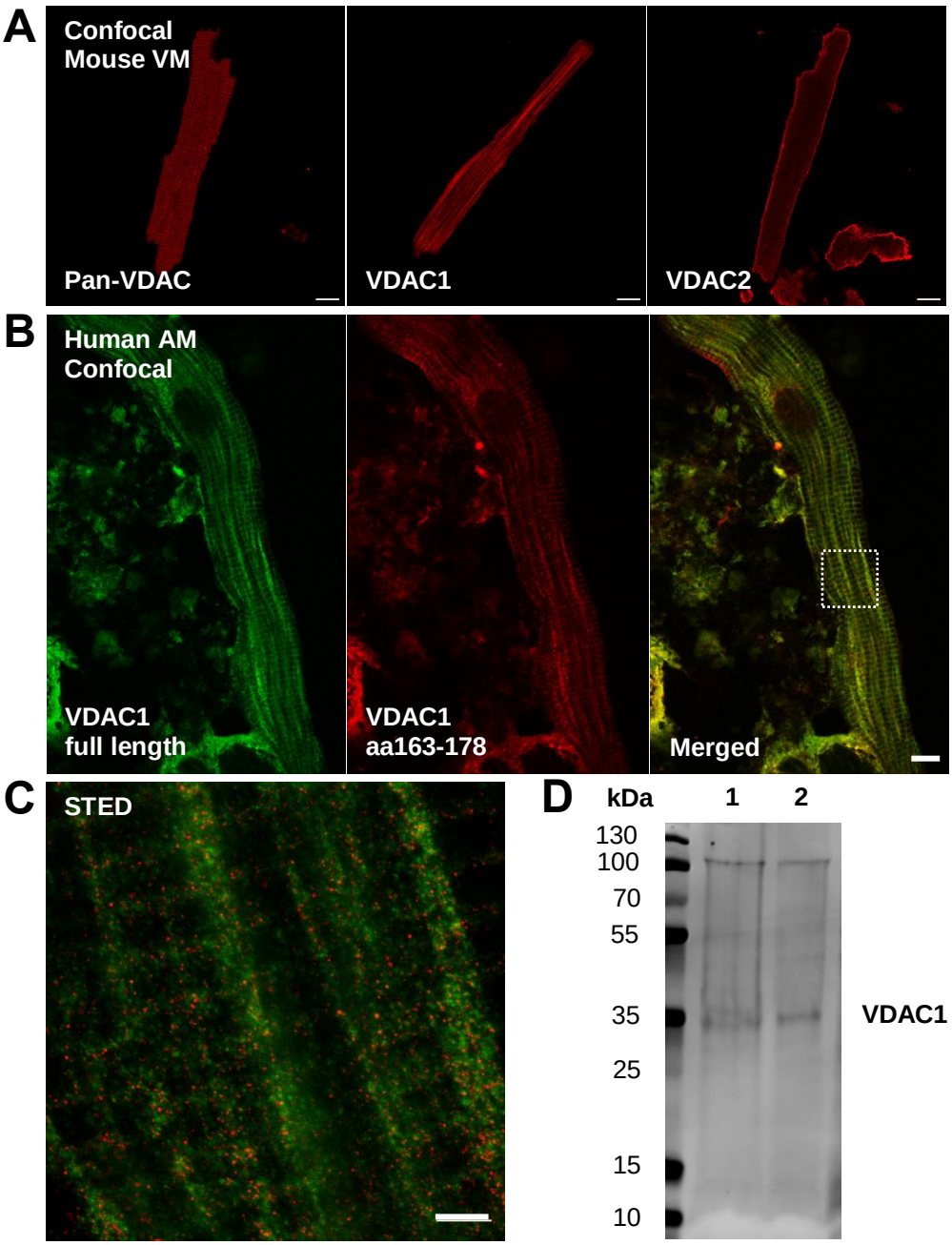

Figure 10. Validation of VDAC1 as mitochondrial marker. A, Initial screening of primary antibodies for VDAC on mouse ventricular myocytes (Mouse VM) staining for Pan-VDAC (Abcam ab15895), VDAC1 (NeuroMab 75-028), and VDAC1+VDAC3 (Abcam ab14734). Scale bar=10µm. Neuromab VDAC1 was further validated by independent antibody strategy using VDAC1 recognising aa163-178 (LSBio LS-C312926), which showed similar staining pattern with NeuroMab VDAC1 with B, confocal (scale bar=2 µm) and C, STED imaging (scale bar=200 nm) D. Immunoblotting, where the band was detected around its expected MW (30 kDa).

2.6.3 Spatial analysis with colocalization

MATLAB (MathWorks, US) was used for colocalisation and statistical analysis. TIFF images were opened in MATLAB. RyR2 spots were designated as reference particles, with which the degree of aggregation of VDAC1 spots within an assigned radius was measured. ROI was assigned arbitrarily avoiding perinuclear regions. Thresholding was performed by spot erosion and dilation. Centroids of each spot were extrapolated and used for distance measurements. The analysis program generates a line scan profile from the averaged spots. Signal was normalized to baseline (points 8 to 16) and a two-way ANOVA was performed on the first 10 points.

2.7 Electron tomography and 3D segmentation

Atrial appendages were immediately transferred to vials with Karnovsky Fixative (Solmedia, UK) and sent to the laboratory of Dr. Eva Rog-Zielinska in University Hospital Freiburg, who performed the electron tomography in EMBL Heidelberg.

2.8 Spontaneous Ca^{2+} release events and Ca^{2+} sparks recording

Spontaneous Ca^{2+} release events were detected using current-clamp in ruptured whole-cell configuration. Myocytes were incubated with Fluo-3 AM (10 µM) for 10 minutes at room temperature, followed by a de-esterification step with indicator-free bath solution for 30 minutes. Myocytes were treated either with 1 µM ezetimibe in EtOH or EtOH alone for 30 minutes. Fluo-3-loaded myocytes were then stimulated at 0.5 Hz and the generation of an action potential was observed by 1 nA increments of 1 ms-long current pulses. If the resting membrane potential is too positive, a hyperpolarising current was applied. APs were recorded at 1.2-1.5x the current pulse where an AP was initially observed. No series resistance compensation was applied. After 1 minute of 0.5 Hz stimulation, a follow-up of 1 minute observation at resting membrane potential. To calibrate the fluorescence signal, maximum and minimum signals were obtained by killing the cell and dragging the cell out of the field of view, respectively. These signals were used to convert fluorescence to Ca^{2+} concentration based on the in vivo k_d of Fluo-3 at 37˚C (864 nM). To count the SCaEs, the Ca^{2+}-converted traces were transferred onto Labchart, where positive deflections during the non-stimulated recording protocol were counted manually. After which, the susceptibility of the myocytes, SCaE frequency, amplitude, and latency of first event could be quantified.

For the Ca^{2+} sparks experiments, atrial human induced pluripotent stem cell-derived cardiac myocytes (hiPSC-CMs) were used because Ca^{2+} sparks recording is achieved by line scanning with confocal microscopy. Atrial hiPSC-CMs were stained with Ca^{2+} indicator Fluo-4 AM (10 µM) at room temperature for 15 minutes, followed by a 15 minute de-esterification step. Cells were treated either with 1 µM ezetimibe in DMSO or DMSO alone for 30 minutes. Line scans were generated using a confocal microscope (LSM 5 Pascal, Carl Zeiss, Germany) at 40x magnification with oil immersion. Using the Zen 2009 acquisition software, the following parameters were assigned: 512 pixels, 37.5 µm, 1302 Hz, 10,000 cycles, pinhole 67 µm. For the sparks recording, cells were preconditioned by field stimulation (MyoPacer, IonOptix, MA, USA) at 2 Hz for 2 minutes. Avoiding the nucleus, a line was drawn across the cell and the line scan was initiated. All experiments were maintained at 37°C (TC-20, NPI, Germany). All solutions used for both experiments were summarised in **Table 5**.

Analysis was done using ImageJ with the SparkMaster plugin and then quantification of spark parameters were done on Microsoft Excel.

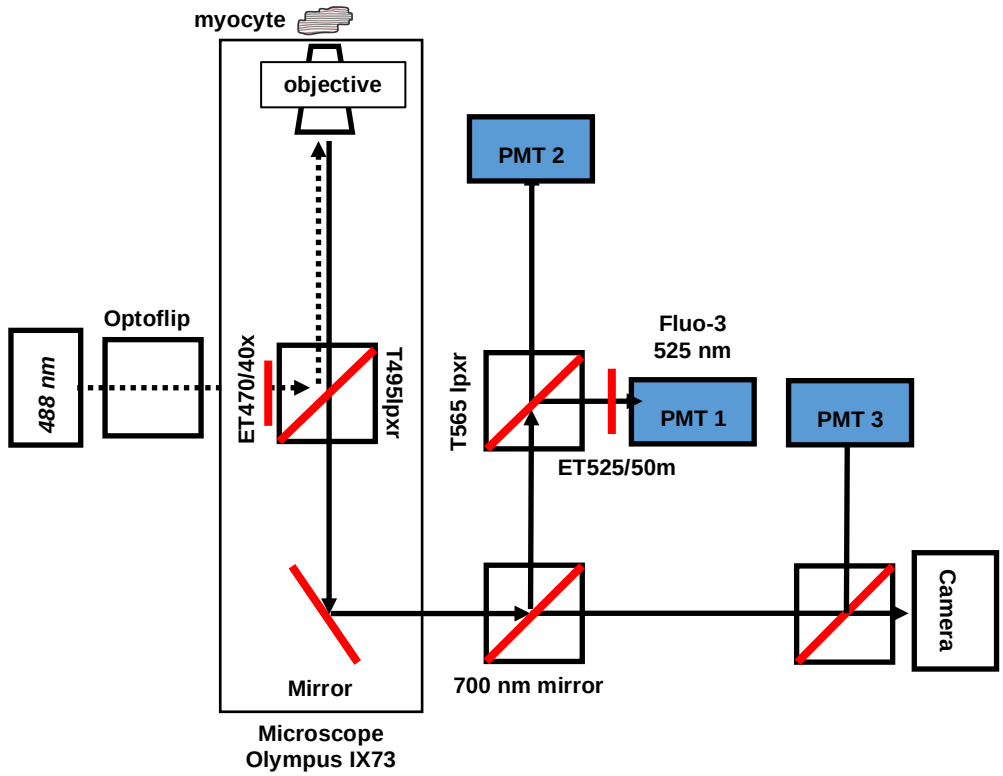

Figure 11. Optical filtering for recording spontaneous Ca^{2+}-release events. Using a monochromator, myocytes were excited at 488 nm. The excitation light goes through a clean-up filter (ET470/40x) before it reaches the myocyte. The light emission from the myocyte then go through beamsplitters that direct it to the appropriate emission filter. Emissions of 525 nm were collected by a PMT.

2.9 COX-SDH staining

Cryosections of frozen RAAs (7 µm) were produced with Leica CM3050 S cryostat, and then mounted on microscope glass slides using Tissue-Tek® O.C.T. Compound (Sakura Finetek, USA), and frozen at -80°C. After unfreezing, the dried Tissue-Tek® was cut away from the tissue with a scalpel.

Sections were incubated with 60 µL of cytochrome *c* Oxidase (COX) stain at 37°C for 30 minutes, followed by the addition of 60 µL of succinate dehydrogenase (SDH) stain and was incubated at 37°C for another 80-90 minutes. Once dried, coverlslips were mounted with a drop of 60°C glycerine gelatine and left overnight. 3,3'-diaminobenzadine acts as an electron donor to COX, which results in a brown indamine polymer product localising in mitochondrial cristae when oxidised. With dysfunctional COX, the nitroblue tetrazolium in the SDH stain acts as an electron acceptor from sodium succinate, resulting in a blue formazan product forming with mitochondrial proliferation. All solutions used are summarized in **Table 9**.

Tissue sections were imaged with ZEISS ApoTome Axio Imager Z1m microscope with immersion oil at 40X magnification. Colour images were taken with the AxioCam MR3 microscope camera. Blue-tinted cardiomyocytes were counted manually in whole slides. Images were processed using AxioVision 4.6.3 SP1, ZEN Blue 3.3.89.0000 and Fiji ImageJ 1.53c.

Table 9. Solutions for COX-SDH staining.

10x PBS Buffer	
Reagent	**Amount**
NaCl	80 g
KCl	2 g
Na_2HPO_4	14.4 g
KH_2PO_4	2.4 g
dH_2O	up to 1 L
Cytochrome *C* oxidase (COX) staining solution	
Reagent	**Amount**
50 mM Na-phosphate buffer, pH 7.4	10 ml
20 mg/ml Catalase	2 µl
Diaminobenzidine	10 mg
Cytochrome *C*	20 mg
Saccharose	750 mg
stored in aliquots at -20°C	
Succinate dehydrogenase (SHD) staining solution	
Reagent	**Amount**
50 mM Tris-HCl, pH 7.4	5 ml
0.2 M Na-succinate	5 ml / 0.2701g
50 mM $MgCl_2$ x $6H_20$	1 ml
40 mg Nitroblue tetrazolium	dissolved in 9 ml dH20
stored in aliquots at -20°C	

2.10 Protein biochemistry

2.10.1 Total protein isolation and quantification

LN_2-frozen RAAs were pulverized in a mortar submerged in LN_2, and were homogenised in Kranias buffer using a dispersing instrument (ULTRA-TURRAX®, IKA, Germany). Homogenates were centrifuged at 900 x *g* for 15 minutes at room temperature. Supernatant was transferred to new tubes. Homogenates were diluted (1:20) in water and kept at -20°C until use.

Protein quantification with bicinchoninic acid (BCA) protein assay (Pierce™ BCA Protein Assay Kit, ThermoScientific, MA, USA) was done according to manufacturer protocol.

2.10.2 Protein detection and visualisation

35-50 µg of protein lysate with Lämmli buffer was loaded onto 10% Mini-PROTEAN® TGX Precast Protein Gels (Bio-Rad, CA, USA) and was resolved by electrophoresis for 65 minutes at 120 V. Protein transfer onto nitrocellulose membranes was done with the Trans-Blot Turbo System for 7 minutes, and then stained with Revert™ Total Protein Stain (LI-COR Biosciences, NE, USA) for 65 minutes and then washed. Fluorescence was detected at 700 nm with a fluorescent scanner (Azure Sapphire, Azure Biosystems, CA, USA). Membranes were blocked with Roti-Block (Carl Roth) for 1 hour at room temperature, followed by primary body incubation at 4°C, overnight. All antibodies are summaries in **Table 11**. Membranes were washed with 0.1% TBST and then incubated with secondary antibody incubation for 90 minutes at room temperature. Membranes were washed and bands were visualised using Azure Sapphire. All solutions used are summarised in **Table 10**.

Table 10. Solutions used for protein biochemistry.

Kranias buffer	
Component	**Concentration**
0.5 M EDTA Solution, pH 8.0	5 mM
Glycerol 99%	10%
NaF / Natriumfluorid (41,99g/mol)	30 mM
SDS	3%
Tris (121,14 g/mol)	30 mM
Lämmli buffer	
Component	**Concentration**
Glycerol 99%	109 mM
SDS / Roti-Stock 20%	2%
Tris	10 mM
Dithiothreitol	60.3 mM
Bromphenol blue	0.17 mM
TBST	
Component	**Concentration**
Tris	10 mM
NaCl	0.17mM
Tween®20	0.01%
Running buffer	
Component	**Concentration**
Tris	25mM
Glycine	192 mM
SDS / Roti-Stock 20%	0.10%

Table 11. Antibodies used for protein biochemistry

Primary Antibody	**Host**	**Catalogue Number**	**Company**	**Dilution**
Mitofusin 2	anti-rabbit	ab56889	Abcam	1:2000
GRP75	anti-rabbit	HPA009975	Sigma	1:2000
VAPB	anti-rabbit	HPA013144	Sigma	1:10000
COX4	anti-mouse	ab15744	Abcam	1:5000
TGM2	anti-rabbit	HPA029518	Sigma	1:3000
TUBB2A	anti-mouse	PAB0379	Abnova	1:1000
HSPA9	anti-rabbit	HPA000898	Sigma	1:2000
VDAC1	anti-rabbit	LS-C312926	LSBio	1:2000
VDAC2	anti-goat	ab37985	Abcam	1:2500
MICU1	anti-rabbit	HPA037480	Sigma	1:1000
MCU	anti-rabbit	HPA016480	Sigma	1:500
Fis1	anti-rabbit	HPA017430	Sigma	1:1000
MCUB	anti-rabbit	HPA048776	Sigma	1:300
MICU2	anti-rabbit	ab101465	Abcam	1:1000
PDP1	anti-rabbit	HPA021152	Sigma	1:5000
PDK4	anti-rabbit	12949-1-AP	Proteintech	1:1000
Secondary Antibody				
IRDye 800CW	anti-rabbit	926-32213	Li-Cor	1:10000
IRDye 800CW	anti-goat	926-32214	Li-Cor	1:10000
AzureSpectra 550	anti-mouse	512159	Azure Biosystems	1:2500

2.11 Statistical analysis

All statistical analyses were performed with GraphPad Prism (Version 9, GraphPad Software, UK), unless otherwise stated. Prior to further statistical testing, Shapiro-Wilk test was performed to test for normal distribution. If normally distributed, CTL and AF were compared with an unpaired t-test with Welch's correction. Otherwise, a Mann-Whitney test was performed. Responses to different stimulation conditions (0.5 Hz vs. 3 Hz vs. 3 Hz + ISO) or response to Ezetimibe (CTL vs. AF vs. AF + Eze) were compared with two-way ANOVA with Bonferroni correction. Data are presented as mean±SEM. *p*-values of <0.5 were considered significant. Non-continuous patient characteristics were presented as mean±SD. All non-continuous data comparisons were done with Fisher's exact test. All graphs and statistical analyses were performed on Prism, unless otherwise stated.

3 Results

3.1 Patient characteristics

Table 12. Cumulative table showing patient characteristcs of the samples used in the project.

	CTL	AF
Patients, n	86	39
Gender, m/f	75/11	30/9
Age, y	64.41±10.11	69.64±7.67**
Body mass index, kg/m^2	28.73±4.85	28.81±4.99
CAD, n	62	22
MVD/AVD, n	14	12
CAD+MVD/AVD, n	11	5
Hypertension, n	75	31
Diabetes, n	24	16
Hyperlipidemia, n	43	22
LVEF, %	50.75±14.72	45.57±14.21
LAD, mm	41.11±6.98	45.91±6.20***
Digitalis, n	0	4
ACE inhibitors, n	39	20
AT1 blockers, n	24	16
β-Blockers, n	55	34##
Calcium, n	20	13
Diuretics, n	29	23#
Nitrates, n	4	7
Lipid-lowering drugs, n	69	28

ACE, angiotensin-converting enzyme; AT, angiotensin receptor; CAD, coronary artery disease; ECC, extracorporeal circulation; LAD, left atrial diameter; LVEF, left ventricular ejection fraction; MVD/AVD, mitral/aortic valve disease. Continuous data are expressed as mean±SD. **P<0.01, ***P<0.005 vs CTL. #P<0.05, ##p<0.01 vs CTL with Fisher's exact test. n=number of patients.

3.2 Redox response of human atrial myocytes to workload transitions

Cellular autofluorescence is a non-invasive method of estimating metabolic state (Abramov & Bartolomé, 2015; Blacker & Duchen, 2016; Kolenc & Quinn, 2019) and has been applied in cardiac cells (Eng et al., 1989; T. Liu & Rourke, 2008; Maack, 2016; Maack et al., 2006), trabecular muscle (Brandes & Bers, 1996, 1997, 2002), and whole-heart preparations (Heineman & Balaban, 1993; Nuutinen, 1984). Among these autofluorescent entities are reduced nicotinamide adenine dinucleotide (NADH, **Figure 12A**) and oxidised flavin adenine dinucleotide (FAD^+) (Chance et al., 1962, 1979). The autofluorescence of pyridine and flavin nucleotides can be isolated by optical filtering. Another autofluorescent molecule is the reduced and phosphorylated form of NAD^+, NADPH. However, NADH and NADPH spectral properties are the same (Blacker & Duchen, 2016), therefore, the emission at 435 nm was notated as NAD(P)H.

To assess the Ca^{2+}-dependent activation of metabolism, a stress protocol was applied to promote Ca^{2+} accumulation. The averaged traces of NAD(P)H/FAD^+ ratio can give us an idea of the redox response of atrial myocytes during workload transitions (**Figure 12B**). Myocytes initially start with similar redox indices (% NAD(P)H, CTL 54.33±2.54, n/N=28myocytes/13 patients vs AF 59.09±3.18, n/N=25 myocytes/4 patients, **Figure 12C**) but during increased workload conditions, redox state tends towards being reduced in AF myocytes compared to CTL. Statistical analysis showed, however, that redox indices at all conditions, were not significantly different between CTL and AF. The redox index during reversion to 0.5 Hz also exhibited similar behaviour in CTL and AF. Interestingly, AF myocytes showed a delayed onset of electron donor regeneration during 3 Hz and β-adrenergic stimulation (ms, CTL 21.33.33±1.96, n/N=21 myocytes/ 13 patients vs AF 30.61±3.74, n/N=23 myocytes/4 patients, p=0.035, **Figure 12E-F**), although the tau values of recovery were comparable (tau, CTL 87.66±8.63 ms vs AF 33.10±28.68 ms; **Figure 12G**). The negative tau values represent cells that exhibited continued oxidation of NAD(P)H and $FADH_2$. Indeed, while all CTL myocytes regenerated reducing equivalents of the electron donors, a fraction of AF myocytes failed to do so during the 1 minute observation period (% of myocytes, CTL 0% vs AF 26%, p<0.001, **Figure 12H**). Furthermore, while NAD(P)H and NADH share similar spectral properties, rendering their fluorescent signals indistinguishable (Blacker &

Duchen, 2016), we can estimate the NADH pool using blockers targeting oxidative phosphorylation, such as the mitochondrial uncoupler FCCP and Complex IV inhibitor Na-cyanide. We can see that after calibration, the estimated NADH pool was similar between CTL and AF (ΔmV, CTL 0.93±0.09 vs AF 0.97±0.08, **Figure 12D**). Therefore, this difference in redox response may be attributed to other mechanisms besides substrate availability.

Regeneration of NADH and $FADH_2$ is more efficient when Ca^{2+} influx is mediated by SERCA, as compared to Ca^{2+} entry via reverse mode of NCX (Kohlhaas & Maack, 2010). To test this, 100 nM ISO with 0.5 Hz stimulation was applied for 1 minute. To promote SR Ca^{2+} release, a 10 mM caffeine pulse was applied, followed by continuous 0.5 Hz stimulation of myocytes (**Figure 13A**). NAD(P)H/FAD^+ ratio was similar in CTL and AF in response to this intervention (CTL 6.76±3.01, n/N=18 myocytes/9 patients vs AF 7.79±2.93, n/N=18 myocytes/9 patients, **Figure 13B and C**).

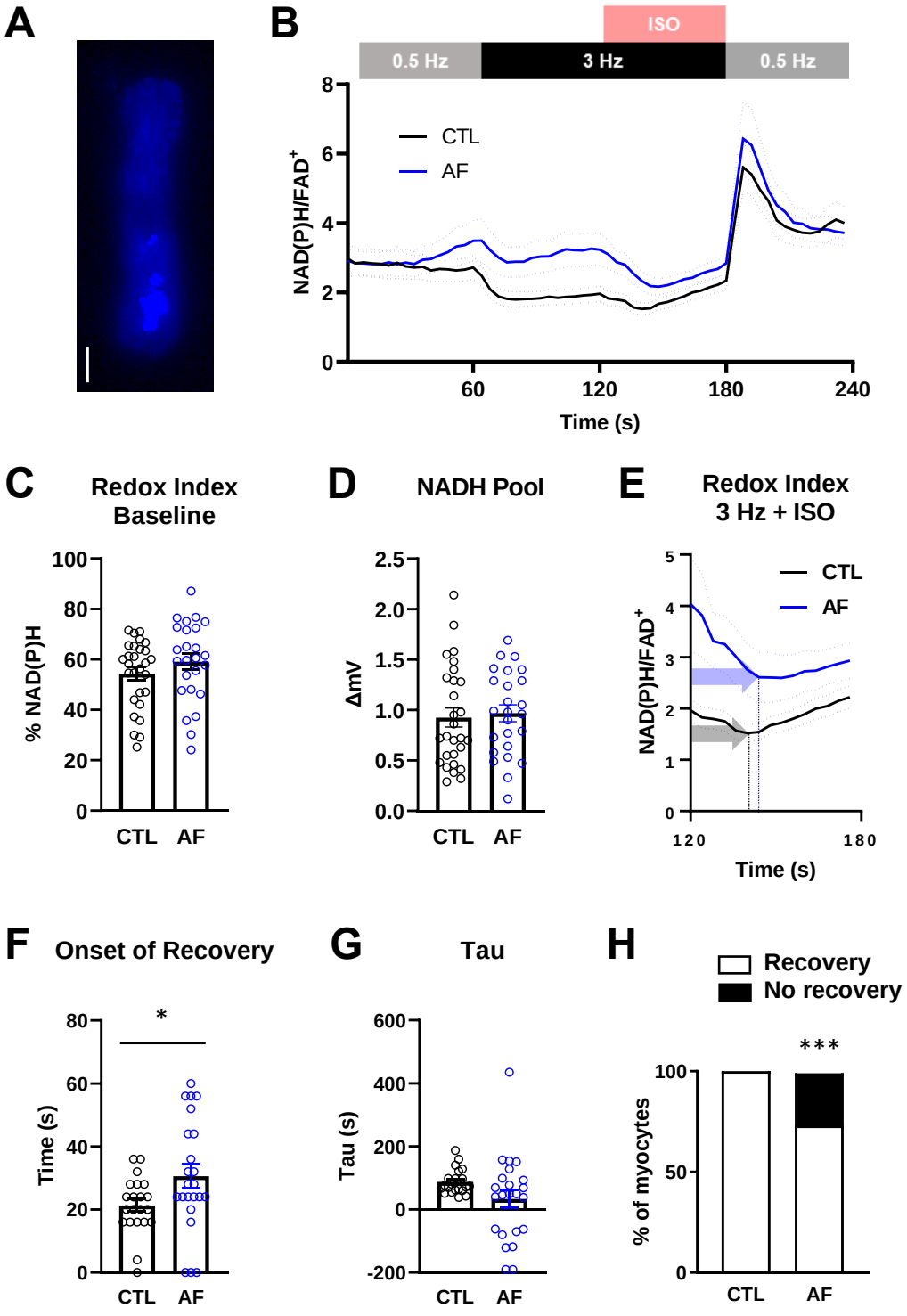

Figure 12. Autofluorescence of NAD(P)H and FAD^+ as an estimate of cellular redox index in atrial myocytes from CTL and AF patients. A, fluorescence image of NAD(P)H autofluorescence obtained using Keyence BZ-X800E (ex 360/40 nm, em 460/50 nm). Scale bar=10 µm. **B,** Averaged traces of NAD(P)H/FAD^+ ratio during workload transitions in CTL (black, n/N=21-28myocytes/13 patients) and AF (blue, n/N=23-25 myocytes/4 patients) myocytes. The following graphs depict mean±SEM of **C,** baseline NAD(P)H redox index; **D,** estimated NADH pool after calibration of NAD(P)H signal with FCCP and Na-CN; **E,** segment of redox index at 3 Hz+100 nM ISO from A, with arrows and dotted lines showing the time before onset of recovery of redox index; **F,** time before onset of recovery of redox index; **G,** rate of recovery quantified as tau of single exponential growth curve; and **H,** % of myocytes with continued oxidation of redox index. *p<0.05 vs CTL with Welch's test. ***p<0.0001 vs. CTL with Fisher's test. Ex=excitation; Em=emission.

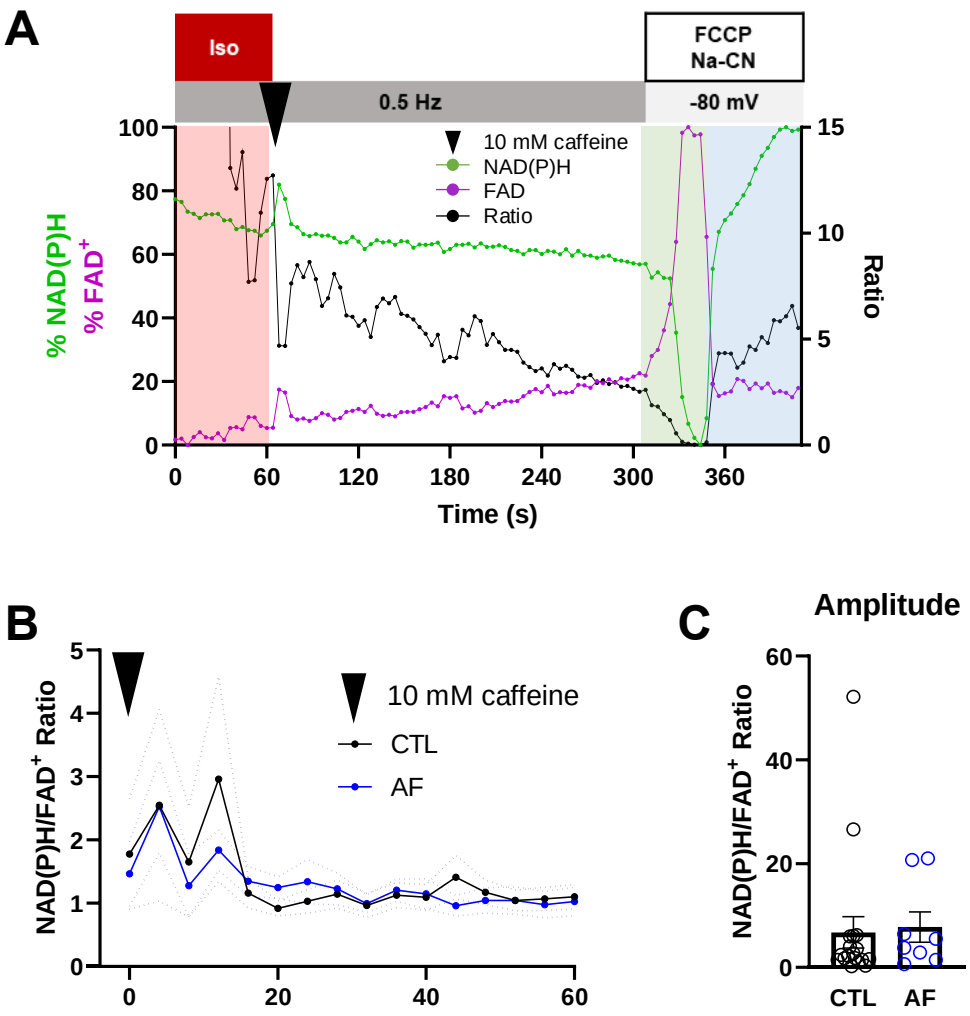

Figure 13. Efficiency of sarcoplasmic reticulum-dependent cytosolic Ca^{2+} increase by caffeine on NADH and FADH2 recovery in atrial myocytes from CTL and AF patients. **A,** Recording protocol where myocytes were stimulated at 0.5 Hz with 100 nM ISO for 1 minute, followed by a pulse of 10 mM caffeine and reversal to 0.5 Hz stimulation for 4 minutes. Same calibration protocol as in Figure 11 was applied. **B,** Averaged traces of the first 60 seconds of $NAD(P)H/FAD^+$ ratio after caffeine pulse in CTL (black, n/N=18 myocytes/9 patiens) and AF (blue, n/N=8 myocytes/4 patients) myocytes. **C,** Mean±SEM of the amplitude of the first peak from B.

3.3 Phosphorylation status of pyruvate dehydrogenase complex

One of the pathways well known to generate NADH and $FADH_2$ is the TCA cycle. ICDH, αKGDH, and malate dehydrogenase transfer electrons to NAD^+ to make NADH and succinate dehydrogenase in turn makes $FADH_2$. Focusing on the pyruvate dehydrogenase (PDH) activity, we checked for the protein expression of its regulators. PDH is kept inactive by PDK-mediated phosphorylation. In AF, PDK4 expression was 21% higher (CTL 1.00±0.03, N=16 vs AF 1.21±0.06, N=16, p=0.0086, **Figure 12A and B**). However, the expression of the Ca^{2+}-sensitive phosphatase, PDP1, was unchanged in AF (**Figure 12A and B**).

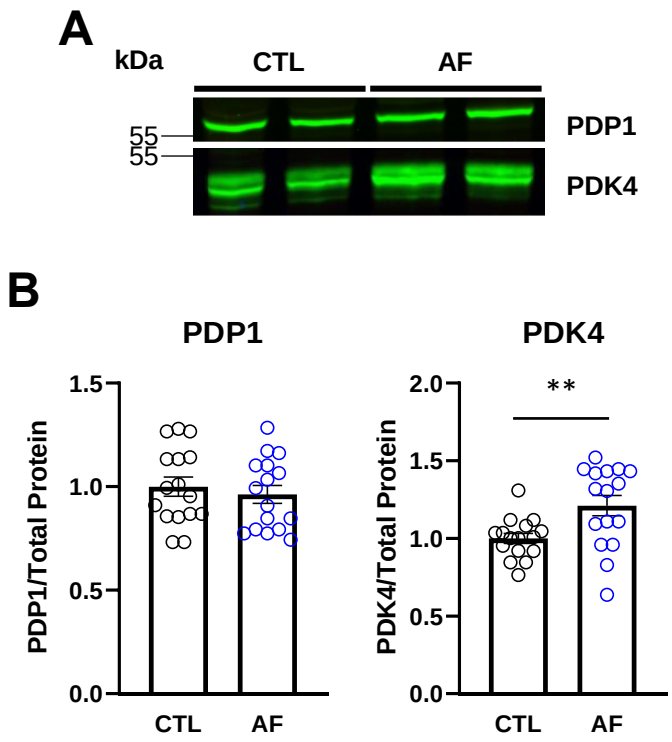

Figure 14. Protein expression pyruvate dehydrogenase regulators detected by immunoblotting of RAAs from CTL and AF patients. A, Representative blots and **B,** Mean±SEM of densitometric analysis of immunoblots (bottom) of PDP1 and PDK4, normalised to total protein.

3.4 L-type Ca^{2+} currents during workload transitions in human atrial myocytes

To monitor the contribution of L-type Ca^{2+} currents in the impaired redox response of AF myocytes during workload transitions, we took advantage of simultaneous voltage-clamp recording during the NAD(P)H and FAD^{+} autofluorescence recording. L-type Ca^{2+} current was measured at 0.5 Hz (**Figure 15A**), 3 Hz, and 3 Hz+ISO (**Figure 15C**). Currents were normalised to cell capacitance. Cell capacitance, which gives an estimate of cell size, was found to be comparable between CTL and AF (pF, CTL 99.18±9.77 vs AF 101.2±8.90, **Figure 15F**). A classic hallmark of electrophysiological remodelling in AF could be observed, where peak Ca^{2+} current was smaller, both at 0.5 Hz (pA/pF, CTL 4.67±0.47, n=19 myocytes/13 patients vs AF 2.58±0.21, n=21 myocytes/4 patients, p=0.0004, **Figure 15B**) and 3 Hz (pA/pF, CTL 4.15±0.46 vs AF 2.11±0.21, p=0.0003, **Figure 15D**) in AF. However, ß-adrenergic stimulation by ISO at 3 Hz eliminated this difference (pA/pF, CTL (pink, left) 11.81±0.84 vs AF (pink, right) 10.36±0.87; **Figure 15E**, left panel). Interestingly, the degree of change after ISO was greater in AF myocytes (% change, CTL 259.60±59.91% vs AF (pink, right) 468.80±74.73, p=0.0022, **Figure 15E**, right panel). Based on this finding, it seems that the L-type Ca^{2+} current has a minimal role in the impaired redox index response to increased workload in AF. Therefore, we proceeded to look at other Ca^{2+} handling mechanisms known to be altered in AF.

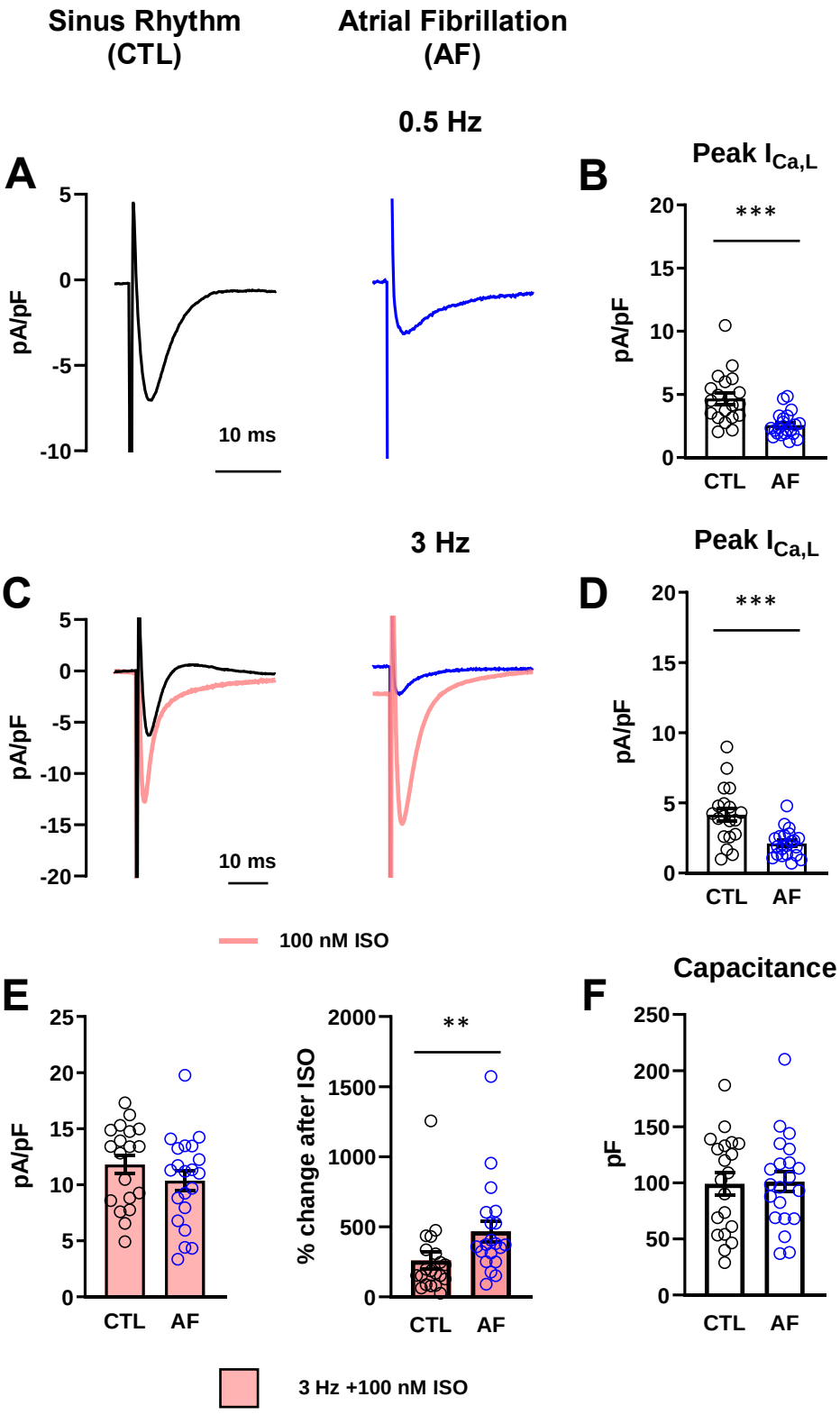

Figure 15. L-type Ca^{2+} current ($I_{Ca,L}$) densities in atrial myocytes from CTL and AF patients. A, Representative $I_{Ca,L}$ from CTL (black, n/N=19 myocytes/13 patients) and AF (blue, n/N=21 myocytes/4 patients) myocytes at 0.5 Hz **B,** Mean±SEM of A. **C,** Superimposed traces of representative $I_{Ca,L}$ at 3 Hz and 3 Hz + 100 nM ISO (pink). **D,** Mean±SEM of C. **E,** Mean±SEM (left) of pink traces on C, and % change of density after ISO (right). **F,** Cell capacitance as estimate of cell size. **p<0.01, ***p<0.001 vs. CTL.

3.5 Cytosolic and mitochondrial Ca^{2+} handling in human atrial myocytes

3.5.1 Mitochondrial Ca^{2+} kinetics in human atrial myocytes

A decrease in the cytosolic Ca^{2+} transient amplitude has previously been observed in AF. Since mitochondria can accumulate Ca^{2+} during increased workload, we used compartment-specific indicators to measure cytosolic and mitochondrial Ca^{2+}. The Ca^{2+} transient kinetics between cytosolic and mitochondrial transients were clearly different (**Figure 16A-E**); time to peak was faster in mito at 0.5 Hz (ms, Cyto. Ca^{2+}, 133.90±6.06, n/N=32 myocytes/patients vs Mito. Ca^{2+}, 105.60±5.02, n=34 myocytes/patients, p=0.0019, **Figure 16D**) and 3 Hz+ISO (ms, Cyto. Ca^{2+}, 133.90±6.06, n/N=32 myocytes/patients vs Mito. Ca^{2+}, 105.60±5.02, n=34 myocytes/patients, p=0.0019, **Figure 16D**). Cytosolic Ca^{2+} extrusion was comparable with mitochondrial Ca^{2+} extrusion in all conditions (**Figure 16E**). However, mitochondrial Ca^{2+} efflux was increasingly faster with increasing degree of workload (**Figure 16E**). These differences in behaviours of Ca^{2+} kinetics suggest that the emissions from Indo-1 and Rhod-2 come from different compartments in the myocyte. Furthermore, a membrane-permeable blocker of mitochondrial Ca^{2+} uptake, Ru265 (1 µM) (**Figure 16F**), abolished mitochondrial Ca^{2+} transients (**Figure 16G and H**). These results suggest that emissions from the Ca^{2+} indicators are cell compartment-specific (cytosolic vs mitochondrial).

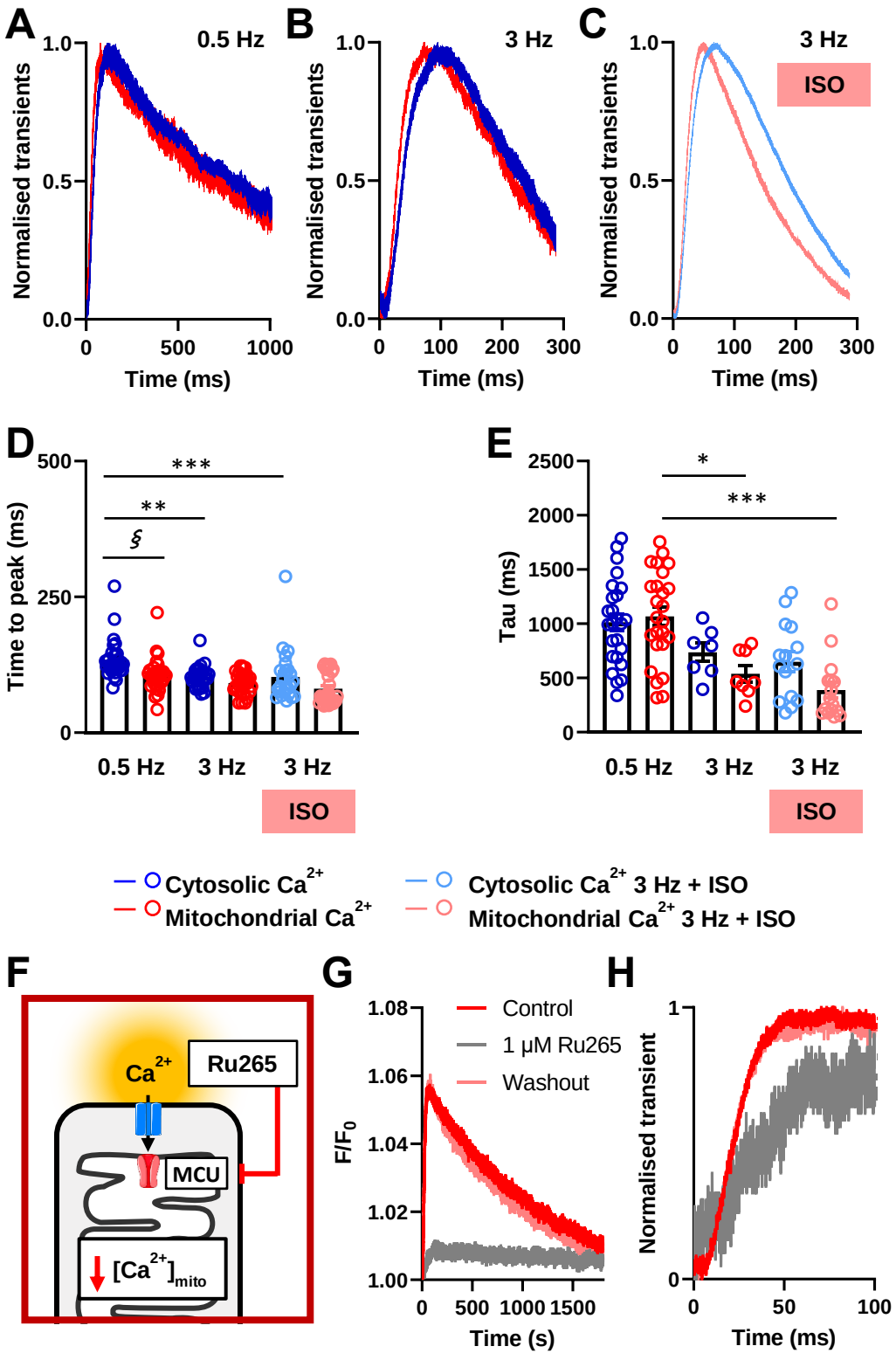

Figure 16. Validation of distinct cytosolic and mitochondrial transients recorded from atrial myocytes isolated from CTL patients. Superimposed traces of Ca^{2+} transients from cytosol (blue) and mitochondria (red) in atrial myocytes stimulated at **A,** 0.5 Hz **B,** 3 Hz and **C,** 3 Hz + ISO. Mean±SEM of **D,** upstroke time to peak and **E,** decay time (tau) of cytosolic and mitochondrial Ca^{2+} transients. **F,** Schematic diagram of mitochondrial Ca^{2+} uptake block by 1 µM Ru265. **G,** Representative traces of reversible mitochondrial Ca^{2+} transient block by 1 µM Ru265. **H,** Upstroke of Ca^{2+} transients from **F**. *p<0.05,**p<0.01,***p<0.001 vs. 0.5 Hz. §p<0.05 vs cytosolic Ca^{2+}.

3.5.2 Cytosolic and mitochondrial Ca^{2+} handling in atrial myocytes

Diastolic levels of Ca^{2+} in the cytosol and mitochondria were analysed in order to investigate Ca^{2+} accumulation upon workload transition (**Figure 17**). Cytosolic diastolic Ca^{2+} levels remained steady in the transient from 0.5 to 3 Hz in both CTL and AF (**Figure 17A and C**). However, when we compare diastolic Ca^{2+} levels in the mitochondria (**Figure 17B and D**), the degree of diastolic Ca^{2+} increase during workload transition in CTL was higher compared to that in AF myocytes. This suggests that Ca^{2+} accumulation is impaired in AF myocytes.

Ca^{2+} transients in CTL and AF were also compared; at 0.5 Hz, both the cytosolic (F_{405}/F_{480}, CTL 0.21±0.04, n/N=11 myocytes/7 patients vs 0.05±0.02, n/N=3 myocytes/3 patients, p=0.006, **Figure 18A and B**) and the mitochondrial Ca^{2+} transient amplitude (F/F_{load}, CTL 0.17±0.06, vs 0.02±0.003, , p=0.022, **Figure 18**F and G) were found to be smaller in AF, compared to CTL. Both the cytosolic (F_{405}/F_{480}*ms^{-1}, CTL 0.00166±0.00032, n/N=11/6 vs 0.00036±0.00011, n/N=3/3, p=0.0055, **Figure 18D**) and the mitochondrial transients (F/F_{load}*ms^{-1}, CTL 0.001704±0.0005455, n/N=11/6 vs 0.0001876±3.739e-5, n/N=3/3, p=0.006, **Figure 18**I) showed slower rise in AF, despite similar time to peak values as CTL. Decay of Ca^{2+} transients (tau, cytosolic and mitochondrial) were also comparable between CTL and AF at 0.5 Hz (**Figure 18E and J**).

At 3 Hz (**Figure 19**), both cytosolic (F_{405}/F_{480}*ms^{-1}, CTL 0.001014±0.0002250, n/N=11/6 vs 0.0002663±5.997e-5, n/N=3/3, p=0.022, **Figure 19C and F**) and mitochondrial Ca^{2+} transients showed a slower rate of rise in AF (F/F_{load}*ms^{-1}, CTL 0.001048±0.0003055, n/N=11/6 vs 9.653e-5±2.463e-5, n/N=3/3, p=0.022, **Figure 19C and F**), compared to CTL. However Ca^{2+} transient amplitudes were not significantly different in AF (**Figure 19A and D**).

At 3 Hz+ISO (**Figure 20**), cytosolic and mitochondrial Ca^{2+} transients were also not significantly different between CTL and AF was maintained, however the slower rate of rise observed at 3Hz (without Iso) in AF was abolished. Ca^{2+} efflux was comparable between CTL and AF during 3 Hz with Iso.

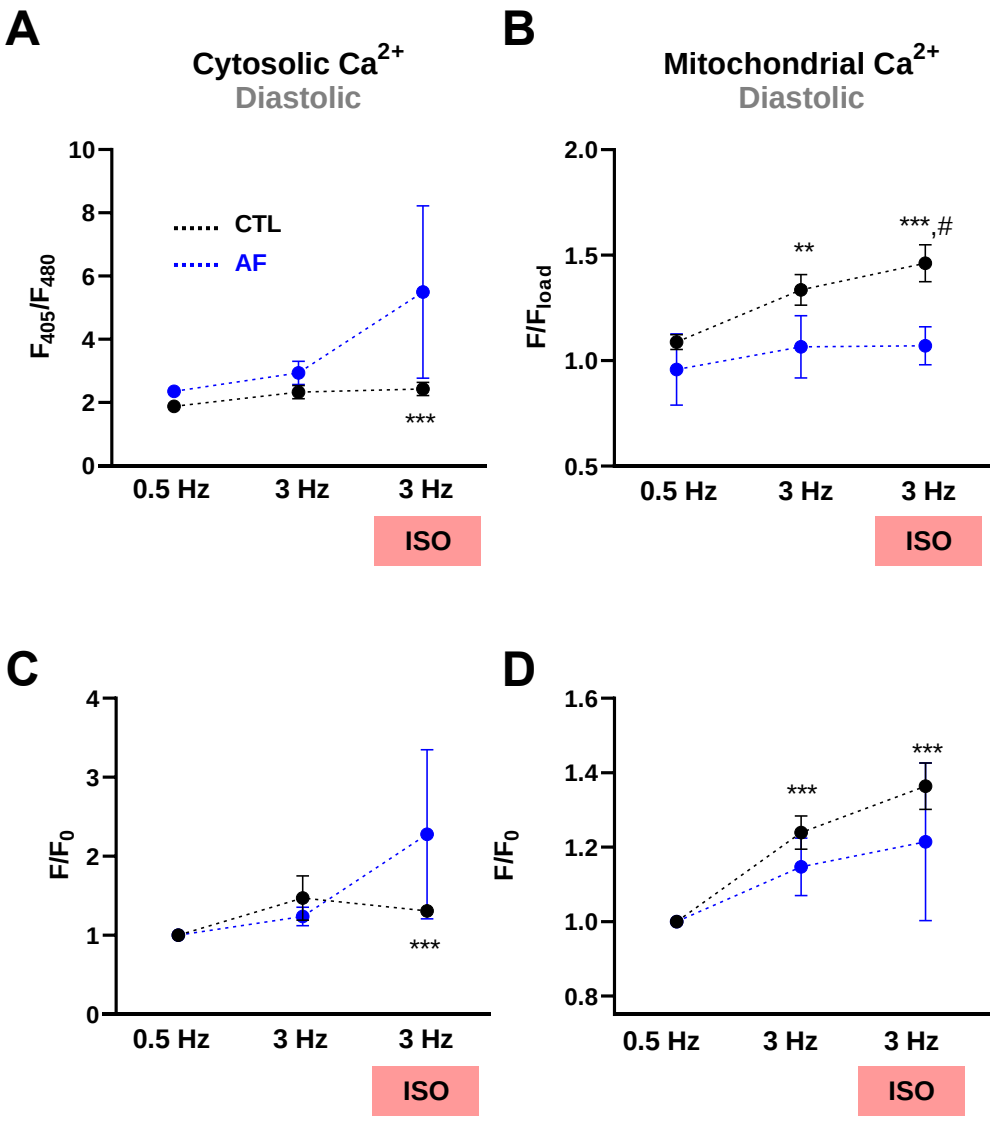

Figure 17. Ca^{2+} accumulation in cytosol and mitochondria during workload transitions. The following graphs represent the mean±SEM of the following: **A,** Diastolic cytosolic Ca^{2+} level from CTL (black, n/N=16 myocytes/7 patients) and AF (blue, n/N=4 myocytes/3 patients) myocytes and **C,** when normalised to 0.5 Hz as F_0 (F/F_0). **B,** Diastolic mitochondrial Ca^{2+} from CTL (black) and AF (blue) myocytes **D,** when normalised to 0.5 Hz as F_0 (F/F_0). #p<0.05 vs. CTL with two-way ANOVA. **p<0.01, ***p<0.001 vs 0.5 Hz with Bonferroni correction.

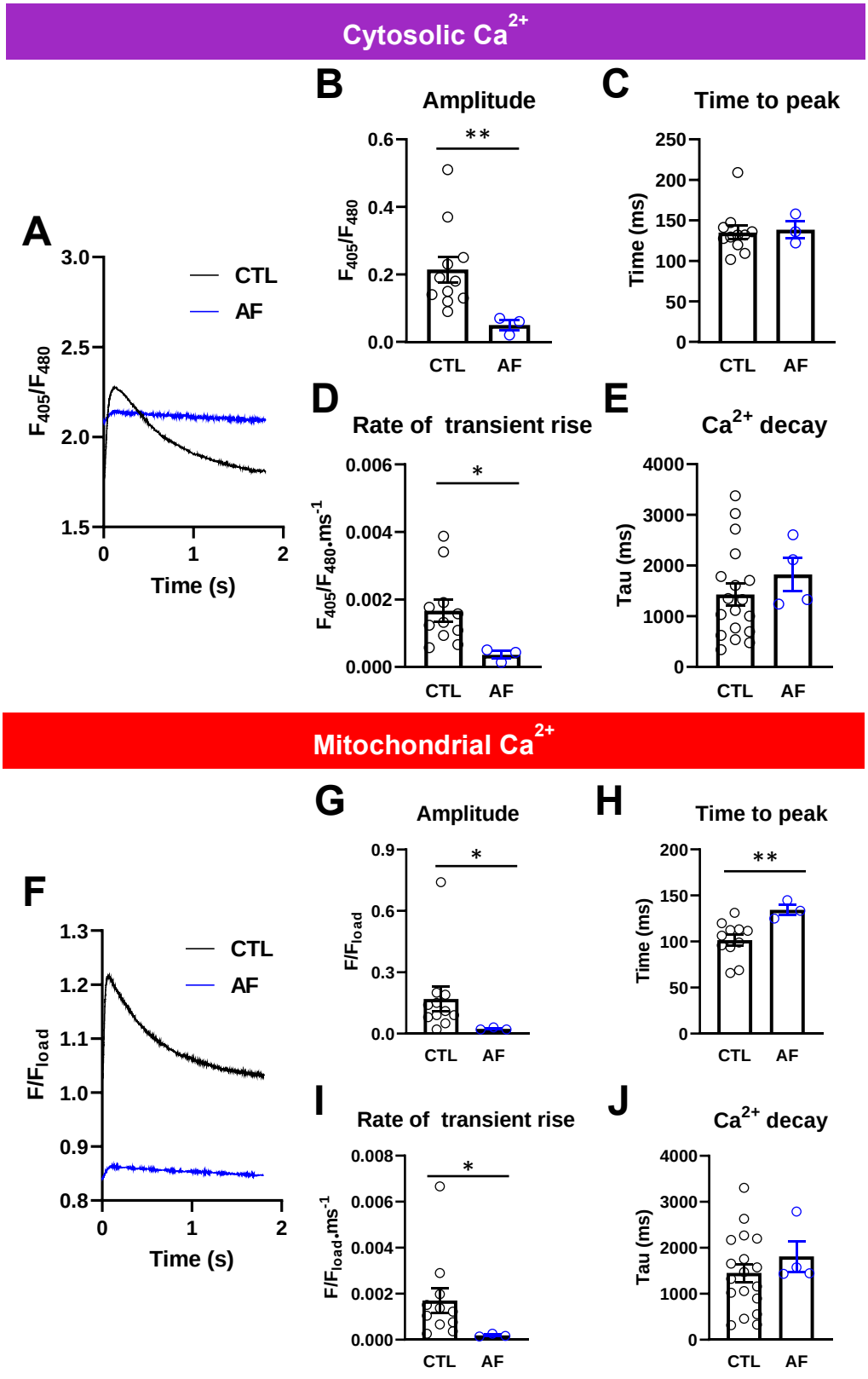

Figure 18. Cytosolic and mitochondrial Ca^{2+} transients recorded from atrial myocytes from CTL and AF patients at 0.5 Hz. A, Representative traces of cytosolic Ca^{2+} transients at 0.5 Hz. The following bar graphs represent the mean±SEM of: **B,** transient amplitude (F_{405}/F_{480}); **C,** time to peak (ms); **D,** rate of amplitude increase (F_{405}/F_{480}•ms^{-1}); and **E,** time constant of decay, τ (ms). **F-J,** same for mitochondrial Ca^{2+}. *p<0.05,**p<0.01 vs CTL.

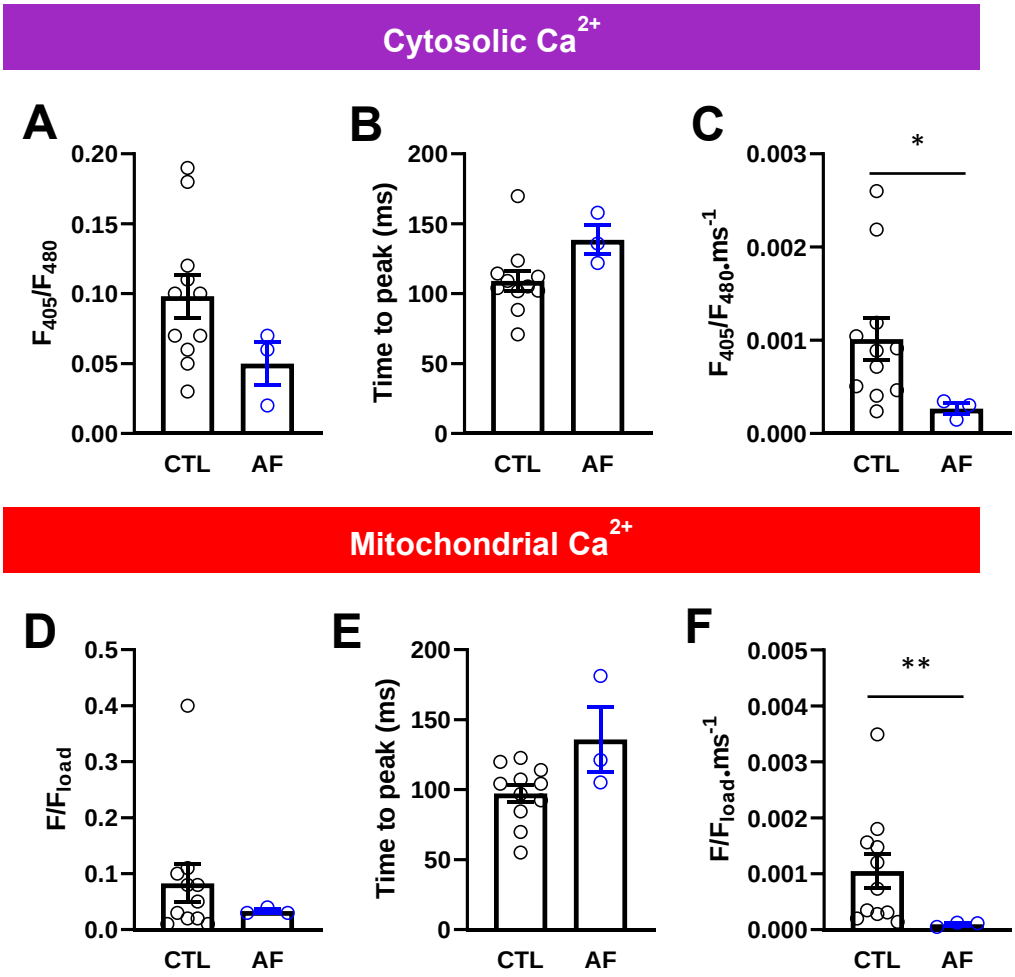

Figure 19. Cytosolic and mitochondrial Ca^{2+} transients recorded from atrial myocytes from CTL and AF patients at 3 Hz. A, Representative traces of cytosolic Ca^{2+} transients at 3 Hz. The following bar graphs represent the mean±SEM of: **B,** transient amplitude (F_{405}/F_{480}); **C,** time to peak (ms); and **D,** rate of amplitude increase (F_{405}/F_{480}•ms^{-1}). **E-H,** same for mitochondrial Ca^{2+}. *p<0.05, **p<0.01 vs. CTL.

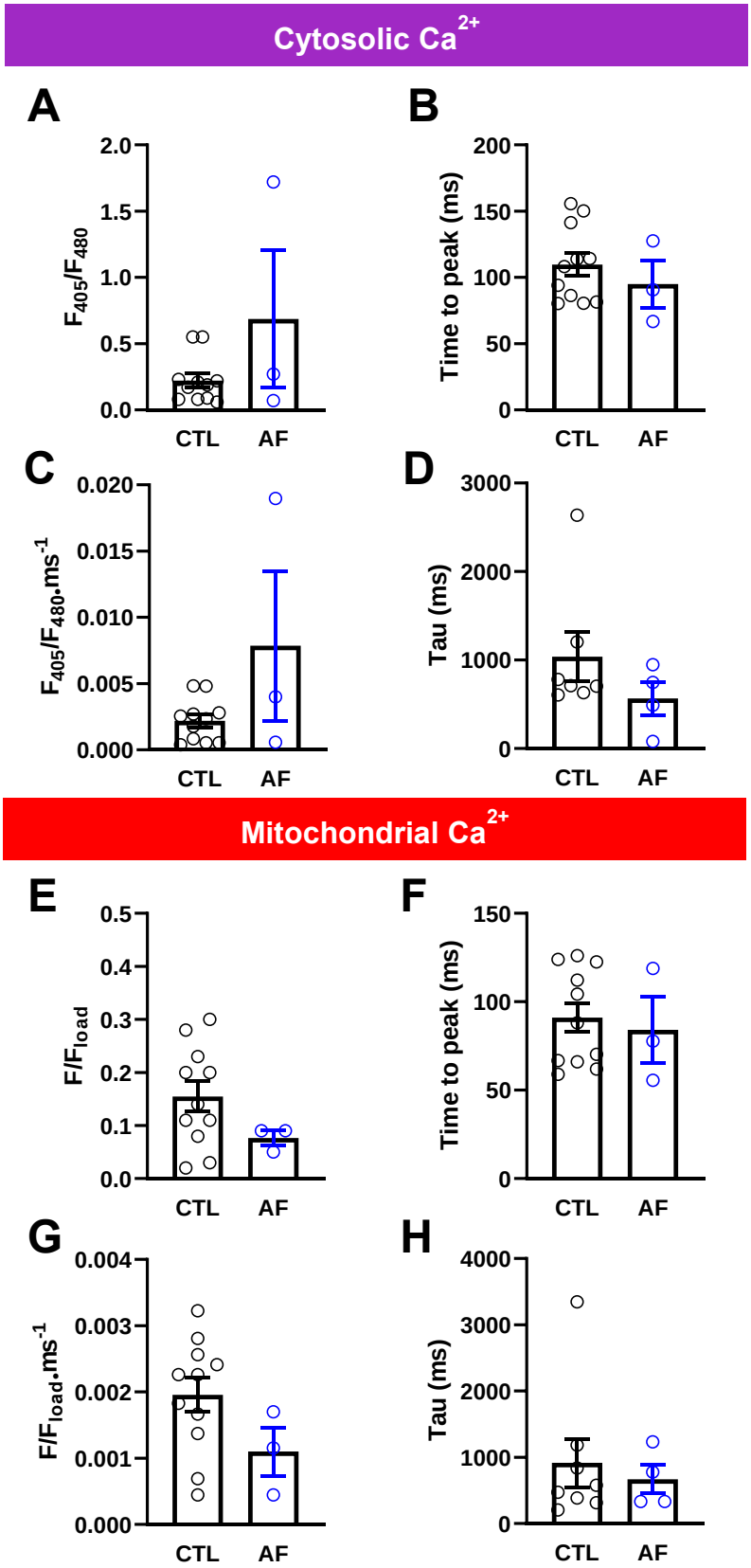

Figure 20. Cytosolic and mitochondrial Ca^{2+} transients recorded from atrial myocytes from CTL and AF patients at 3 Hz + ISO. A, Representative traces of cytosolic Ca^{2+} transients at 3 Hz + ISO. The following bar graphs represent the mean±SEM of: **B,** transient amplitude (F_{405}/F_{480}); **C,** time to peak (ms); **D,** rate of amplitude increase (F_{405}/F_{480}•ms^{-1}); and **E,** time constant of decay, τ (ms). **F-J,** same for mitochondrial Ca^{2+}.

3.6 Calcium handling proteins in the mitochondria

Proteins involved in Ca^{2+} handling between ER/SR and mitochondria which have previously been observed in cardiac tissue or otherwise were investigated in this study. OMM proteins, VDAC1 and VDAC2, adaptor proteins GRP75 and TGM2, ER protein VAPB and its mitochondrial partner, PTPIP51, as well as PDZD8 all showed similar protein expression levels between CTL and AF (**Figure 21**).

Interestingly, higher MCU expression was detected in tissue from AF patients (CTL 1.000±0.03, N=15 patients vs AF 1.543±0.18, N=15 patients, p=0.039, **Figure 22B and C**), while both its Ca^{2+}-sensing-regulator, MICU1, and negative regulator, MCUB, were comparable between CTL and AF (**Figure 22A and B**). Interestingly, MICU2 (CTL 1.067±0.26, N=15 patients vs AF 0.2602±0.07, N=15 patients, p=0.0003, **Figure 22A and B**), and thus its ratio with MCU (MICU2/MCU) expression was significantly lower in AF tissue (**Figure 22C**).

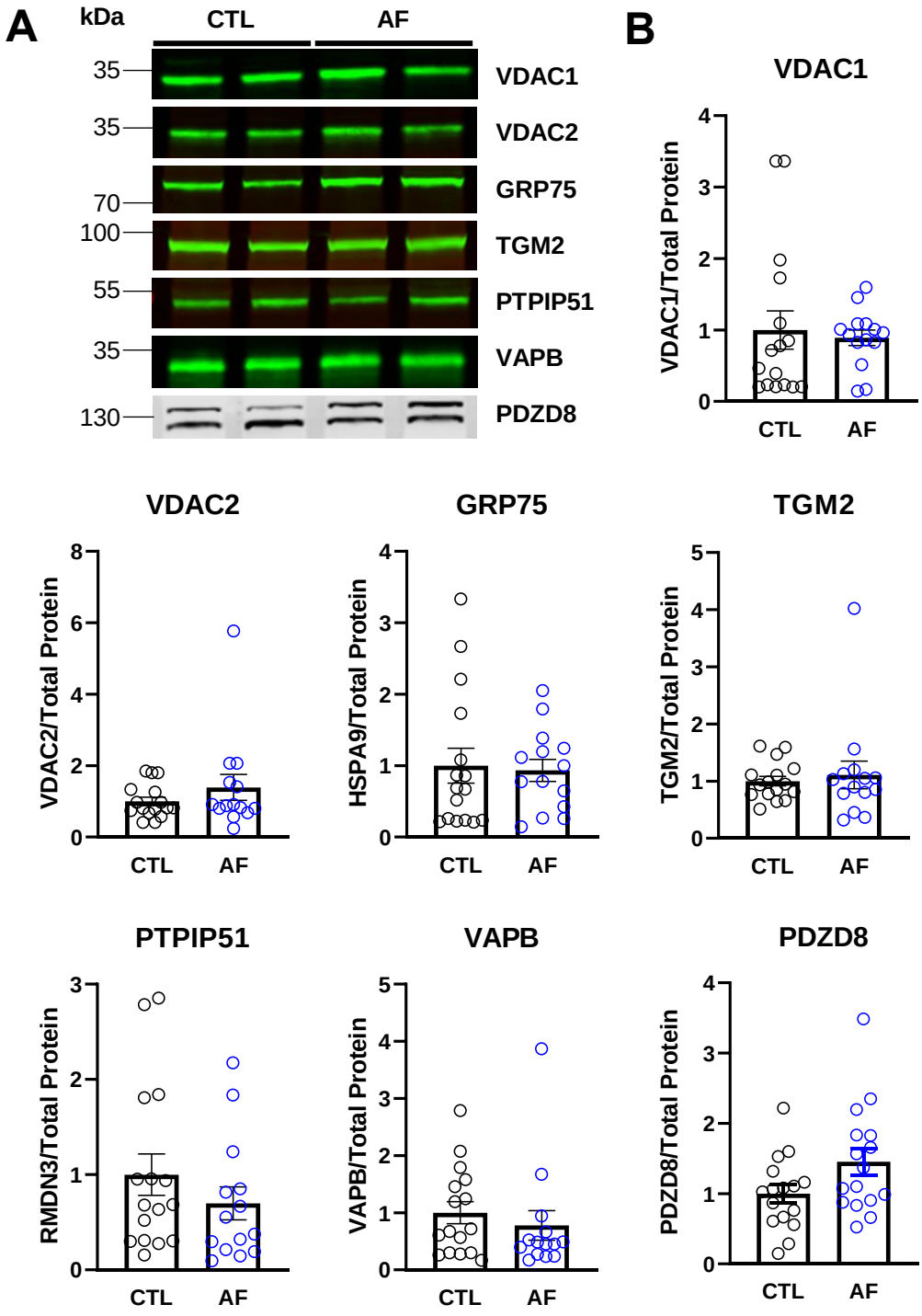

Figure 21. Protein expression of proteins involved Ca^{2+} handling between SR and mitochondria detected by immunoblotting of RAAs from CTL and AF patients. A, Representative blots from CTL (N=16) and AF (N=14) and **B,** Mean±SEM of densitometric analysis of immunoblots of VDAC**1**, VDAC2, GRP75, TGM2, PTPIP51, VAPB, and PDZD8 normalised to total protein.

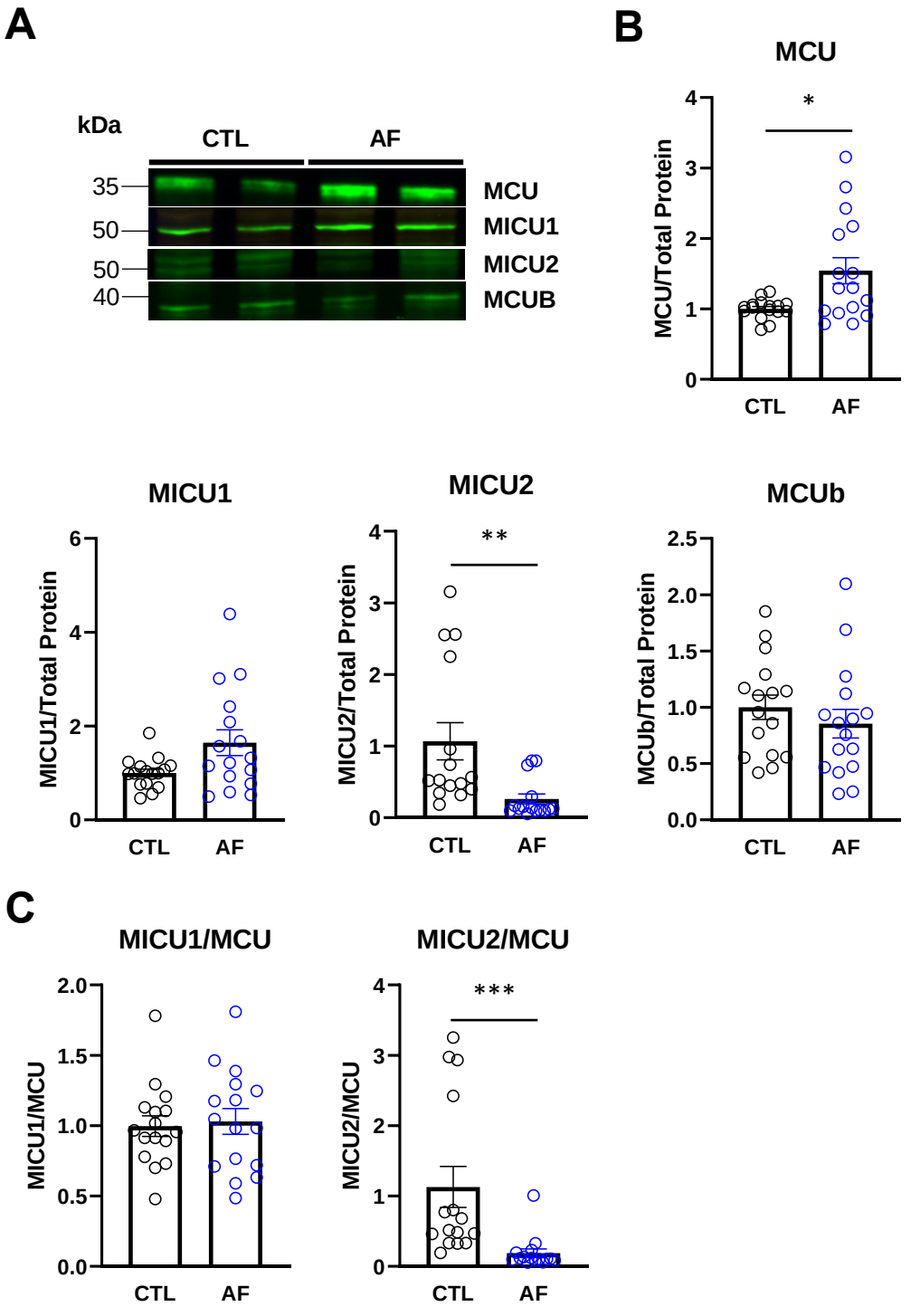

Figure 22. Protein expression of mitochondrial Ca^{2+} uniporter (MCU) complex detected by immunoblotting of RAAs from CTL and AF patients. A, Representative blots (top) and **B,** Mean±SEM of densitometric analysis of immunoblots (bottom) of MCU, MICU1, MICU2, and MCUb normalised to total protein, and **C,** ratios of MICU1 and MICU2 to MCU. *p<0.05, **p<0.05, ***p<0.001 vs CTL with Student's t-test.

3.7 Structural differences in the mitochondria of human atrial appendages

Pixel-based measures of colocalisation are not ideal with super-resolution (Tameling et al., 2021). The degree of clustering of VDAC1 relative to RyR2 signals was used as a measure of correlation between SR and mitochondria. Ripley's K function was applied to measure VDAC1 and RyR2 colocalisation (**Figure 24**). This is an object-based (spatial) analysis where spots are detected after a process of (pixel) erosion and dilation. The centers of these points are the used for spatial analysis between two fluorophores within a given radius. This object-based method of analysis overcomes the noisy nature of images generated from paraffin sections and is therefore preferable to pixel-based methods.

Here, we show that mitochondria in CTL myocytes appear as packages running parallel along the length of the myocyte, and the gaps in between these mitochondrial packages are occupied by RyR2, as shown in the merged image **Figure 23**). AF tissue displayed non-distinct mitochondrial patterns, but rather aggregation of smaller mitochondria, filling areas which would normally be occupied by SR (**Figure 24**). Ripley curve analysis revealed a lesser degree of VDAC1 spot aggregation with respect to RyR2 spots (CTL n/N=122/8 patients vs AF (115/8 patients, p=0.0018, **Figure 24**).

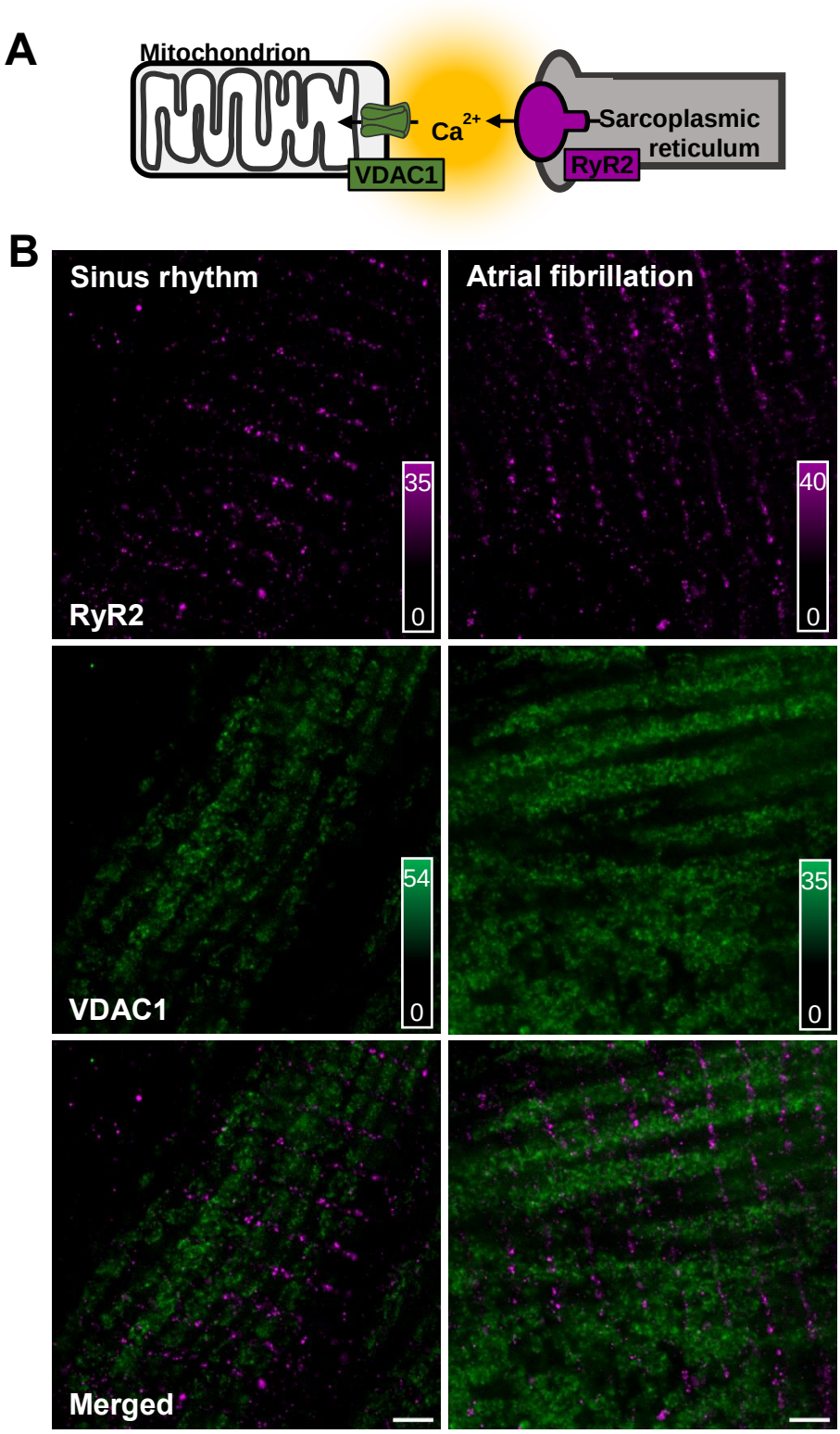

Figure 23. Stimulated Emission Depletion (STED) images of paraffin sections of RAAs from CTL and AF patients showing mitochondrial and SR localisation. A. Schematic diagram of a Ca^{2+} microdomain formed by the close apposition of a mitochondrion and SR. Mitochondrial outer membrane was labelled with VDAC1 (green) and SR was labelled with RyR2 (magenta). B. STED images showing RyR2, stained with a secondary antibody conjugated to STAR635P (top, magenta), VDAC1, stained with a secondary antibody conjugated to STAR580 (middle, green), and the merged images (bottom). Scale bar=2 µm.

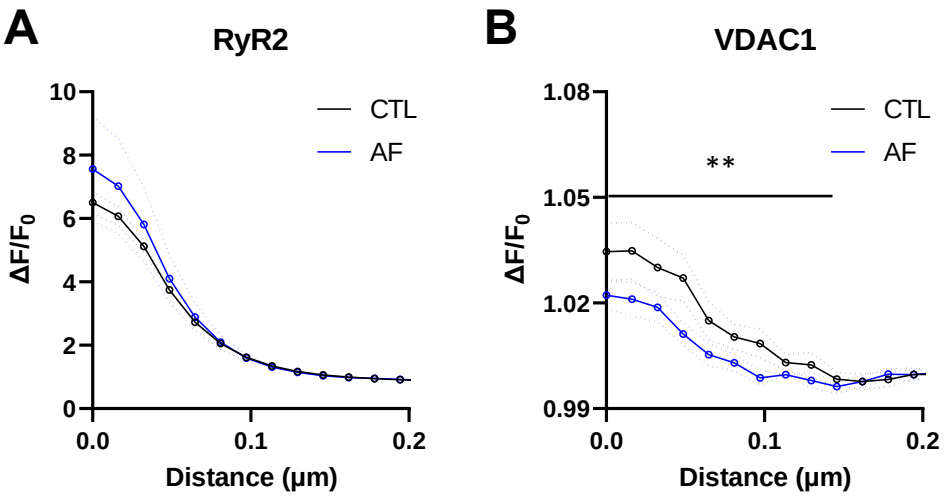

Figure 24. Colocalisation of RyR2 and VDAC1 in paraffin sections of RAAs from CTL and AF patients. A, Ripley K analysis of RyR2 as reference signal. B, Ripley K analysis of VDAC1 as reference signal. Traces were normalised between points 8-16 and a two-way ANOVA was performed on the first 10 points of the curve. **p<0.01 vs. CTL with Friedman's test.

3.8 Ultrastructural changes in the mitochondria in human atrial appendages

In order to more accurately quantify the interaction between mitochondria and SR, electron tomography (ET) was employed which allows for 3D reconstruction of the subcellular organisation. As can be seen in the 2D electron microscopy images (**Figure 25**), the organisation of the mitochondria replicates the observations made with STED microscopy. Moreover, the sarcomeres can be visualised with electron microscopy and the location of mitochondria in between the z-lines of the sarcomeres can be observed. This positioning results in a greater degree of interaction between mitochondria and SR, which is enriched in this area. Despite the similar density of mitochondria in CTL and AF (**Figure 26B)**, mitochondria are smaller in AF (nm, CTL 480.30±8.95, n/N=376 vs AF 404.20±6.079, n/N=445/, $p<0.001$, **Figure 26C**) Of particular significance is that the mitochondria and SR are further apart from each other in AF (nm, CTL 39.60±1.64, n/N=355/13 patients vs AF 404.2±6.079, n/N=347/5 patients, $p<0.001$, **Figure 26A (arrowheads) and D)**, which agrees with the STED colocalisation analysis. Despite the larger left atrial (LA) diameter in AF patients (**Table 12**), there was no correlation with SR-mitochondria distance (**Figure 26E)**. No significant differences were detected in the tethering protein, mitofusin2, or in the fission protein, Fis1, or mitochondria-associated tubulin, TUBB2A in AF compared to CTL (**Figure 27**).

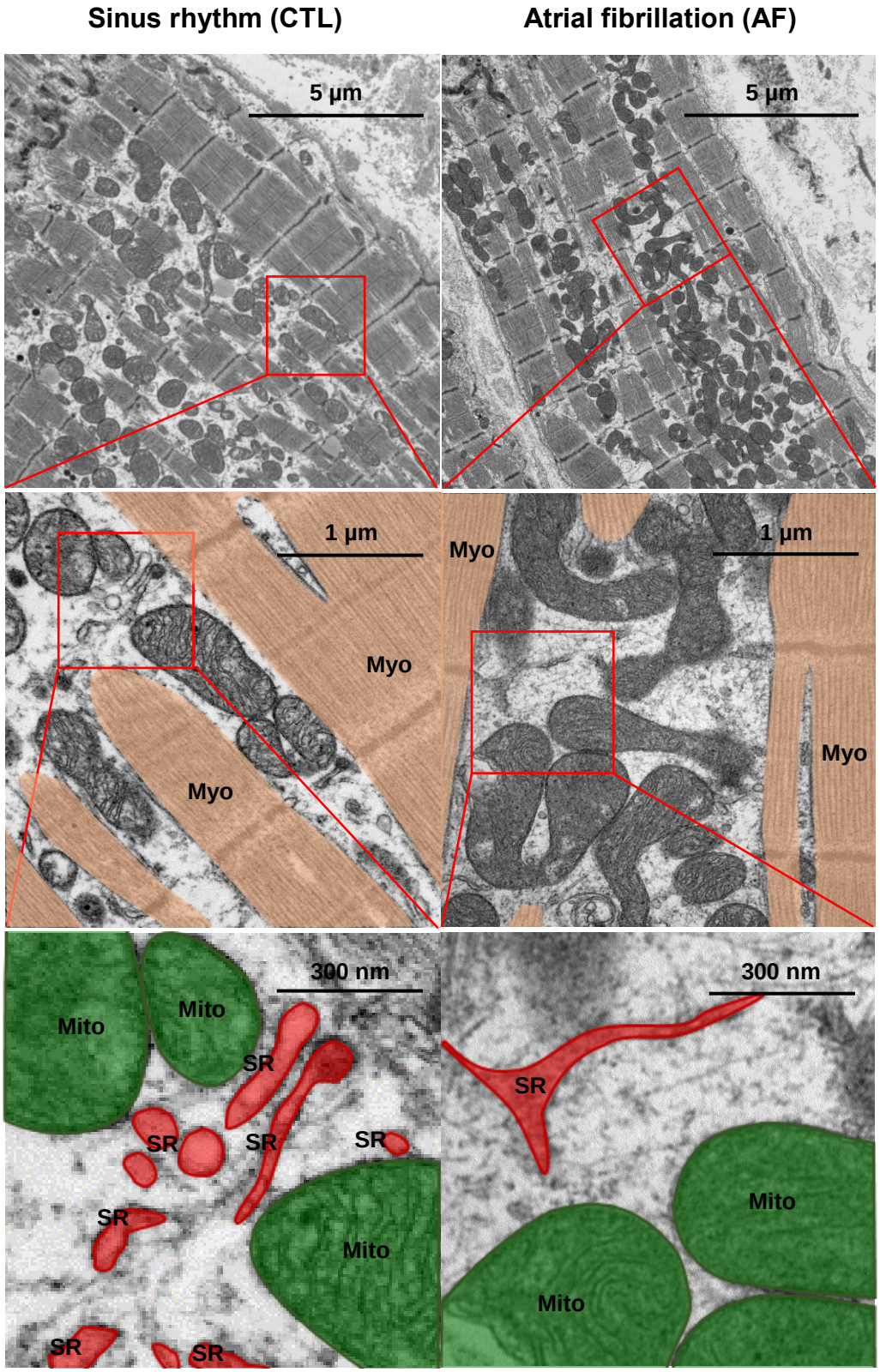

Figure 25. Ultrastructural changes of the RAA from CTL and AF patients observed by transmission electron microscopy (TEM). Representative images of RAAs from CTL (left panel) and AF (right panel) patients. (Top) Mitochondrial arrangement in between myofibrils, with mitochondria in between z-lines of sarcomeres in CTL but less so in AF, as well as smaller mitochondria in AF. Scale bar=5 µm. (Middle) Zoomed in image of inset from the top, showing mitochondrial arrangement. Scale bar=1 µm. (Right) Zoomed in image of inset from the middle, showing SR and mitochondria interaction. Scale bar=300 nm. Myo=myofilament; SR=sarcoplasmic reticulum; Mito=mitochondrion.

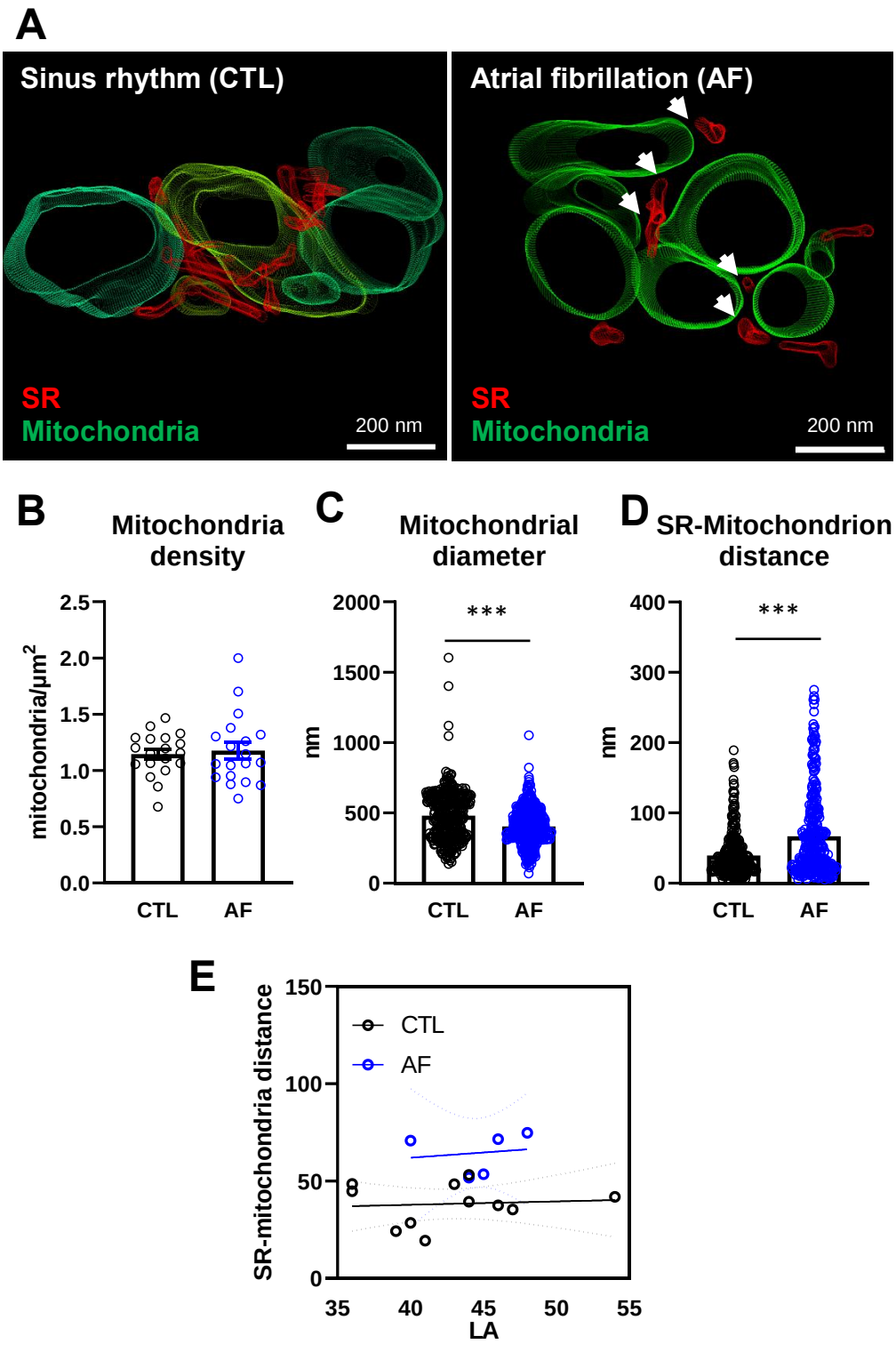

Figure 26. Sarcoplasmic reticulum and mitochondria interaction in RAAs from CTL and AF patients visualised by electron tomography (ET). A, Representative images ET 3D reconstructions of the SR (red) and mitochondria (green) from CTL and AF RAAs. Scale bar=200 nm. The following bar graphs represent the mean±SEM of: **B,** Mitochondria density; **C,** Mitochondrial diameter; and **D,** Distance between SR and mitochondria. E, correlations of SR-mitochondria distance to left atrial (LA) diameter of patients. ***p<0.001vs CTL.

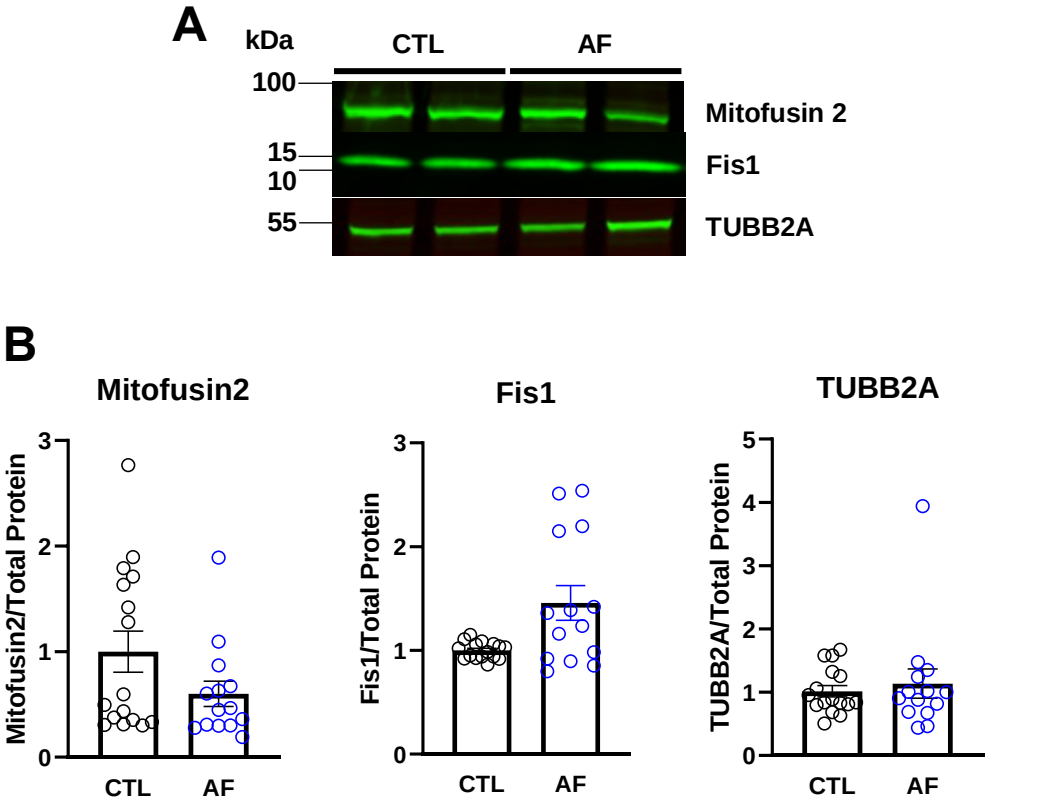

Figure 27. Protein expression of structural proteins detected by immunoblotting of RAAs from CTL and AF patients. A, Representative blots and **B,** Mean±SEM of densitometric analysis of immunoblots of Mitofusin2, Fis1, and TUBB2A normalised to total protein.

3.9 Accumulation of defective OXPHOS components as pro-arrhythmic substrate

Age is the most important risk factor in AF, and older patients are also at higher risk for stroke (Laredo et al., 2018). Ageing also results in the accumulation of mtDNA deletions, that have been recently found to be a pro-arrhythmic substrate (Baris et al., 2015). This can be visualised by enzymatic staining of mitochondrial enzymes, COXIV and SDH. However, the degree of COX-deficient cells in the RAAs of CTL and AF patients were found to be similar (**Figure 28A**), as well as the age-dependence of this mosaic COX deficiency (**Figure 28B**).

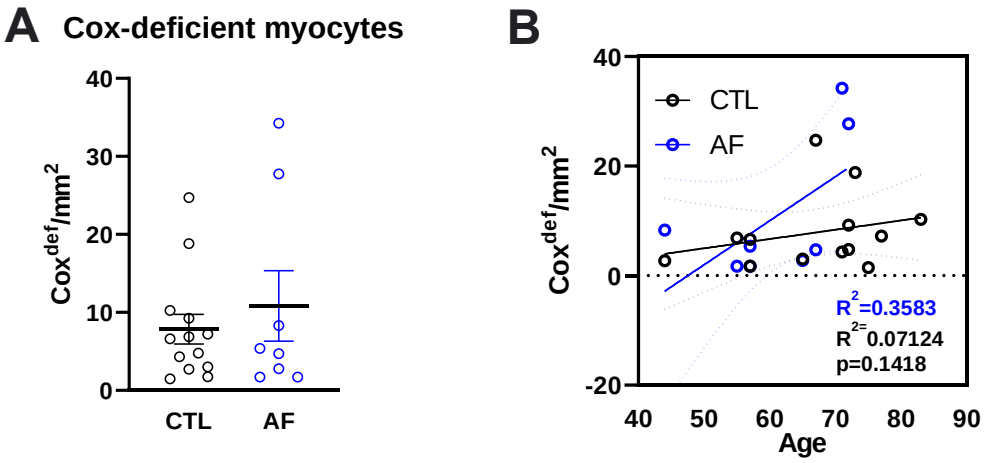

Figure 28. COX-deficient myocytes in RAAs from CTL and AF patients. A, Mean±SEM of blue-stained myocytes after double-staining of COX/SDH of RAA cryosections in CTL (black) and AF (blue) patients. **B,** Correlation of age and frequency of COX-deficient myocytes with simple linear regression analyses.

3.10 Ezetimibe and its effects on spontaneous Ca^{2+}-release events in human atrial myocytes

Triggered events, like DADs, can arise when spontaneous Ca^{2+}-release events (SCaEs) trigger an inward current on the NCX, thereby depolarizing the cell. This activity can be arrhythmogenic (Voigt et al., 2012).To assess whether Ezetimibe can reduce spontaneous activity, current-clamp configuration was used to stimulate atrial myocytes at 0.5 Hz. After stimulation for 1 minute, fluorescence of Fluo-2 in unstimulated myocytes were recorded for another minute. The incidence of SCaEs (measured as the percentage of cells exhibiting this activity) was higher in AF myocytes, compared to CTL (% myocytes with positive events, CTL 60% vs AF 83%, p=0.0002; CTL 83% vs AF+Eze 71%, p=0.0402, **Figure 29A and B**). The frequency (**Figure 29C**), amplitude (**Figure 29D**) and latency of the SCaEs (**Figure 29E**) in AF were, however not significantly different between the two groups, despite showing a tendency towards an increase in AF (particularly in event frequency). Upon treatment with 1 µM Ezetimibe, susceptibility to spontaneous Ca^{2+} events was comparable with CTL.

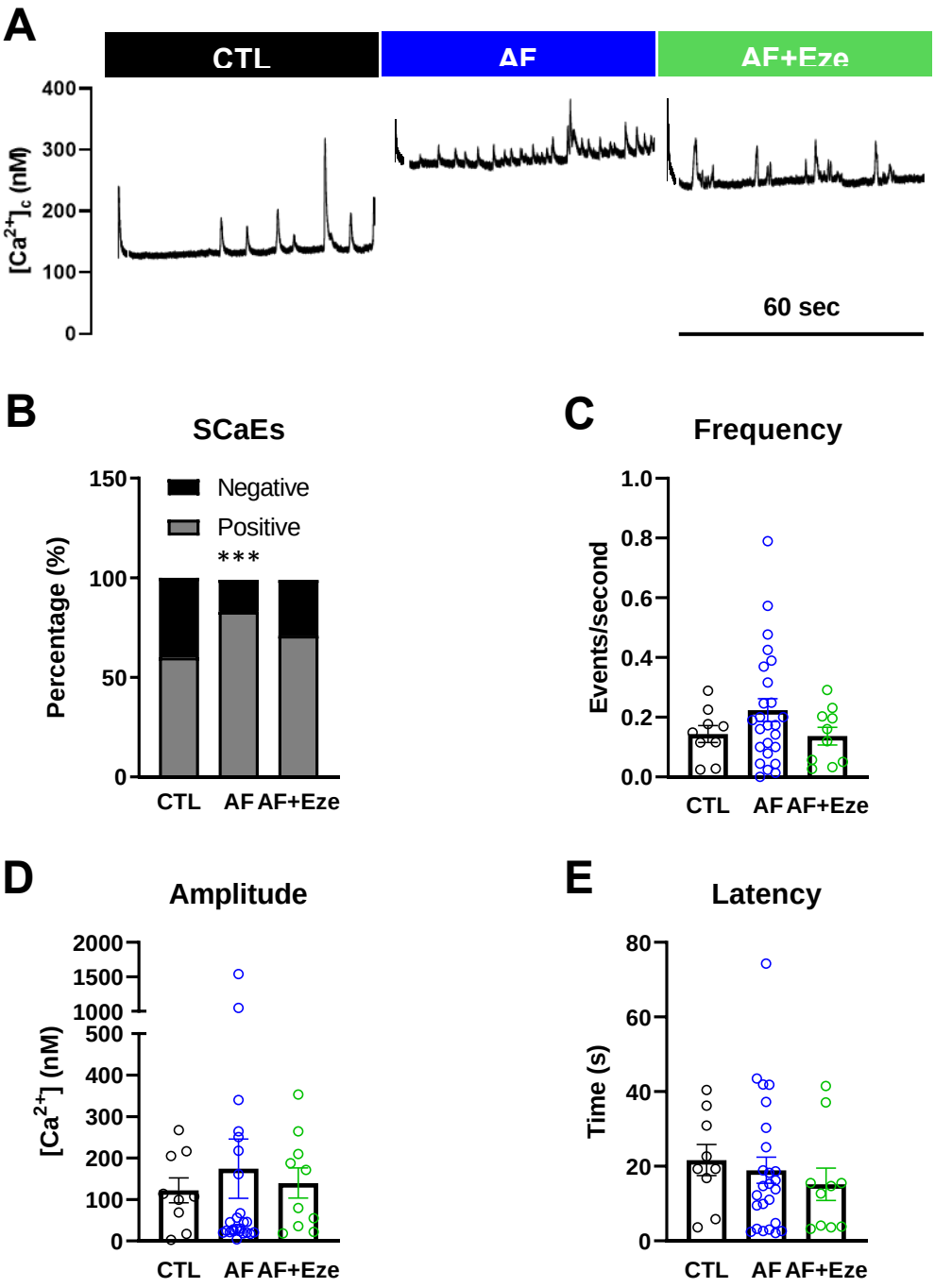

Figure 29. Spontaneous Ca^{2+}-release events (SCaEs) in atrial myocytes from CTL patients and AF patients with or without Ezetimibe. A, Representative recordings of SCaEs in CTL, AF, and AF myocytes treated with 1 μM ezetimibe, 1 minute after 0.5 Hz stimulation by current-clamp. **B,** Susceptibility of myocytes to spontaneous Ca^{2+} events. The following bar graphs represent mean±SEM of: C, Frequency of SCaEs; D, Amplitude of SCaEs; and E, Latency of first event. ***p<0.001 vs CTL with Fischer's test.

3.11 Ezetimibe and its effects on Ca^{2+} sparks in atrial human induced stem cell-derives cardiac myocytes

Afterdepolarisations can be caused by spontaneous Ca^{2+} releases (Schlotthauer & Bers, 2000), such as sparks and waves, and have an increased occurrence in AF (Hove-Madsen, Llach, Bayes-Genis, et al., 2004). Ca^{2+} sparks are localised Ca^{2+} release events in quiescent myocytes, mainly occurring via RyR2 (Cheng et al., 1993). hiPSC-CMs, despite their immaturity, exhibit comparable Ca^{2+} spark properties with adult cardiac myocytes (S. Li et al., 2014; Zhang et al., 2013), and can be used as a surrogate myocyte model for this experiment. A lower frequency of sparks was observed in the presence of 1 µM Ezetimibe (100 $\mu m^{-1}*s^{-1}$, DMSO 2.40±0.51 vs Eze 0.63±0.17, p=0.0053, **Figure 30A and B**). Ca^{2+} spark amplitude was also lower with 1 µM Ezetimibe (F/F_0, DMSO 1.75±0.03 vs Eze 1.66±0.06, p=0.049, **Figure 30C**, as was calculated total Ca^{2+} leak (F/F_0*ms*µm*(100 $\mu m^{-1}*s^{-1}$), DMSO 306.90±98.27 vs Eze 78.51±37.91, p=0.046, **Figure 30D**). Furthermore, Ezetimibe caused Ca^{2+} sparks to terminate faster (ms, DMSO 12.59±0.81 vs Eze 9.41±1.55, p=0.0022, **Figure 30G**).

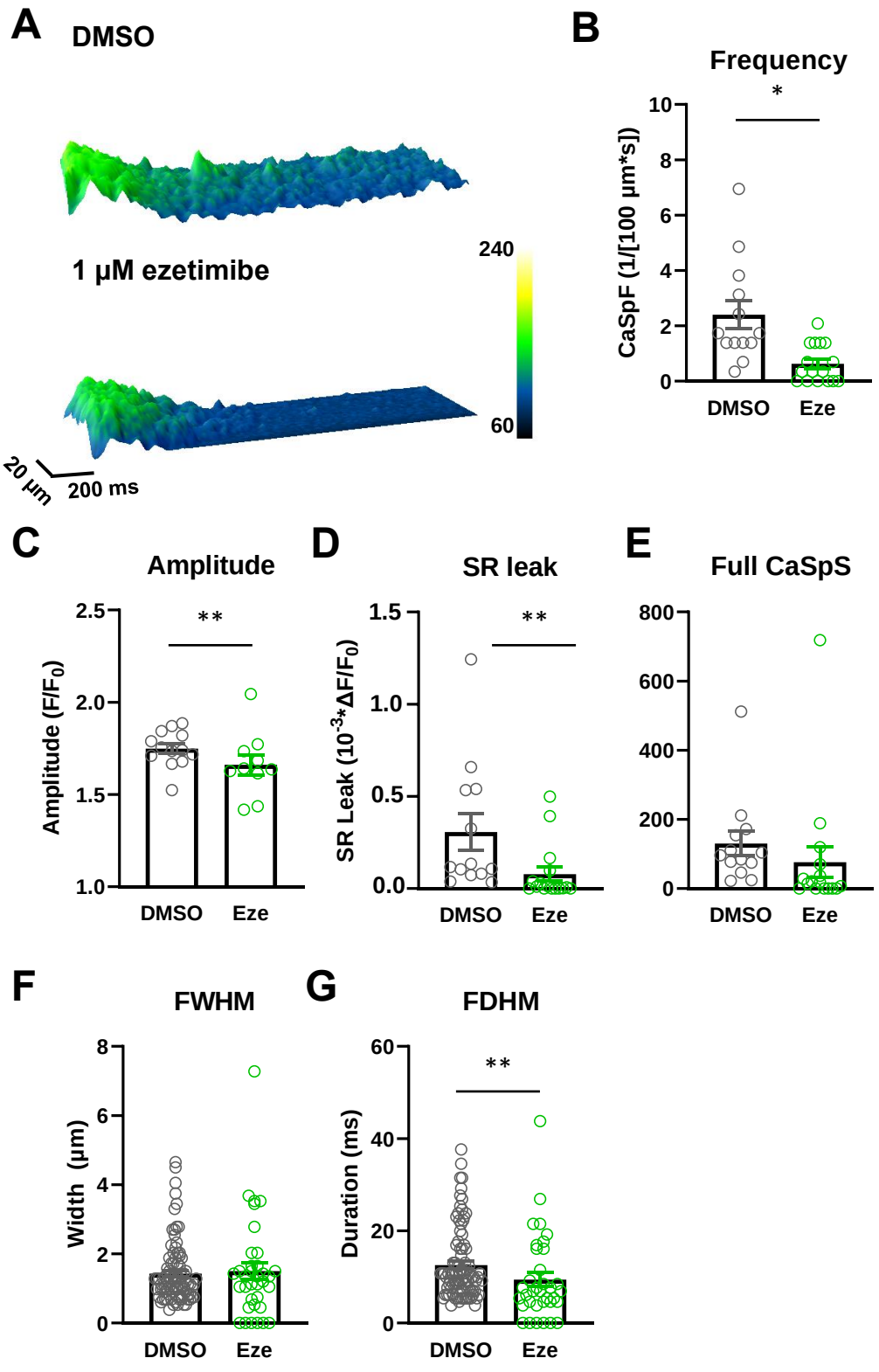

Figure 30. Ca^{2+} spark measurements in human induced pluripotent stem cell-derived atrial myocytes (hiPSC-AMs). A, Representative surface plots of line scans from hiPSC-AMs without (top) and with 1 µM Ezetimibe. The following bar graphs represent the mean±SEM of: **B,** Ca^{2+} spark frequency (CaSpF); **C,** SR leak (F/F_0*ms*µm*(100 µm-1*s-1)); **D,** Ca^{2+} spark amplitude (F/F_0); **E,** Estimated Ca^{2+} spark size (Full CaSpS); **F,** Spark full width at half-maximum (FWHM, µm); and **G,** Spark full duration at half-maximum (FDHM, ms). *p<0.05, **p<0.01 vs DMSO.

4 Discussion

4.1 Summary of results

The findings of this study collectively allude to the significance of Ca^{2+} microdomains in the Ca^{2+}-activated redox response of atrial myocytes during workload transitions in the atria, and how this is disturbed in AF. To our knowledge, we are first to present dynamic observations of the redox response and mitochondrial Ca^{2+} handling of human atrial myocytes, made possible by simultaneous fluorescence and patch-clamp experiments. The results of this study show that in AF myocytes, the mitochondrial Ca^{2+} transient amplitude and the capacity of the mitochondria to accumulate Ca^{2+} is impaired. This can affect Ca^{2+}-activated mechanisms in the mitochondria (Kohlhaas et al., 2017; Maack & O'Rourke, 2007), particularly during increased workload, such as the recovery of electron donors NADH and $FADH_2$. Indeed, we found evidence of potential reduction in PDH activity, mediated by PDK4. Furthermore, nanoscale imaging techniques used in this study revealed increased distance between SR and mitochondria in AF. This was coupled by reduced interaction between VDAC1 on the mitochondria and RyR2 on the SR, which is necessary for the occurrence of functional Ca^{2+} microdomains. The contribution of the L-type Ca^{2+} current to impaired mitochondrial redox response appeared to be inconsequential in conditions of increased workload. Interestingly, protein biochemistry analysis suggested remodelling of the MCU complex, revealing a decreased MICU2/MCU ratio. Ca^{2+} microdomains are necessary to regulate mitochondrial Ca^{2+} handling, for example in response to increased workload. Therefore, one could speculate that the increased MICU2/MCU ratio in AF, observed here, could be a compensatory response, in the face of impaired mitochondrial handling, to boost mitochondrial Ca^{2+} uptake. Finally, we attempted to test effect of Ezetimibe, a lipid-lowering drug recently shown to increase mitochondrial Ca^{2+} uptake, on pro-arrhythmic spontaneous Ca^{2+} events (SCaEs) and Ca^{2+} waves in atrial myocytes and iPSC-derived cardiac myocytes, respectively. Treatment of 1 µM Ezetimibe showed a tendency to decrease the occurrence of SCaEs, possibly due to a reduction of Ca^{2+} spark frequency. This highlights the possibility of modulating mitochondrial Ca^{2+} handling as a potential treatment modality, at least in long-standing persistent AF. Altogether, the current work

provides structural and functional characterisation of mitochondria and mitochondrial Ca^{2+} handling in AF and may point to potential therapeutic targets.

4.2 Impaired redox response during increased workload in AF

Brandes and Bers were first to show that increased stimulation frequency of cardiac muscle uses up NADH but is followed by a slow recovery of its reduced equivalents, due to an accumulation of Ca^{2+} in mitochondria (Brandes & Bers, 1996, 1997). To our knowledge, we are the first to recapitulate this finding in human atrial myocytes. We found that in AF, despite the similar baseline redox indices and NADH pools, compared to CTL myocytes, recovery of NADH and $FADH_2$ after initial oxidation is delayed during increased workload in AF. While the actual rate of recovery was comparable between CTL and AF, a higher fraction of myocytes from the AF patients showed continued oxidation, i.e. a failure to recover NADH and $FADH_2$ within the time period investigated. However, since each experimental step was recorded for 1 minute in order not to cause excessive stress to the myocytes, we cannot exclude the possibility that the myocytes in question were exhibiting prolonged delay of recovery, rather than lack of recovery at all.

During conditions of increased workload, AF myocytes showed a tendency to have a higher $NAD(P)H/FAD^+$ ratio, which may possibly be attributed to the decreased activity of the ETC Complexes I and II, as no structural alterations on the complexes were observed (Emelyanova, Ashary, Cosic, Negmadjanov, Ross, Rizvi, Olet, Kress, Sra, Tajik, et al., 2016). Another possibility is that CTL myocytes tend to be more oxidised than AF myocytes, and one could hypothesise that this is because these cells have not undergone remodelling caused by increased atrial activation rates. Moreover, a higher $NADH/NAD^+$ ratio has previously been associated with increased lactate (Cross et al., 1995) and decreased PDH activity (Randle, 1981). While we did observe increased PDK4 expression, which inhibits PDH activity by phosphorylation, Ca^{2+}-sensitive PDP1 was unchanged between CTL and AF. Therefore, phosphorylated forms of PDH must be investigated.

4.3 Contribution of L-Type Ca^{2+} currents in the redox response of atrial myocytes during increased workload and β-adrenergic stimulation

A hallmark of electrophysiological remodelling in patients with chronic forms of AF is decreased L-type Ca^{2+} current. This has been shown to contribute to APD shortening in AF (Bosch et al., 1999; Skasa et al., 2001; Van Wagoner et al., 1999; Voigt et al., 2012; Workman et al., 2001). Workman et al., (2001) measured $I_{Ca,L}$ in atrial myocytes at various stimulation rates (0.33-10 Hz) and found that, at around 5 Hz, atrial myocytes show a similar of degree of $I_{Ca,L}$ reduction. Therefore, the fast stimulation frequency appropriate for our stress protocol is 3 Hz. In this frequency, the potential role of L-type Ca^{2+} reduction in AF in mitochondrial Ca^{2+} handling can be accounted for. While we also observed smaller $I_{Ca,L}$ in AF myocytes at 0.5 Hz and 3 Hz, compared to CTL - potentially due to the downregulation or posttranslational modifications (i.e. oxidation or hypophosphorylation) of the channel (Christ et al., 2004; Reinhardt et al., 2021) - β-adrenergic stimulation negated this difference, a finding which has previously observed at lower stimulation frequencies (Voigt et al., 2012). Moreover, the effect of ISO on $I_{Ca,L}$ was greater in AF, similar to previous findings (Skasa et al., 2001; Van Wagoner et al., 1999), suggesting that there is no desensitisation to β-adrenergic stimulation in AF (Schotten et al., 2002). Voigt et al. (Voigt et al., 2012) also detected a doubling of cAMP levels in AF patients, which could explain this response to ISO. We conclude, therefore, that L-type Ca^{2+} channels do not play a major role in the redox response of the mitochondria to changes in workload; a reason for this could be the distance between the plasma membrane and mitochondria. Moreover, the lack of extensive t-tubules in atrial myocytes, where L-type Ca^{2+} channels are typically located, further decreases the probability of a direct interaction with mitochondria.

4.4 Oscillatory Ca^{2+} kinetics in human atrial myocytes

Mitochondria Ca^{2+} uptake kinetics is controversial because of a lack of consensus on which model (integrator or oscillatory) prevails in cardiac myocytes (Mason et al., 2020). To our knowledge, we are the first to describe mitochondrial Ca^{2+} handling in human atrial myocytes, where we found oscillatory mitochondrial Ca^{2+} dynamics,

and how this is altered in AF. Oscillatory mitochondrial Ca^{2+} uptake has previously been observed in rat atrial myocytes (Mackenzie et al., 2004). Using Rhod-2 as mitochondrial Ca^{2+} indicator, they also found that subpopulations of mitochondria exhibit varied mitochondrial Ca^{2+} kinetic profiles, where SSM Ca^{2+} transient amplitudes are higher than in IFM. In atria, SSM, together with SERCA on the junctional SR, prevent the formation of Ca^{2+} waves by buffering local SR Ca^{2+} releases and are enriched near the sarcolemma (Bootman et al., 2006; Kockskämper et al., 2001). This restricted Ca^{2+} increase on the periphery of atrial myocytes result in modest twitches, compared to ventricular myocytes. Therefore, Ca^{2+} buffering is possibly more relevant to atrial architecture than that of the ventricles.

Cytosolic Ca^{2+} indicator-loading with cell-impermeant Indo-1 into myocytes incubated with a mitochondrial Ca^{2+} indicator Rhod-2 AM has been previously utilised on ventricular guinea pig myocytes (Kohlhaas & Maack, 2010; Maack et al., 2006). This method displayed oscillatory Ca^{2+} movement in the mitochondria during myocyte contraction at 0.5 Hz and a concomitant increase in diastolic Ca^{2+} level during stress. Wescott et al. (Wescott et al., 2019) used a variation of Ca^{2+} indicator loading, whereby Mitycam-infected cells were dialysed with a pipette solution containing membrane-impermeable Rhod-2 salt, which prevents it from accumulating in the mitochondria. Mitycam is a genetically-encoded Ca^{2+} sensor based on an inverse pericam construct that binds to the Complex IV of the ETC, thus improving specificity (Kettlewell et al., 2009). Their findings dispute the Ca^{2+} threshold for MCU opening and beat-to-beat oscillations in mitochondria Ca^{2+} transients, as they observed a steady-state increase in mitochondrial Ca^{2+}, as well as a sub-micromolar half-activation for mitochondrial Ca^{2+} uptake. Experiments using genetically encoded Ca^{2+} sensors, such as Mitycam, have previously been performed on myocytes from animals with higher heart rates than human (Milani-Nejad & Janssen, 2014) and show higher mitochondrial Ca^{2+} content at higher stimulation rates. It is also possible that the expression of mitochondrial Ca^{2+} handling proteins is different in mammals with higher versus lower heart rates. For example, the resting heart rates of human and mouse are at 80 and 600 beats per minute, respectively. However, during stress, heart rate can increase to a greater extent in human than in mouse. In order to investigate the effect of heart rate on mitochondrial Ca^{2+} accumulation, it would also be important to assess inter-species

differences in mNCLX expression, which is responsible for mitochondrial Ca^{2+} extrusion.

The use of Rhod-2 as a mitochondrial Ca^{2+} indicator is well-established (Andrienko et al., 2009; Kohlhaas et al., 2010; Maack et al., 2006; Trollinger et al., 1997, 2000), with the main concern being remaining cytosolic traces (Dedkova & Blatter, 2012; Fonteriz et al., 2010). The O'Rourke group, used a patch pipette to dialyse the cytosol of cells previously incubated with Rhod-2 and this resulted in a decreased in Rhod-2 signal, to a similar extent as cell permeabilisation (Kohlhaas et al., 2010). Such short dialysis (6 minutes) is arguably a better alternative to the 48-hour incubation time required with adenoviral transfection of mitochondrial Ca^{2+} sensors such as Mitycam (Kettlewell et al., 2009; Lu et al., 2013), as culture of myocytes can affect the morphology of cells overtime (Leach et al., 2005; Louch et al., 2004) and potentially affect ECC mechanisms (Banyasz et al., 2008; Mitcheson et al., 1996). Indeed, investigators using Mitycam have had to address these alterations by doubling extracellular Ca^{2+} concentration and applying ß-adrenergic stimulation (Kettlewell et al., 2009) Moreover, we have performed the Ca^{2+} measurements at physiological rates and temperatures, which were either not applied or were not disclosed in studies using Mitycam (Kettlewell et al., 2009; Lu et al., 2013; Wescott et al., 2019). While we did not calibrate for $[Ca^{2+}]_m$, Ca^{2+} concentrations quantified by genetically encoded Ca^{2+} sensors versus other Ca^{2+} indicators have been reported to be similar (Andrienko et al., 2009; Fernandez-Sanz et al., 2019; Lu et al., 2013). Thus, we believe that the use of Rhod-2 as a mitochondrial Ca^{2+} indicator is an appropriate choice for our investigation. Moreover, computational modelling predicts that very high local Ca^{2+} concentrations in microdomains persist for around 10 ms, which is much less than the observed mitochondrial Ca^{2+} transient rise time in myocytes with Mitycam (Hamilton et al., 2021). Therefore, our observations on the kinetics of mitochondrial Ca^{2+} handling agrees with the structural considerations of SR-mitochondria interaction and the concept of Ca^{2+} microdomains.

4.5 Impaired mitochondrial Ca^{2+} handling in AF atrial myocytes

Ca^{2+} accumulation during changes in workload promotes the parallel activation of ATP hydrolysis (energy utilisation) and regeneration of NADH and $FADH_2$ (energy

production) (Bertero & Maack, 2018; Brandes & Bers, 1997; Saks et al., 2006) and we show here that in AF atrial myocytes the latter is impaired (later onset of recovery during increased workload). Using compartment-specific Ca^{2+} indicators, we were able to show that the rate of uptake and the amplitude of mitochondrial Ca^{2+} transients are smaller in AF atrial myocytes compared to CTL myocytes. Moreover, the Ca^{2+} accumulation in the mitochondria, exhibited by increasing diastolic levels of mitochondrial Ca^{2+}, is less apparent in AF myocytes. Given that the regeneration of NADH and $FADH_2$, at least by the TCA cycle, is Ca^{2+}-activated during increased workload, the impaired mitochondrial Ca^{2+} handling observed in the present study could explain the impaired redox response during increased workload. Additionally, the expression of PDK4 is increased in AF, which phosphorylates the PDH, thus inhibiting this enyzyme.

There are limited information on mitochondrial Ca^{2+} handling in human AF, and the functional investigations of observed mitochondrial function changes in human samples were validated in non-human AF models (J. Li et al., 2022; Wiersma et al., 2019). Wiersma et al. (Wiersma et al., 2019) showed a decrease in mitochondrial Ca^{2+} transient amplitude with tachypacing in HL-1 cells and a Drosophila model (Wiersma et al., 2019), which can be rescued by sub-optimal concentrations of Ru360 (5 µM). Mitochondrial Ca^{2+} uptake block by Ru360 is relevant in protecting against I/R injury by preventing organellar Ca^{2+} overload. Since a transient Ca^{2+} overload might be relevant in the earlier stages of AF (Greiser, 2017; Greiser & Schotten, 2013), the duration of tachypacing might not exactly recapitulate more chronic forms of AF. Moreover, HL-1 cells exhibit neonatal-like mitochondrial organization, where the tight arrangement of mitochondria in between sarcomeres of myocytes relies on efficient phosphotransfer of creatine kinases (Saks et al., 2006), which is not the case in the filamentous and relatively more dynamic mitochondria of HL-1 cells (Anmann et al., 2006; Kuznetsov et al., 2006).

Unexpectedly, we observed increased MCU expression, which was recently shown to be unchanged in tachypaced HL-1 cells (Wiersma et al., 2019). The same group also showed that MCU overexpression and knockdown do *not* alter the mitochondrial Ca^{2+} transient, suggesting the potential role of MCU regulators. Interestingly, we observed unchanged MICU1 but lower MICU2 protein expression

in the AF group, compared to CTL. Unchanged MICU1 expression relative to reduced MICU2 expression has previously been shown (Payne et al., 2017). Loss of MICU2 increases mitochondrial Ca^{2+} uptake, due to reduced gatekeeping (Payne et al., 2017), a role initially attributed exclusively to MICU2. We speculate, therefore, that the decreased MICU2/MCU ratio we observe is a compensatory mechanism to try to maintain mitochondrial Ca^{2+}. This furthers the notion that Ca^{2+} microdomain must be indispensable for efficient mitochondrial Ca^{2+} uptake. Computational modelling predicts that MICU1/2 heterodimers bound to MCU can be activated within 60 nm from IP_3R, to activate mitochondrial Ca^{2+} entry (Payne et al., 2017). However, since cooperative activation of MCU requires Ca^{2+} binding to the EF hands in both MICU subunits (Kamer & Mootha, 2014; Payne et al., 2017), the reduced amount of MICU2 in AF could affect dimer formation with MICU1 and cause MCU complex destabilisation, and we suggest this could be responsible for reduced mitochondrial Ca^{2+} entry observed in AF. Cardiac Ca^{2+} signals have been shown to recruit MCU preferentially on the SR-mitochondria interface (De la Fuente et al., 2016), and this could explain the increased MCU expression in human AF tissue versus the unchanged tachypaced HL-1 cells. Ca^{2+} signals – oscillations (Dolmetsch et al., 1998) and sparks (W. H. Li et al., 1998) – can results in long-lasting effects on the nucleus by regulating gene expression. The idea of a mitochondrial memory mechanism (Jouaville et al., 1999) was introduced by the Rizzuto group, and describes a process where Ca^{2+} signals experienced by the mitochondria can result in a persistent change, so as to still provide the required amount of energy without the risk of Ca^{2+} overload. Changes in mitochondrial morphology is one of the possible long-term effects of this signal (Jouaville et al., 1999), and we show that mitochondria in AF are seemingly smaller and located further from the SR.

Altogether, in the context of intact myocytes, the reduced mitochondrial Ca^{2+} transients might point to an indispensable role of SR mitochondria interaction in mitochondrial Ca^{2+} handling, and its disturbance in AF might be counterbalanced by a compensatory regulation of MCU complex activity.

4.6 Impaired interaction of mitochondria and SR in AF

The present study demonstrated that the mitochondrial Ca^{2+} transient peaks before the cytosolic Ca^{2+} transient, in agreement with, previous observations in guinea pig cardiac myocytes (Kohlhaas & Maack, 2010). This difference in kinetics has been attributed to the presence of Ca^{2+} microdomains between SR and mitochondria, where the latter acts as a Ca^{2+} sink during global increases in Ca^{2+}.

The close interaction of SR, mitochondria and myofilaments is integral to ECC and bioenergetic coupling, facilitating efficient responses to transitions in workload (Maack & O'Rourke, 2007). We have employed super-resolution microscopy and electron tomography to investigate structural changes involving mitochondria and SR in AF, which could be consequential for Ca^{2+} handling.

First, we showed using STED nanoscopy of CTL tissue sections, the ultrastructure which is important for maintaining Ca^{2+} microdomains. The use of VDAC1 antibody to label mitochondria can be justified by 1) its greatest abundance among the three VDAC isoforms in mammals (Camara et al., 2017), 2) the similar colocalisation of VDAC1 and VDAC2 previously observed in human U2OS cells (U2OS) using two-color STED (Neumann et al., 2010), and 3) the specific antibody used for VDAC1 staining exhibited the expected mitochondrial staining pattern in the preliminary antibody screening using mouse ventricular myocytes. The VDAC2 isoform has been shown to associate with RyR2 in rat ventricular cardiomyocytes (Min et al., 2012), however its expression was restricted to the subsarcolemmal region. These heterogeneity in VDAC isoform expression might be explained by differences in atrial and ventricular myocyte architecture, where a denser occurrence of mitochondria in between the filaments has been suggested (Brandenburg et al., 2016).

RyR2 hyperactivity has been associated with AF (Neef et al., 2010; Voigt et al., 2012, 2014; Xie et al., 2015), where a reduction in SR Ca^{2+} release threshold contributes to higher diastolic Ca^{2+} leak, potentiating the occurrence of DADs (Voigt et al., 2012). Such hyperactivity can be attributed to RyR2 phosphorylation or oxidation (Waddell et al., 2016), although RyR2 cluster fragmentation and

displacement from the Z-line have also been observed in tachypaced sheep atria, resulting in higher Ca^{2+} spark frequency and dimensions (Macquaide et al., 2015). This cross-species heterogeneity can attributed to differences of arrhythmogenesis aetiology between these models (Munro et al., 2021). Therefore, further analysis of our RyR2 STED images could help in identifying mechanisms underlying the Ca^{2+} leak results. Turning to the mitochondria, we observed reduced clustering of VDAC1 with RyR2 in AF tissue. This is supported by electron microscopy and tomography data, which showed increased distance between SR and mitochondria, and this provides a mechanistic basis for the Ca^{2+} handling findings, as disturbance of Ca^{2+} microdomains would likely affect mitochondrial Ca^{2+} uptake.

Changes in mitochondrial morphology have been shown to contribute to cardiac arrhythmia; a model of late I_{Na}-induced atrial fibrillation showed changes in mitochondrial structure and function, as well as decreased Mfn2 expression, which were all reversed when mice were crossed with mice exhibiting increased antioxidative capacity (Avula et al., 2021; Xie et al., 2015). Sinoatrial nodal cells from a TAC-induced heart failure mouse model exhibited compromised automaticity, which was attributed to mitochondrial dysfunction following SR-mitochondrial disruption. This phenotype was mimicked by Mfn2 knockdown specific to the SAN (Ren et al., 2022). Mfn2 knockdown in mice caused dysfunction of Ca^{2+}-dependent mechanisms in the mitochondria (Chen et al., 2012). More recently, Mfn2 downregulation has been observed in experimental models and samples from patients with AF, where mitochondria associate less with the SR on account of microtubule disruption (J. Li et al., 2022). Microtubule disruption can also prevent transport of defective mitochondria from the intermyofibrillar to the perinuclear region for mitophagy (Lu et al., 2019), a process which appears to be defective in human AF (Andres et al., 2017). Moreover, perinuclear mitochondria have also been shown to experience low Ca^{2+} exposure, owing to their distance from RyR2 clusters (Lu et al., 2019), resulting in reduced and slow Ca^{2+} accumulation. These findings demonstrate that Ca^{2+} handling by different cardiac subpopulations of mitochondria play different roles. In the present study, however, we did not observe any differences in Ca^{2+} handling proteins present on the interface between SR and OMM.

Our data show smaller mitochondria in AF tissue and this could be due to mitochondrial fission. Intracellular Ca^{2+} can influence mitochondrial morphology in cardiac myocytes (J. Hom et al., 2010; J. R. Hom et al., 2007; Szabadkai, Simoni, et al., 2006), whereby increases in intracellular Ca^{2+} can transiently promote mitochondrial fragmentation by promoting mitochondrial translocation of Dlp1 (Smirnova et al., 1998), also known as Drp1, a process facilitated by Fis1 (Yoon et al., 2003). However, we did not observe differences in expression of fission proteins in AF.

The role of cytoskeletal elements in maintaining SR-mitochondria contact has recently been demonstrated in AF models (J. Li et al., 2022). βII-tubulin has been shown to associate with VDAC in adult rat cardiac myocytes, which was not present in HL-1 cells (Guzun et al., 2011). The presence of βII-tubulin is argued to help maintain the compartmentalisation of phosphocreatine systems in cardiac myocytes. However, we did not observe a difference in the expression of TUBB2A between CTL and AF.

4.7 Normalisation of mitochondrial Ca^{2+} uptake as a potential therapeutic for AF

Targeting ROS using antioxidants decreased the incidence of postoperative AF in some clinical trials (Carnes et al., 2001; Rodrigo et al., 2013). However, antioxidant therapy needs fine-tuning as different stages of AF have varied predominant ROS sources, so such targeted suppression can affect physiological ROS signalling. Therefore, it might be more beneficial to target the sources of ROS instead of ROS *per se*. Here, we showed that 1 µM Ezetimibe tends to decrease the presence of spontaneous Ca^{2+} releases in AF atrial myocytes, and it reduced the occurrence of Ca^{2+} sparks in iPSC-derived atrial myocytes – known phenomena in arrhythmic events.

Blocking of mitochondrial Ca^{2+} uptake, dissipation of $\Delta\psi_m$, and inhibition of ATP synthesis and the ETC complexes, as well as αKGDH, have been shown to promote Ca^{2+} alternans in rabbit and cat atrial myocytes, with the MCU activator spermine, reversing such effect in these myocytes (Florea & Blatter, 2010; Oropeza-Almazán

& Blatter, 2020). Also, mitochondrial depolarisation has also been suggested to be the culprit for alternans in ventricles (Smith et al., 2013). Recently, restoration of ventricular rhythmicity by improved Ca^{2+} uptake in small animal and iPSC-derived cardiomyocyte models of ventricular arrhythmia (Sander et al., 2020; Shimizu et al., 2015). Activators of mitochondrial Ca^{2+} uptake such as the VDAC2 activator efsevin and the MCU activator kaempferol show a capacity to improve mitochondrial Ca^{2+} uptake but have poor translational potential due to the high effective concentrations observed in previous studies. Recently, the screening of the clinically-approved drugs Ezetimibe and disulfiram enhanced mitochondrial Ca^{2+} uptake with an EC_{50} in the nanomolar range (Sander, Feng, et al., 2021). However, disulfiram, used to treat alcohol dependence, exerts developmental effects in zebrafish, leaving Ezetimibe as the more viable candidate due to its minimal side effects. Whether the favourable effects of Ezetimibe can be recapitulated in clinically-relevant models of AF remains to be seen.

Ezetimibe is currently used, either in monotherapy or in combination with statins, to inhibit cholesterol absorption (Kosoglou et al., 2005). Its role in inhibiting cholesterol uptake is associated to its putative target, the Niemann-Pick C1 Like 1 (NPC1L1) protein (Kosoglou et al., 2005). The cardiovascular benefits of Ezetimibe has been demonstrated in clinical trials, where using it in conjunction with a statin, it can reduce atherosclerotic cardiovascular diseases, especially in older patients. In patients with aortic stenosis, AF burden was unchanged whether Ezetimibe was used with simvastatin or not (Bang et al., 2012). Therefore, further investigation on the pleiotropic effect of these drugs would be a valuable area of research.

5 Limitations

We only had access to RAAs, which are routinely excised during open heart surgeries. While biochemical data on mitochondrial parameters have been previously reported in left atrial appendages, mitochondrial function on live atrial myocytes must be explored. However, right atrial tissue is also a relevant source of ectopic impulses and rotors. Confounding clinical factors such as differences in ß-blocker and diuretic intake (**Table 12**) may be better analysed with substratification of patients.

The techniques used in the present study are likely to have subjected the myocytes to considerable stress, thus limiting the time that experimental observations could be made. While there were no dynamic measurements of ROS and mitochondrial membrane potential, these will be addressed in future investigations. Immunoblotting of mitochondrial proteins were performed on tissue lysates, rather than mitochondrial extracts or membrane-associated membrane isolations. However, we were still able to observe discernable bands for all mitochondrial and other membrane proteins assessed. The physical association of SR and mitochondrial tethers can further be examined by imaging by biochemical methods, such as proximity ligation assay and co-immunopecipitation. Since the major Ca^{2+} efflux mechanism in mitochondria is Na^{+}-dependent, and Na^{+} currents have been reported to be altered in AF (Sossalla et al., 2010), the mitochondrial function of atrial myocytes in response to higher Na^{+} concentration must be examine. Furthermore, modulation of the mNCLX in AF would be worth checking, as its benefits in improving mitochondrial Ca^{2+} retention in the context of elevated Na^{+} levels (Kohlhaas et al., 2010; T. Liu & Rourke, 2008). With regard to investigations of Ezetimibe, its effects should be compared with an established Ca^{2+} uptake enhancer, such as kaempferol. Moreover, it cannot be discounted that Ezetimibe can affect other Ca^{2+} handling proteins, such as RyR2, which can also promote increased available Ca^{2+} for mitochondrial uptake. Therefore, this must be examined, potentially by single channel recording of RyR2 in the presence of Ezetimibe.

6 Conclusion and Outlook

Altogether, we found that the mitochondrial-SR distance widening, given the architecture of the atrial myocyte where mitochondria are able to buffer Ca^{2+} in the subsarcolemmal space, can further prevent effective mitochondrial Ca^{2+} transfer. This is particularly worse in conditions of increased workload, where impaired mitochondrial Ca^{2+} handling affects Ca^{2+}-activated processes in the mitochondria, such as the regeneration of electron donors NADH and $FADH_{2.}$ However, potential compensatory mechanisms involving mitochondrial Ca2+ uptake via the IMM were unraveled, which could prevent detrimental mitochondrial Ca^{2+} loss.

Overall, the study highlights the alterations in mitochondrial Ca^{2+} in long-standing persistent AF, and adds to the growing field of research focussed on normalisation of mitochondrial Ca^{2+} uptake as a potential therapeutic target in AF. Their pleiotropic effects on the mitochondria could pave the way for drug repurposing of Ezetimibe, due to its low effective concentration in improving rhythmicity in tachycardia models due to improved mitochondrial Ca^{2+} uptake, with minimal side-effects. This warrants long-term studies with patients taking Ezetimibe and whether this is associated with lowering AF burden.

7 Bibliography

Abramov, A. Y., & Bartolomé, F. (2015). Measurement of Mitochondrial NADH and FAD Autofluorescence in Live Cells Chapter 23 Measurement of Mitochondrial NADH and FAD Autofl uorescence in Live Cells. *Methods in Molecular Biology*, *1264*.

Abu-Alrub, S., Strik, M., Ramirez, F. D., Moussaoui, N., Racine, H. P., Marchand, H., Buliard, S., Haïssaguerre, M., Ploux, S., & Bordachar, P. (2022). Smartwatch Electrocardiograms for Automated and Manual Diagnosis of Atrial Fibrillation: A Comparative Analysis of Three Models. *Frontiers in Cardiovascular Medicine*, *9*. https://doi.org/10.3389/fcvm.2022.836375

Akar, F. G., Aon, M. A., Tomaselli, G. F., & O'Rourke, B. (2005). The mitochondrial origin of postischemic arrhythmias. *Journal of Clinical Investigation*, *115*(12), 3527–3535. https://doi.org/10.1172/JCI25371

Ambrus, A. (2019). An Updated View on the Molecular Pathomechanisms of Human Dihydrolipoamide Dehydrogenase Deficiency in Light of Novel Crystallographic Evidence. *Neurochemical Research*, *44*(10), 2307–2313. https://doi.org/10.1007/s11064-019-02766-9

Anderson, E. J., Efird, J. T., Davies, S. W., O'Neal, W. T., Darden, T. M., Thayne, K. A., Katunga, L. A., Kindell, L. C., Ferguson, T. B., Anderson, C. A., Chitwood, W. R., Koutlas, T. C., Williams, J. M., Rodriguez, E., & Kypson, A. P. (2014). Monoamine oxidase is a major determinant of redox balance in human atrial myocardium and is associated with postoperative atrial fibrillation. *J Am Heart Assoc*, *3*(1), e000713. https://doi.org/10.1161/jaha.113.000713

Andres, A. M., Tucker, K. C., Thomas, A., Taylor, D. J., Sengstock, D., Jahania, S. M., Dabir, R., Pourpirali, S., Brown, J. A., Westbrook, D. G., Ballinger, S. W., Mentzer Jr., R. M., & Gottlieb, R. A. (2017). Mitophagy and mitochondrial biogenesis in atrial tissue of patients undergoing heart surgery with cardiopulmonary bypass. *JCI Insight*, *2*(4), e89303. https://doi.org/10.1172/jci.insight.89303

Andrienko, T. N., Picht, E., & Bers, D. M. (2009). Mitochondrial free calcium regulation during sarcoplasmic reticulum calcium release in rat cardiac myocytes. *Journal of Molecular and Cellular Cardiology*, *46*(6). https://doi.org/10.1016/j.yjmcc.2009.03.015

Anmann, T., Guzun, R., Beraud, N., Pelloux, S., Kuznetsov, A. V., Kogerman, L., Kaambre, T., Sikk, P., Paju, K., Peet, N., Seppet, E., Ojeda, C., Tourneur, Y., & Saks, V. (2006). Different kinetics of the regulation of respiration in permeabilized cardiomyocytes and in HL-1 cardiac cells. Importance of cell structure/organization for respiration regulation. *Biochimica et Biophysica Acta - Bioenergetics*, *1757*(12). https://doi.org/10.1016/j.bbabio.2006.09.008

Aon, M. A., Cortassa, S., Marbán, E., & O'Rourke, B. (2003). Synchronized Whole Cell Oscillations in Mitochondrial Metabolism Triggered by a Local Release of Reactive Oxygen Species in Cardiac Myocytes. *Journal of Biological Chemistry*, *278*(45), 44735–44744. https://doi.org/10.1074/jbc.M302673200

Aon, M. A., Cortassa, S., & O'Rourke, B. (2010). Redox-optimized ROS balance: a unifying hypothesis. *Biochim Biophys Acta*, *1797*(6–7), 865–877. https://doi.org/10.1016/j.bbabio.2010.02.016

Armoundas, A. A., Tomaselli, G. F., & Esperer, H. D. (2002). Pathophysiological basis and clinical application of T-wave alternans. In *Journal of the American*

College of Cardiology (Vol. 40, Issue 2). https://doi.org/10.1016/S0735-1097(02)01960-5

Avula, U. M. R., Dridi, H., Chen, B. X., Yuan, Q., Katchman, A. N., Reiken, S. R., Desai, A. D., Parsons, S., Baksh, H., Ma, E., Dasrat, P., Ji, R., Lin, Y., Sison, C., Lederer, W. J., Joca, H. C., Ward, C. W., Greiser, M., Marks, A. R., … Wan, E. Y. (2021). Attenuating persistent sodium current- induced atrial myopathy and fibrillation by preventing mitochondrial oxidative stress. *JCI Insight*, *6*(23). https://doi.org/10.1172/jci.insight.147371

Balaban, R. S. (2002). Cardiac Energy Metabolism Homeostasis: Role of Cytosolic Calcium. *Journal of Molecular and Cellular Cardiology*, *34*(10). https://doi.org/10.1006/jmcc.2002.2082

Balaban, R. S., Nemoto, S., & Finkel, T. (2005). Mitochondria, oxidants, and aging. *Cell*, *120*(4), 483–495. https://doi.org/10.1016/j.cell.2005.02.001

Bang, C. N., Greve, A. M., Boman, K., Egstrup, K., Gohlke-Baerwolf, C., Køber, L., Nienaber, C. A., Ray, S., Rossebø, A. B., & Wachtell, K. (2012). Effect of lipid lowering on new-onset atrial fibrillation in patients with asymptomatic aortic stenosis: The Simvastatin and Ezetimibe in Aortic Stenosis (SEAS) study. *American Heart Journal*, *163*(4). https://doi.org/10.1016/j.ahj.2012.01.026

Banyasz, T., Lozinskiy, I., Payne, C. E., Edelmann, S., Norton, B., Chen, B., Chen-Izu, Y., Izu, L. T., & Balke, C. W. (2008). Transformation of adult rat cardiac myocytes in primary culture. *Experimental Physiology*, *93*(3). https://doi.org/10.1113/expphysiol.2007.040659

Baris, O. R., Ederer, S., Neuhaus, J. F. G., von Kleist-Retzow, J. C., Wunderlich, C. M., Pal, M., Wunderlich, F. T., Peeva, V., Zsurka, G., Kunz, W. S., Hickethier, T., Bunck, A. C., Stöckigt, F., Schrickel, J. W., & Wiesner, R. J. (2015). Mosaic Deficiency in Mitochondrial Oxidative Metabolism Promotes Cardiac Arrhythmia during Aging. *Cell Metabolism*, *21*(5), 667–677. https://doi.org/10.1016/j.cmet.2015.04.005

Barth, A. S., Merk, S., Arnoldi, E., Zwermann, L., Kloos, P., Gebauer, M., Steinmeyer, K., Bleich, M., Kääb, S., Hinterseer, M., Kartmann, H., Kreuzer, E., Dugas, M., Steinbeck, G., & Nabauer, M. (2005). Reprogramming of the Human Atrial Transcriptome in Permanent Atrial Fibrillation. *Circulation Research*, *96*(9), 1022–1029. https://doi.org/10.1161/01.RES.0000165480.82737.33

Bay, J., Kohlhaas, M., & Maack, C. (2013). Intracellular Na+ and cardiac metabolism. *Journal of Molecular and Cellular Cardiology*, *61*, 20–27. https://doi.org/10.1016/j.yjmcc.2013.05.010

Bedard, K., & Krause, K. H. (2007). The NOX family of ROS-generating NADPH oxidases: Physiology and pathophysiology. In *Physiological Reviews* (Vol. 87, Issue 1). https://doi.org/10.1152/physrev.00044.2005

Belevych, A. E., Terentyev, D., Viatchenko-Karpinski, S., Terentyeva, R., Sridhar, A., Nishijima, Y., Wilson, L. D., Cardounel, A. J., Laurita, K. R., Carnes, C. A., Billman, G. E., & Gyorke, S. (2009). Redox modification of ryanodine receptors underlies calcium alternans in a canine model of sudden cardiac death. *Cardiovascular Research*, *84*(3). https://doi.org/10.1093/cvr/cvp246

Benjamin, E. J., Levy, D., Vaziri, S. M., D'agostino, R. B., Belanger, A. J., & Wolf, P. A. (1994). Independent Risk Factors for Atrial Fibrillation in a Population-Based Cohort: The Framingham Heart Study. *JAMA: The Journal of the American Medical Association*. https://doi.org/10.1001/jama.1994.03510350050036

Bers, D. M. (2008). Calcium cycling and signaling in cardiac myocytes. In *Annual Review of Physiology* (Vol. 70). https://doi.org/10.1146/annurev.physiol.70.113006.100455

Bers, D. M., Bassani, J. W. M., & Bassani, R. A. (1996). Na-Ca exchange and Ca fluxes during contraction and relaxation in mammalian ventricular muscle. *Annals of the New York Academy of Sciences*, *779*. https://doi.org/10.1111/j.1749-6632.1996.tb44818.x

Bertero, E., & Maack, C. (2018). Calcium signaling and reactive oxygen species in Mitochondria. In *Circulation Research*. https://doi.org/10.1161/CIRCRESAHA.118.310082

Beutner, G., Sharma, V. K., Lin, L., Ryu, S.-Y., Dirksen, R. T., & Sheu, S.-S. (2005). Type 1 ryanodine receptor in cardiac mitochondria: Transducer of excitation–metabolism coupling. *Biochimica et Biophysica Acta (BBA) - Biomembranes*, *1717*(1), 1–10. https://doi.org/10.1016/j.bbamem.2005.09.016

Bhosale, G., Sharpe, J. A., Sundier, S. Y., & Duchen, M. R. (2015). Calcium signaling as a mediator of cell energy demand and a trigger to cell death. *Annals of the New York Academy of Sciences*. https://doi.org/10.1111/nyas.12885

Blacker, T. S., & Duchen, M. R. (2016). Investigating mitochondrial redox state using NADH and NADPH autofluorescence. In *Free Radical Biology and Medicine* (Vol. 100). https://doi.org/10.1016/j.freeradbiomed.2016.08.010

Bootman, M. D., Higazi, D. R., Coombes, S., & Roderick, H. L. (2006). Calcium signalling during excitation-contraction coupling in mammalian atrial myocytes. *Journal of Cell Science*, *119*(19). https://doi.org/10.1242/jcs.03223

Bosch, R. F., Zeng, X., Grammer, J. B., Popovic, K., Mewis, C., & Kühlkamp, V. (1999). Ionic mechanisms of electrical remodeling in human atrial fibrillation. *Cardiovascular Research*, *44*(1). https://doi.org/10.1016/S0008-6363(99)00178-9

Bragadin, M., Pozzan, T., & Azzone, G. F. (1979). Kinetics of Ca2+ Carrier in Rat Liver Mitochondria†. *Biochemistry*, *18*(26). https://doi.org/10.1021/bi00593a033

Brandenburg, S., Arakel, E. C., Schwappach, B., & Lehnart, S. E. (2016). The molecular and functional identities of atrial cardiomyocytes in health and disease. *Biochim Biophys Acta*, *1863*(7 Pt B), 1882–1893. https://doi.org/10.1016/j.bbamcr.2015.11.025

Brandes, R., & Bers, D. M. (1996). Increased work in cardiac trabeculae causes decreased mitochondrial NADH fluorescence followed by slow recovery. *Biophysical Journal*, *71*(2). https://doi.org/10.1016/S0006-3495(96)79303-7

Brandes, R., & Bers, D. M. (1997). Intracellular Ca2+ increases the mitochondrial NADH concentration during elevated work in intact cardiac muscle. *Circulation Research*, *80*(1). https://doi.org/10.1161/01.RES.80.1.82

Brandes, R., & Bers, D. M. (2002). Simultaneous measurements of mitochondrial NADH and Ca2+ during increased work in intact rat heart trabeculae. *Biophysical Journal*, *83*(2). https://doi.org/10.1016/S0006-3495(02)75194-1

Brown, D. A., Perry, J. B., Allen, M. E., Sabbah, H. N., Stauffer, B. L., Shaikh, S. R., Cleland, J. G. F., Colucci, W. S., Butler, J., Voors, A. A., Anker, S. D., Pitt, B., Pieske, B., Filippatos, G., Greene, S. J., & Gheorghiade, M. (2017). Expert consensus document: Mitochondrial function as a therapeutic target in heart failure. *Nature Reviews Cardiology*, *14*(4). https://doi.org/10.1038/nrcardio.2016.203

Brundel, B. J. J. M., Ai, X., Hills, M. T., Kuipers, M. F., Lip, G. Y. H., & de Groot, N. M. S. (2022). Atrial fibrillation. *Nature Reviews Disease Primers*, *8*(1), 21. https://doi.org/10.1038/s41572-022-00347-9

Bukowska, A., Schild, L., Keilhoff, G., Hirte, D., Neumann, M., Gardemann, A., Neumann, K. H., Rohl, F. W., Huth, C., Goette, A., & Lendeckel, U. (2008). Mitochondrial dysfunction and redox signaling in atrial tachyarrhythmia. *Exp Biol Med (Maywood)*, *233*(5), 558–574. https://doi.org/10.3181/0706-rm-155

Buntinas, L., Gunter, K. K., Sparagna, G. C., & Gunter, T. E. (2001). The rapid mode of calcium uptake into heart mitochondria (RaM): comparison to RaM in liver mitochondria. *Biochimica et Biophysica Acta (BBA) - Bioenergetics*, *1504*(2–3), 248–261. https://doi.org/10.1016/S0005-2728(00)00254-1

Camara, A. K. S., Zhou, Y. F., Wen, P. C., Tajkhorshid, E., & Kwok, W. M. (2017). Mitochondrial VDAC1: A key gatekeeper as potential therapeutic target. In *Frontiers in Physiology* (Vol. 8, Issue JUN). https://doi.org/10.3389/fphys.2017.00460

Cao, Y., Xu, C., Ye, J., He, Q., Zhang, X., Jia, S., Qiao, X., Zhang, C., Liu, R., Weng, L., Liu, Y., Liu, L., & Zheng, M. (2019). Miro2 regulates inter-mitochondrial communication in the heart and protects against TAC-Induced cardiac dysfunction. *Circulation Research*, *125*(8). https://doi.org/10.1161/CIRCRESAHA.119.315432

Carafoli, E., Tiozzo, R., Lugli, G., Crovetti, F., & Kratzing, C. (1974). The release of calcium from heart mitochondria by sodium. *Journal of Molecular and Cellular Cardiology*, *6*(4), 361–371. https://doi.org/10.1016/0022-2828(74)90077-7

Carnes, C. A., Chung, M. K., Nakayama, T., Nakayama, H., Baliga, R. S., Piao, S., Kanderian, A., Pavia, S., Hamlin, R. L., McCarthy, P. M., Bauer, J. A., & Van Wagoner, D. R. (2001). Ascorbate attenuates atrial pacing-induced peroxynitrite formation and electrical remodeling and decreases the incidence of postoperative atrial fibrillation. *Circulation Research*, *89*(6). https://doi.org/10.1161/hh1801.097644

Chance, B., Cohen, P., Jobsis, F., & Schoener, B. (1962). Intracellular Oxidation-reduction states in vivo. *Science*, *137*(3529). https://doi.org/10.1126/science.137.3529.499

Chance, B., Schoener, B., Oshino, R., Itshak, F., & Nakase, Y. (1979). Oxidation-reduction ratio studies of mitochondria in freeze-trapped samples. NADH and flavoprotein fluorescence signals. *Journal of Biological Chemistry*, *254*(11). https://doi.org/10.1016/s0021-9258(17)30079-0

Chen, Y., Csordás, G., Jowdy, C., Schneider, T. G., Csordás, N., Wang, W., Liu, Y., Kohlhaas, M., Meiser, M., Bergem, S., Nerbonne, J. M., Dorn, G. W., & Maack, C. (2012). Mitofusin 2-containing mitochondrial-reticular microdomains direct rapid cardiomyocyte bioenergetic responses via interorganelle Ca2+ crosstalk. *Circulation Research*. https://doi.org/10.1161/CIRCRESAHA.112.266585

Cheng, H., Lederer, W. J., & Cannell, M. B. (1993). Calcium sparks: Elementary events underlying excitation-contraction coupling in heart muscle. *Science*, *262*(5134). https://doi.org/10.1126/science.8235594

Chiang, D. Y., Li, N., Wang, Q., Alsina, K. M., Quick, A. P., Reynolds, J. O., Wang, G., Skapura, D., Voigt, N., Dobrev, D., & Wehrens, X. H. T. (2014). Impaired local regulation of ryanodine receptor type 2 by protein phosphatase 1 promotes atrial fibrillation. *Cardiovascular Research*, *103*(1), 178–187. https://doi.org/10.1093/cvr/cvu123

Christ, T., Boknik, P., Wöhrl, S., Wettwer, E., Graf, E. M., Bosch, R. F., Knaut, M.,

Schmitz, W., Ravens, U., & Dobrev, D. (2004). L-type Ca2+ current downregulation in chronic human atrial fibrillation is associated with increased activity of protein phosphatases. *Circulation*. https://doi.org/10.1161/01.CIR.0000145659.80212.6A

Cooper, L. L., Li, W., Lu, Y., Centracchio, J., Terentyeva, R., Koren, G., & Terentyev, D. (2013). Redox modification of ryanodine receptors by mitochondria-derived reactive oxygen species contributes to aberrant Ca2+ handling in ageing rabbit hearts. *Journal of Physiology*. https://doi.org/10.1113/jphysiol.2013.260521

Cortassa, S., Aon, M. A., Winslow, R. L., & O'Rourke, B. (2004). A Mitochondrial Oscillator Dependent on Reactive Oxygen Species. *Biophysical Journal*, *87*(3), 2060–2073. https://doi.org/10.1529/biophysj.104.041749

Cortassa, S., O'Rourke, B., & Aon, M. A. (2014). Redox-optimized ROS balance and the relationship between mitochondrial respiration and ROS. *Biochim Biophys Acta*, *1837*(2), 287–295. https://doi.org/10.1016/j.bbabio.2013.11.007

Cross, H. R., Clarke, K., Opie, L. H., & Radda, G. K. (1995). Is lactate-induced myocardial ischaemic injury mediated by decreased pH or increased intracellular lactate? *Journal of Molecular and Cellular Cardiology*, *27*(7). https://doi.org/10.1006/jmcc.1995.0130

Csordás, G., Várnai, P., Golenár, T., Roy, S., Purkins, G., Schneider, T. G., Balla, T., & Hajnóczky, G. (2010). Imaging Interorganelle Contacts and Local Calcium Dynamics at the ER-Mitochondrial Interface. *Molecular Cell*, *39*(1). https://doi.org/10.1016/j.molcel.2010.06.029

D'Autréaux, B., & Toledano, M. B. (2007). ROS as signalling molecules: Mechanisms that generate specificity in ROS homeostasis. In *Nature Reviews Molecular Cell Biology* (Vol. 8, Issue 10). https://doi.org/10.1038/nrm2256

D'Eletto, M., Rossin, F., Occhigrossi, L., Farrace, M. G., Faccenda, D., Desai, R., Marchi, S., Refolo, G., Falasca, L., Antonioli, M., Ciccosanti, F., Fimia, G. M., Pinton, P., Campanella, M., & Piacentini, M. (2018). Transglutaminase Type 2 Regulates ER-Mitochondria Contact Sites by Interacting with GRP75. *Cell Reports*, *25*(13). https://doi.org/10.1016/j.celrep.2018.11.094

de Brito, O. M., & Scorrano, L. (2008). Mitofusin 2 tethers endoplasmic reticulum to mitochondria. *Nature*, *456*(7222), 605–610. https://doi.org/10.1038/nature07534

De la Fuente, S., Fernandez-Sanz, C., Vail, C., Agra, E. J., Holmstrom, K., Sun, J., Mishra, J., Williams, D., Finkel, T., Murphy, E., Joseph, S. K., Sheu, S. S., & Csordás, G. (2016). Strategic positioning and biased activity of the mitochondrial calcium uniporter in cardiac muscle. *Journal of Biological Chemistry*, *291*(44). https://doi.org/10.1074/jbc.M116.755496

De La Fuente, S., Lambert, J. P., Nichtova, Z., Fernandez Sanz, C., Elrod, J. W., Sheu, S. S., & Csordás, G. (2018). Spatial Separation of Mitochondrial Calcium Uptake and Extrusion for Energy-Efficient Mitochondrial Calcium Signaling in the Heart. *Cell Reports*, *24*(12). https://doi.org/10.1016/j.celrep.2018.08.040

De Stefani, D., Raffaello, A., Teardo, E., Szabó, I., & Rizzuto, R. (2011). A forty-kilodalton protein of the inner membrane is the mitochondrial calcium uniporter. *Nature*. https://doi.org/10.1038/nature10230

De Stefani, D., Rizzuto, R., & Pozzan, T. (2016). Enjoy the Trip: Calcium in Mitochondria Back and Forth. *Annual Review of Biochemistry*, *85*(1), 161–192. https://doi.org/10.1146/annurev-biochem-060614-034216

De vos, K. J., Mórotz, G. M., Stoica, R., Tudor, E. L., Lau, K. F., Ackerley, S., Warley, A., Shaw, C. E., & Miller, C. C. J. (2012). VAPB interacts with the mitochondrial

protein PTPIP51 to regulate calcium homeostasis. *Human Molecular Genetics*, *21*(6). https://doi.org/10.1093/hmg/ddr559

Dedkova, E. N., & Blatter, L. A. (2012). Measuring mitochondrial function in intact cardiac myocytes. In *Journal of Molecular and Cellular Cardiology* (Vol. 52, Issue 1). https://doi.org/10.1016/j.yjmcc.2011.08.030

Denton, R. M., Randle, P. J., & Martin, B. R. (1972). Stimulation by calcium ions of pyruvate dehydrogenase phosphate phosphatase. *The Biochemical Journal*. https://doi.org/10.1042/bj1280161

Denton, R. M., Richards, D. A., & Chin, J. G. (1978). Calcium ions and the regulation of NAD+-linked isocitrate dehydrogenase from the mitochondria of rat heart and other tissues. *Biochemical Journal*. https://doi.org/10.1042/bj1760899

Dolmetsch, R. E., Xu, K., & Lewis, R. S. (1998). Calcium oscillations increase the efficiency and specificity of gene expression. *Nature*, *392*(6679). https://doi.org/10.1038/31960

Dorn, G. W. (2009). Apoptotic and non-apoptotic programmed cardiomyocyte death in ventricular remodelling. In *Cardiovascular Research* (Vol. 81, Issue 3). https://doi.org/10.1093/cvr/cvn243

Dorn, G. W., & Maack, C. (2013). SR and mitochondria: Calcium cross-talk between kissing cousins. In *Journal of Molecular and Cellular Cardiology* (Vol. 55, Issue 1). https://doi.org/10.1016/j.yjmcc.2012.07.015

Dudley, S. C., Hoch, N. E., McCann, L. A., Honeycutt, C., Diamandopoulos, L., Fukai, T., Harrison, D. G., Dikalov, S. I., & Langberg, J. (2005). Atrial fibrillation increases production of superoxide by the left atrium and left atrial appendage: Role of the NADPH and xanthine oxidases. *Circulation*, *112*(9). https://doi.org/10.1161/CIRCULATIONAHA.105.538108

Edfors, F., Hober, A., Linderbäck, K., Maddalo, G., Azimi, A., Sivertsson, Å., Tegel, H., Hober, S., Szigyarto, C. A. K., Fagerberg, L., von Feilitzen, K., Oksvold, P., Lindskog, C., Forsström, B., & Uhlen, M. (2018). Enhanced validation of antibodies for research applications. *Nature Communications*, *9*(1). https://doi.org/10.1038/s41467-018-06642-y

Edwards, J. N., & Blatter, L. A. (2014). Cardiac alternans and intracellular calcium cycling. *Clinical and Experimental Pharmacology and Physiology*, *41*(7), 524–532. https://doi.org/10.1111/1440-1681.12231

Einthoven, W. (1997). THE GALVANOMETRIC REGISTRATION OF THE HUMAN ELECTROCARDIOGRAM, LIKEWISE A REVIEW OF THE USE OF THE CAPILLARY-ELECTROMETER IN PHYSIOLOGY *. *Annals of Noninvasive Electrocardiology*, *2*(1). https://doi.org/10.1111/j.1542-474x.1997.tb00314.x

Eisner, D. A., Caldwell, J. L., Kistamás, K., & Trafford, A. W. (2017). Calcium and Excitation-Contraction Coupling in the Heart. In *Circulation Research* (Vol. 121, Issue 2). https://doi.org/10.1161/CIRCRESAHA.117.310230

Eisner, V., Cupo, R. R., Gao, E., Csordás, G., Slovinsky, W. S., Paillard, M., Cheng, L., Ibetti, J., Chen, S. R. W., Chuprun, J. K., Hoek, J. B., Koch, W. J., & Hajnóczky, G. (2017). Mitochondrial fusion dynamics is robust in the heart and depends on calcium oscillations and contractile activity. *Proceedings of the National Academy of Sciences of the United States of America*, *114*(5). https://doi.org/10.1073/pnas.1617288114

Emelyanova, L., Ashary, Z., Cosic, M., Negmadjanov, U., Ross, G., Rizvi, F., Olet, S., Kress, D., Sra, J., Jamil Tajik, A., Holmuhamedov, E. L., Shi, Y., & Jahangir, A. (2016). Selective downregulation of mitochondrial electron transport chain activity and increased oxidative stress in human atrial fibrillation. *American*

Journal of Physiology - Heart and Circulatory Physiology. https://doi.org/10.1152/ajpheart.00699.2015

Emelyanova, L., Ashary, Z., Cosic, M., Negmadjanov, U., Ross, G., Rizvi, F., Olet, S., Kress, D., Sra, J., Tajik, A. J., Holmuhamedov, E. L., Shi, Y., & Jahangir, A. (2016). Selective downregulation of mitochondrial electron transport chain activity and increased oxidative stress in human atrial fibrillation. *Am J Physiol Heart Circ Physiol*, *311*(1), H54-63. https://doi.org/10.1152/ajpheart.00699.2015

Eng, J., Lynch, R. M., & Balaban, R. S. (1989). Nicotinamide adenine dinucleotide fluorescence spectroscopy and imaging of isolated cardiac myocytes. *Biophysical Journal*, *55*(4). https://doi.org/10.1016/S0006-3495(89)82859-0

Fakuade, F. E., Steckmeister, V., Seibertz, F., Gronwald, J., Kestel, S., Menzel, J., Pronto, J. R. D., Taha, K., Haghighi, F., Kensah, G., Pearman, C. M., Wiedmann, F., Teske, A. J., Schmidt, C., Dibb, K. M., El-Essawi, A., Danner, B. C., Baraki, H., Schwappach, B., … Voigt, N. (2021). Altered atrial cytosolic calcium handling contributes to the development of postoperative atrial fibrillation. *Cardiovascular Research*. https://doi.org/10.1093/cvr/cvaa162

Fernandez-Sanz, C., De la Fuente, S., & Sheu, S. S. (2019). Mitochondrial Ca2+ concentrations in live cells: quantification methods and discrepancies. In *FEBS Letters* (Vol. 593, Issue 13). https://doi.org/10.1002/1873-3468.13427

Florea, S. M., & Blatter, L. A. (2010). The role of mitochondria for the regulation of cardiac alternans. *Front Physiol*, *1*, 141. https://doi.org/10.3389/fphys.2010.00141

Fonteriz, R. I., de la Fuente, S., Moreno, A., Lobatón, C. D., Montero, M., & Alvarez, J. (2010). Monitoring mitochondrial [Ca2+] dynamics with rhod-2, ratiometric pericam and aequorin. *Cell Calcium*, *48*(1). https://doi.org/10.1016/j.ceca.2010.07.001

Garbincius, J. F., & Elrod, J. W. (2022). MITOCHONDRIAL CALCIUM EXCHANGE IN PHYSIOLOGY AND DISEASE. In *Physiological Reviews* (Vol. 102, Issue 2). https://doi.org/10.1152/physrev.00041.2020

Giacomello, M., Drago, I., Bortolozzi, M., Scorzeto, M., Gianelle, A., Pizzo, P., & Pozzan, T. (2010). Ca2+ Hot Spots on the Mitochondrial Surface Are Generated by Ca2+ Mobilization from Stores, but Not by Activation of Store-Operated Ca2+ Channels. *Molecular Cell*, *38*(2). https://doi.org/10.1016/j.molcel.2010.04.003

Giorgi, C., Marchi, S., & Pinton, P. (2018). The machineries, regulation and cellular functions of mitochondrial calcium. In *Nature Reviews Molecular Cell Biology* (Vol. 19, Issue 11). https://doi.org/10.1038/s41580-018-0052-8

Glancy, B., & Balaban, R. S. (2012). Role of mitochondrial Ca 2+ in the regulation of cellular energetics. *Biochemistry*, *51*(14). https://doi.org/10.1021/bi2018909

Greiser, M. (2017). Calcium signalling silencing in atrial fibrillation. In *Journal of Physiology* (Vol. 595, Issue 12). https://doi.org/10.1113/JP273045

Greiser, M., & Schotten, U. (2013). Dynamic remodeling of intracellular Ca2+ signaling during atrial fibrillation. In *Journal of Molecular and Cellular Cardiology* (Vol. 58, Issue 1). https://doi.org/10.1016/j.yjmcc.2012.12.020

Guzun, R., Karu-Varikmaa, M., Gonzalez-Granillo, M., Kuznetsov, A. V., Michel, L., Cottet-Rousselle, C., Saaremäe, M., Kaambre, T., Metsis, M., Grimm, M., Auffray, C., & Saks, V. (2011). Mitochondria-cytoskeleton interaction: Distribution of β-tubulins in cardiomyocytes and HL-1 cells. *Biochimica et Biophysica Acta - Bioenergetics*, *1807*(4).

https://doi.org/10.1016/j.bbabio.2011.01.010

Haïssaguerre, M., Jaïs, P., Shah, D. C., Takahashi, A., Hocini, M., Quiniou, G., Garrigue, S., Le Mouroux, A., Le Métayer, P., & Clémenty, J. (1998). Spontaneous Initiation of Atrial Fibrillation by Ectopic Beats Originating in the Pulmonary Veins. *New England Journal of Medicine*, *339*(10). https://doi.org/10.1056/nejm199809033391003

Halestrap, A. P., Clarke, S. J., & Javadov, S. A. (2004). Mitochondrial permeability transition pore opening during myocardial reperfusion - A target for cardioprotection. In *Cardiovascular Research* (Vol. 61, Issue 3). https://doi.org/10.1016/S0008-6363(03)00533-9

Hamilton, S., Terentyeva, R., Clements, R. T., Belevych, A. E., & Terentyev, D. (2021). Sarcoplasmic reticulum-mitochondria communication; implications for cardiac arrhythmia. In *Journal of Molecular and Cellular Cardiology*. https://doi.org/10.1016/j.yjmcc.2021.04.002

Harada, M., Melka, J., Sobue, Y., & Nattel, S. (2017). Metabolic Considerations in Atrial Fibrillation — Mechanistic Insights and Therapeutic Opportunities. *Circulation Journal*, *81*(12), 1749–1757. https://doi.org/10.1253/circj.CJ-17-1058

Heijman, J., Voigt, N., Nattel, S., & Dobrev, D. (2014). Cellular and molecular electrophysiology of atrial fibrillation initiation, maintenance, and progression. *Circ Res*, *114*(9), 1483–1499. https://doi.org/10.1161/circresaha.114.302226

Heijman, J., Voigt, N., Wehrens, X. H. T., & Dobrev, D. (2014). Calcium dysregulation in atrial fibrillation: the role of CaMKII. *Frontiers in Pharmacology*, *5*, 30. https://doi.org/10.3389/fphar.2014.00030

Heineman, F. W., & Balaban, R. S. (1993). Effects of afterload and heart rate on NAD(P)H redox state in the isolated rabbit heart. *American Journal of Physiology - Heart and Circulatory Physiology*, *264*(2 33-2). https://doi.org/10.1152/ajpheart.1993.264.2.h433

Heinzel, F. R., Luo, Y., Dodoni, G., Boengler, K., Petrat, F., Di Lisa, F., de Groot, H., Schulz, R., & Heusch, G. (2006). Formation of reactive oxygen species at increased contraction frequency in rat cardiomyocytes. *Cardiovasc Res*, *71*(2), 374–382. https://doi.org/10.1016/j.cardiores.2006.05.014

Hermans, A. N. L., Gawalko, M., Dohmen, L., van der Velden, R. M. J., Betz, K., Duncker, D., Verhaert, D. V. M., Heidbuchel, H., Svennberg, E., Neubeck, L., Eckstein, J., Lane, D. A., Lip, G. Y. H., Crijns, H. J. G. M., Sanders, P., Hendriks, J. M., Pluymaekers, N. A. H. A., & Linz, D. (2022). Mobile health solutions for atrial fibrillation detection and management: a systematic review. In *Clinical Research in Cardiology* (Vol. 111, Issue 5). https://doi.org/10.1007/s00392-021-01941-9

Hirabayashi, Y., Kwon, S. K., Paek, H., Pernice, W. M., Paul, M. A., Lee, J., Erfani, P., Raczkowski, A., Petrey, D. S., Pon, L. A., & Polleux, F. (2017). ER-mitochondria tethering by PDZD8 regulates Ca2+ dynamics in mammalian neurons. *Science*, *358*(6363). https://doi.org/10.1126/science.aan6009

Hom, J. R., Gewandter, J. S., Michael, L., Sheu, S. S., & Yoon, Y. (2007). Thapsigargin induces biphasic fragmentation of mitochondria through calcium-mediated mitochondrial fission and apoptosis. *Journal of Cellular Physiology*, *212*(2). https://doi.org/10.1002/jcp.21051

Hom, J., Yu, T., Yoon, Y., Porter, G., & Sheu, S. S. (2010). Regulation of mitochondrial fission by intracellular Ca2+ in rat ventricular myocytes. *Biochimica et Biophysica Acta - Bioenergetics*, *1797*(6–7).

https://doi.org/10.1016/j.bbabio.2010.03.018

Hove-Madsen, L., Llach, A., Bayes-Genís, A., Roura, S., Font, E. R., Arís, A., & Cinca, J. (2004). Atrial fibrillation is associated with increased spontaneous calcium release from the sarcoplasmic reticulum in human atrial myocytes. *Circulation*. https://doi.org/10.1161/01.CIR.0000141296.59876.87

Hove-Madsen, L., Llach, A., Bayes-Genis, A., Roura, S., Rodriguez Font, E., Aris, A., & Cinca, J. (2004). Atrial fibrillation is associated with increased spontaneous calcium release from the sarcoplasmic reticulum in human atrial myocytes. *Circulation*, *110*(11), 1358–1363. https://doi.org/10.1161/01.Cir.0000141296.59876.87

Huang, X., Sun, L., Ji, S., Zhao, T., Zhang, W., Xu, J., Zhang, J., Wang, Y., Wang, X., Franzini-Armstrong, C., Zheng, M., & Cheng, H. (2013). Kissing and nanotunneling mediate intermitochondrial communication in the heart. *Proceedings of the National Academy of Sciences of the United States of America*, *110*(8). https://doi.org/10.1073/pnas.1300741110

Hüser, J., Wang, Y. G., Sheehan, K. A., Cifuentes, F., Lipsius, S. L., & Blatter, L. A. (2000). Functional coupling between glycolysis and excitation-contraction coupling underlies alternans in cat heart cells. *Journal of Physiology*, *524*(3). https://doi.org/10.1111/j.1469-7793.2000.00795.x

Iwasaki, Y., Nishida, K., Kato, T., & Nattel, S. (2011). Atrial Fibrillation Pathophysiology. *Circulation*, *124*(20). https://doi.org/10.1161/circulationaha.111.019893

James, S. L., Abate, D., Abate, K. H., Abay, S. M., Abbafati, C., Abbasi, N., Abbastabar, H., Abd-Allah, F., Abdela, J., Abdelalim, A., Abdollahpour, I., Abdulkader, R. S., Abebe, Z., Abera, S. F., Abil, O. Z., Abraha, H. N., Abu-Raddad, L. J., Abu-Rmeileh, N. M. E., Accrombessi, M. M. K., … Murray, C. J. L. (2018). Global, regional, and national incidence, prevalence, and years lived with disability for 354 Diseases and Injuries for 195 countries and territories, 1990-2017: A systematic analysis for the Global Burden of Disease Study 2017. *The Lancet*, *392*(10159). https://doi.org/10.1016/S0140-6736(18)32279-7

Jouaville, L. S., Pinton, P., Bastianutto, C., Rutter, G. A., & Rizzuto, R. (1999). Regulation of mitochondrial ATP synthesis by calcium: Evidence for a long-term metabolic priming. *Proceedings of the National Academy of Sciences of the United States of America*, *96*(24). https://doi.org/10.1073/pnas.96.24.13807

Kamer, K. J., Grabarek, Z., & Mootha, V. K. (2017). High-affinity cooperative Ca 2+ binding by MICU 1– MICU 2 serves as an on–off switch for the uniporter . *EMBO Reports*, *18*(8). https://doi.org/10.15252/embr.201643748

Kamer, K. J., & Mootha, V. K. (2014). MICU1 and MICU2 play nonredundant roles in the regulation of the mitochondrial calcium uniporter. *EMBO Reports*, *15*(3). https://doi.org/10.1002/embr.201337946

Kanaan, G. N., Patten, D. A., Redpath, C. J., & Harper, M. E. (2019). Atrial Fibrillation Is Associated With Impaired Atrial Mitochondrial Energetics and Supercomplex Formation in Adults With Type 2 Diabetes. *Can J Diabetes*, *43*(1), 67-75.e1. https://doi.org/10.1016/j.jcjd.2018.05.007

Kettlewell, S., Cabrero, P., Nicklin, S. A., Dow, J. A. T., Davies, S., & Smith, G. L. (2009). Changes of intra-mitochondrial Ca2+ in adult ventricular cardiomyocytes examined using a novel fluorescent Ca2+ indicator targeted to mitochondria. *Journal of Molecular and Cellular Cardiology*, *46*(6). https://doi.org/10.1016/j.yjmcc.2009.02.016

Kim, Y. H., Lim, D. S., Lee, J. H., Shim, W. J., Ro, Y. M., Park, G. H., Becker, K. G., Cho-Chung, Y. S., & Kim, M. (2003). Gene expression profiling of oxidative stress on atrial fibrillation in humans. *Experimental & Molecular Medicine*, *35*(5), 336–349. https://doi.org/10.1038/emm.2003.45

Kim, Y. M., Guzik, T. J., Zhang, Y. H., Zhang, M. H., Kattach, H., Ratnatunga, C., Pillai, R., Channon, K. M., & Casadei, B. (2005). A myocardial Nox2 containing NAD(P)H oxidase contributes to oxidative stress in human atrial fibrillation. *Circulation Research*, *97*(7). https://doi.org/10.1161/01.RES.0000183735.09871.61

Kim, Y. M., Kattach, H., Ratnatunga, C., Pillai, R., Channon, K. M., & Casadei, B. (2008). Association of Atrial Nicotinamide Adenine Dinucleotide Phosphate Oxidase Activity With the Development of Atrial Fibrillation After Cardiac Surgery. *Journal of the American College of Cardiology*, *51*(1). https://doi.org/10.1016/j.jacc.2007.07.085

Kirchhof, P., Benussi, S., Kotecha, D., Ahlsson, A., Atar, D., Casadei, B., Castella, M., Diener, H. C., Heidbuchel, H., Hendriks, J., Hindricks, G., Manolis, A. S., Oldgren, J., Popescu, B. A., Schotten, U., Van Putte, B., Vardas, P., Agewall, S., Camm, J., … Duncan, E. (2016). 2016 ESC Guidelines for the management of atrial fibrillation developed in collaboration with EACTS. In *European Heart Journal* (Vol. 37, Issue 38). https://doi.org/10.1093/eurheartj/ehw210

Kleinsorge, M., & Cyganek, L. (2020). Subtype-Directed Differentiation of Human iPSCs into Atrial and Ventricular Cardiomyocytes. *STAR Protocols*, *1*(1). https://doi.org/10.1016/j.xpro.2020.100026

Kockskämper, J., Sheehan, K. A., Bare, D. J., Lipsius, S. L., Mignery, G. A., & Blatter, L. A. (2001). Activation and propagation of Ca2+ release during excitation-contraction coupling in atrial myocytes. *Biophysical Journal*, *81*(5). https://doi.org/10.1016/S0006-3495(01)75903-6

Kohlhaas, M., Liu, T., Knopp, A., Zeller, T., Ong, M. F., Böhm, M., O'Rourke, B., & Maack, C. (2010). Elevated cytosolic Na+ increases mitochondrial formation of reactive oxygen species in failing cardiac myocytes. *Circulation*. https://doi.org/10.1161/CIRCULATIONAHA.109.914911

Kohlhaas, M., & Maack, C. (2010). Adverse bioenergetic consequences of Na+-Ca2+ exchanger-mediated Ca2+ influx in cardiac myocytes. *Circulation*. https://doi.org/10.1161/CIRCULATIONAHA.110.968057

Kohlhaas, M., & Maack, C. (2013). Calcium release microdomains and mitochondria. In *Cardiovascular Research*. https://doi.org/10.1093/cvr/cvt032

Kohlhaas, M., Nickel, A. G., & Maack, C. (2017). Mitochondrial energetics and calcium coupling in the heart. *Journal of Physiology*, *595*(12), 5753–5763. https://doi.org/10.1113/JP273609

Kolenc, O. I., & Quinn, K. P. (2019). Evaluating cell metabolism through autofluorescence imaging of NAD(P)H and FAD. In *Antioxidants and Redox Signaling* (Vol. 30, Issue 6). https://doi.org/10.1089/ars.2017.7451

Kornej, J., Börschel, C. S., Benjamin, E. J., & Schnabel, R. B. (2020). Epidemiology of Atrial Fibrillation in the 21st Century. *Circulation Research*, *127*(1). https://doi.org/10.1161/circresaha.120.316340

Kosoglou, T., Statkevich, P., Johnson-Levonas, A. O., Paolini, J. F., Bergman, A. J., & Alton, K. B. (2005). Ezetimibe: A review of its metabolism, pharmacokinetics and drug interactions. In *Clinical Pharmacokinetics* (Vol. 44, Issue 5). https://doi.org/10.2165/00003088-200544050-00002

Kottkamp, H., Tanner, H., Kobza, R., Schirdewahn, P., Dorszewski, A., Gerds-Li, J.

H., Carbucicchio, C., Piorkowski, C., & Hindricks, G. (2004). Time courses and quantitative analysis of atrial fibrillation episode number and duration after circular plus linear left atrial lesions: Trigger elimination or substrate modification: Early or delayed cure? *Journal of the American College of Cardiology*, *44*(4). https://doi.org/10.1016/j.jacc.2004.04.049

Krijthe, B. P., Kunst, A., Benjamin, E. J., Lip, G. Y. H., Franco, O. H., Hofman, A., Witteman, J. C. M., Stricker, B. H., & Heeringa, J. (2013). Projections on the number of individuals with atrial fibrillation in the European Union, from 2000 to 2060. *European Heart Journal*, *34*(35). https://doi.org/10.1093/eurheartj/eht280

Krumova, K., & Cosa, G. (2016). *Chapter 1. Overview of Reactive Oxygen Species. In: Singlet Oxygen: Applications in Biosciences and Nanosciences, Volume 1* (pp. 1–21). The Royal Society of Chemistry. https://doi.org/10.1039/9781782622208-00001

Kuznetsov, A. V., Troppmair, J., Sucher, R., Hermann, M., Saks, V., & Margreiter, R. (2006). Mitochondrial subpopulations and heterogeneity revealed by confocal imaging: Possible physiological role? *Biochimica et Biophysica Acta - Bioenergetics*, *1757*(5–6). https://doi.org/10.1016/j.bbabio.2006.03.014

Kwong, J. Q., Lu, X., Correll, R. N., Schwanekamp, J. A., Vagnozzi, R. J., Sargent, M. A., York, A. J., Zhang, J., Bers, D. M., & Molkentin, J. D. (2015). The Mitochondrial Calcium Uniporter Selectively Matches Metabolic Output to Acute Contractile Stress in the Heart. *Cell Reports*. https://doi.org/10.1016/j.celrep.2015.06.002

Lambert, J. P., Luongo, T. S., Tomar, D., Jadiya, P., Gao, E., Zhang, X., Lucchese, A. M., Kolmetzky, D. W., Shah, N. S., & Elrod, J. W. (2019). MCUB Regulates the Molecular Composition of the Mitochondrial Calcium Uniporter Channel to Limit Mitochondrial Calcium Overload during Stress. *Circulation*, *140*(21). https://doi.org/10.1161/CIRCULATIONAHA.118.037968

Laredo, M., Waldmann, V., Khairy, P., & Nattel, S. (2018). Age as a Critical Determinant of Atrial Fibrillation: A Two-sided Relationship. *Canadian Journal of Cardiology*, *34*(11), 1396–1406. https://doi.org/10.1016/j.cjca.2018.08.007

Leach, R. N., Desai, J. C., & Orchard, C. H. (2005). Effect of cytoskeleton disruptors on L-type Ca channel distribution in rat ventricular myocytes. *Cell Calcium*, *38*(5). https://doi.org/10.1016/j.ceca.2005.07.006

Lenski, M., Schleider, G., Kohlhaas, M., Adrian, L., Adam, O., Tian, Q., Kaestner, L., Lipp, P., Lehrke, M., Maack, C., Böhm, M., & Laufs, U. (2015). Arrhythmia causes lipid accumulation and reduced glucose uptake. *Basic Research in Cardiology*, *110*(4), 40. https://doi.org/10.1007/s00395-015-0497-2

Li, J., Qi, X., Ramos, K. S., Lanters, E., Keijer, J., de Groot, N., Brundel, B., & Zhang, D. (2022). Disruption of Sarcoplasmic Reticulum-Mitochondrial Contacts Underlies Contractile Dysfunction in Experimental and Human Atrial Fibrillation: A Key Role of Mitofusin 2. *Journal of the American Heart Association*, *11*(19), e024478. https://doi.org/10.1161/JAHA.121.024478

Li, S., Cheng, H., Tomaselli, G. F., & Li, R. A. (2014). Mechanistic basis of excitation-contraction coupling in human pluripotent stem cell-derived ventricular cardiomyocytes revealed by Ca2+ spark characteristics: Direct evidence of functional Ca2+-induced Ca 2+ release. *Heart Rhythm*, *11*(1). https://doi.org/10.1016/j.hrthm.2013.10.006

Li, W. H., Llopis, J., Whitney, M., Zlokarnik, G., & Tsien, R. Y. (1998). Cell-permeant caged InsP3 ester shows that Ca2+ spike frequency can optimize gene

expression. *Nature*, *392*(6679). https://doi.org/10.1038/31965

Liu, J. C., Syder, N. C., Ghorashi, N. S., Willingham, T. B., Parks, R. J., Sun, J., Fergusson, M. M., Liu, J., Holmström, K. M., Menazza, S., Springer, D. A., Liu, C., Glancy, B., Finkel, T., & Murphy, E. (2020). EMRE is essential for mitochondrial calcium uniporter activity in a mouse model. *JCI Insight*, *5*(4). https://doi.org/10.1172/jci.insight.134063

Liu, T., & Rourke, B. O. (2008). Enhancing mitochondrial Ca2+ uptake in myocytes from failing hearts restores energy supply and demand matching. *Circulation Research*, *103*(3). https://doi.org/10.1161/CIRCRESAHA.108.175919

Ljubojevic-Holzer, S. (2018). The Secret of the Kissing Cousins: An ER-mitochondrial tethering protein regulates Ca 2+ crosstalk in mammalian neurons. In *Cardiovascular Research* (Vol. 114, Issue 3). https://doi.org/10.1093/cvr/cvy020

Lopaschuk, G. D., Karwi, Q. G., Tian, R., Wende, A. R., & Abel, E. D. (2021). Cardiac Energy Metabolism in Heart Failure. *Circulation Research*, *128*(10). https://doi.org/10.1161/CIRCRESAHA.121.318241

Lopez-Crisosto, C., Pennanen, C., Vasquez-Trincado, C., Morales, P. E., Bravo-Sagua, R., Quest, A. F. G., Chiong, M., & Lavandero, S. (2017). Sarcoplasmic reticulum-mitochondria communication in cardiovascular pathophysiology. In *Nature Reviews Cardiology*. https://doi.org/10.1038/nrcardio.2017.23

Louch, W. E., Bito, V., Heinzel, F. R., Macianskiene, R., Vanhaecke, J., Flameng, W., Mubagwa, K., & Sipido, K. R. (2004). Reduced synchrony of Ca2+ release with loss of T-tubules - A comparison to Ca2+ release in human failing cardiomyocytes. *Cardiovascular Research*, *62*(1). https://doi.org/10.1016/j.cardiores.2003.12.031

Lu, X., Ginsburg, K. S., Kettlewell, S., Bossuyt, J., Smith, G. L., & Bers, D. M. (2013). Measuring local gradients of intramitochondrial [Ca2+] in cardiac myocytes during sarcoplasmic reticulum Ca2+ release. *Circulation Research*. https://doi.org/10.1161/CIRCRESAHA.111.300501

Lu, X., Kwong, J. Q., Molkentin, J. D., & Bers, D. M. (2016). Individual Cardiac Mitochondria Undergo Rare Transient Permeability Transition Pore Openings. *Circulation Research*, *118*(5), 834–841. https://doi.org/10.1161/CIRCRESAHA.115.308093

Lu, X., Thai, P. N., Lu, S., Pu, J., & Bers, D. M. (2019). Intrafibrillar and perinuclear mitochondrial heterogeneity in adult cardiac myocytes. *Journal of Molecular and Cellular Cardiology*, *136*. https://doi.org/10.1016/j.yjmcc.2019.08.013

Luongo, T. S., Lambert, J. P., Gross, P., Nwokedi, M., Lombardi, A. A., Shanmughapriya, S., Carpenter, A. C., Kolmetzky, D., Gao, E., van Berlo, J. H., Tsai, E. J., Molkentin, J. D., Chen, X., Madesh, M., Houser, S. R., & Elrod, J. W. (2017). The mitochondrial Na+/Ca2+ exchanger is essential for Ca2+ homeostasis and viability. *Nature*, *545*(7652), 93–97. https://doi.org/10.1038/nature22082

Maack, C. (2016). Orphaned mitochondria in heart failure. *Cardiovasc Res*, *109*(1), 6–8. https://doi.org/10.1093/cvr/cvv262

Maack, C., Cortassa, S., Aon, M. A., Ganesan, A. N., Liu, T., & O'Rourke, B. (2006). Elevated cytosolic Na+ decreases mitochondrial Ca2+ uptake during excitation-contraction coupling and impairs energetic adaptation in cardiac myocytes. *Circulation Research*. https://doi.org/10.1161/01.RES.0000232546.92777.05

Maack, C., & O'Rourke, B. (2007). Excitation-contraction coupling and

mitochondrial energetics. In *Basic Research in Cardiology* (Vol. 102, Issue 5). https://doi.org/10.1007/s00395-007-0666-z

Mackenzie, L., Roderick, H. L., Berridge, M. J., Conway, S. J., & Bootman, M. D. (2004). The spatial pattern of atrial cardiomyocyte calcium signalling modulates contraction. *Journal of Cell Science*, *117*(26). https://doi.org/10.1242/jcs.01559

Macquaide, N., Tuan, H. T. M., Hotta, J. I., Sempels, W., Lenaerts, I., Holemans, P., Hofkens, J., Jafri, M. S., Willems, R., & Sipido, K. R. (2015). Ryanodine receptor cluster fragmentation and redistribution in persistent atrial fibrillation enhance calcium release. *Cardiovascular Research*, *108*(3). https://doi.org/10.1093/cvr/cvv231

Mary-Rabine, L., Albert, A., Pham, T. D., Hordof, A., Fenoglio Jr., J. J., Malm, J. R., & Rosen, M. R. (1983). The relationship of human atrial cellular electrophysiology to clinical function and ultrastructure. *Circ Res*, *52*(2), 188–199. https://doi.org/10.1161/01.res.52.2.188

Mason, F. E., Pronto, J. R. D., Alhussini, K., Maack, C., & Voigt, N. (2020). Cellular and mitochondrial mechanisms of atrial fibrillation. In *Basic Research in Cardiology*. https://doi.org/10.1007/s00395-020-00827-7

Mayr, M., Yusuf, S., Weir, G., Chung, Y.-L., Mayr, U., Yin, X., Ladroue, C., Madhu, B., Roberts, N., De Souza, A., Fredericks, S., Stubbs, M., Griffiths, J. R., Jahangiri, M., Xu, Q., & Camm, A. J. (2008). Combined Metabolomic and Proteomic Analysis of Human Atrial Fibrillation. *Journal of the American College of Cardiology*, *51*(5), 585–594. https://doi.org/10.1016/j.jacc.2007.09.055

McCormack, J. G., & Denton, R. M. (1979). The effects of calcium ions and adenine nucleotides on the activity of pig heart 2-oxoglutarate dehydrogenase complex. *Biochemical Journal*. https://doi.org/10.1042/bj1800533

Mihm, M. J., Yu, F., Carnes, C. A., Reiser, P. J., McCarthy, P. M., Van Wagoner, D. R., & Bauer, J. A. (2001). Impaired myofibrillar energetics and oxidative injury during human atrial fibrillation. *Circulation*, *104*(2). https://doi.org/10.1161/01.CIR.104.2.174

Milani-Nejad, N., & Janssen, P. M. L. (2014). Small and large animal models in cardiac contraction research: Advantages and disadvantages. In *Pharmacology and Therapeutics* (Vol. 141, Issue 3). https://doi.org/10.1016/j.pharmthera.2013.10.007

Min, C. K., Yeom, D. R., Lee, K. E., Kwon, H. K., Kang, M., Kim, Y. S., Park, Z. Y., Jeon, H., & Kim, D. H. (2012). Coupling of ryanodine receptor 2 and voltage-dependent anion channel 2 is essential for Ca2+ transfer from the sarcoplasmic reticulum to the mitochondria in the heart. *Biochemical Journal*. https://doi.org/10.1042/BJ20120705

Mitcheson, J. S., Hancox, J. C., & Levi, A. J. (1996). Action potentials, ion channel currents and transverse tubule density in adult rabbit ventricular myocytes maintained for 6 days in cell culture. *Pflugers Archiv European Journal of Physiology*, *431*(6). https://doi.org/10.1007/s004240050073

Montaigne, D., Marechal, X., Lefebvre, P., Modine, T., Fayad, G., Dehondt, H., Hurt, C., Coisne, A., Koussa, M., Remy-Jouet, I., Zerimech, F., Boulanger, E., Lacroix, D., Staels, B., & Neviere, R. (2013). Mitochondrial Dysfunction as an Arrhythmogenic Substrate. *Journal of the American College of Cardiology*, *62*(16), 1466–1473. https://doi.org/10.1016/j.jacc.2013.03.061

Munro, M. L., van Hout, I., Aitken-Buck, H. M., Sugunesegran, R., Bhagwat, K., Davis, P. J., Lamberts, R. R., Coffey, S., Soeller, C., & Jones, P. P. (2021).

Human Atrial Fibrillation Is Not Associated With Remodeling of Ryanodine Receptor Clusters. *Frontiers in Cell and Developmental Biology*, *9*. https://doi.org/10.3389/fcell.2021.633704

Murphy, E., & Eisner, D. A. (2009). Regulation of Intracellular and Mitochondrial Sodium in Health and Disease. *Circulation Research*, *104*(3), 292–303. https://doi.org/10.1161/CIRCRESAHA.108.189050

Murphy, M. P. (2009). How mitochondria produce reactive oxygen species. *Biochemical Journal*, *417*(1), 1–13. https://doi.org/10.1042/BJ20081386

Najbauer, E. E., Becker, S., Giller, K., Zweckstetter, M., Lange, A., Steinem, C., de Groot, B. L., Griesinger, C., & Andreas, L. B. (2021). Structure, gating and interactions of the voltage-dependent anion channel. *European Biophysics Journal*, *50*(2). https://doi.org/10.1007/s00249-021-01515-7

Naon, D., Zaninello, M., Giacomello, M., Varanita, T., Grespi, F., Lakshminaranayan, S., Serafini, A., Semenzato, M., Herkenne, S., Hernández-Alvarez, M. I., Zorzano, A., De Stefani, D., Dorn, G. W., & Scorrano, L. (2016). Critical reappraisal confirms that Mitofusin 2 is an endoplasmic reticulum–mitochondria tether. *Proceedings of the National Academy of Sciences*, *113*(40), 11249–11254. https://doi.org/10.1073/pnas.1606786113

Nattel, S. (2017). Molecular and Cellular Mechanisms of Atrial Fibrosis in Atrial Fibrillation. *JACC: Clinical Electrophysiology*, *3*(5), 425–435. https://doi.org/10.1016/j.jacep.2017.03.002

Neef, S., Dybkova, N., Sossalla, S., Ort, K. R., Fluschnik, N., Neumann, K., Seipelt, R., Schöndube, F. A., Hasenfuss, G., & Maier, L. S. (2010). CaMKII-Dependent diastolic SR Ca2+ leak and elevated diastolic Ca2+ levels in right atrial myocardium of patients with atrial fibrillation. *Circulation Research*. https://doi.org/10.1161/CIRCRESAHA.109.203836

Neumann, D., Bückers, J., Kastrup, L., Hell, S. W., & Jakobs, S. (2010). Two-color STED microscopy reveals different degrees of colocalization between hexokinase-I and the three human VDAC isoforms. *PMC Biophysics*, *3*(1). https://doi.org/10.1186/1757-5036-3-4

Newton, A. C., Bootman, M. D., & Scott, J. (2016). Second messengers. *Cold Spring Harbor Perspectives in Biology*, *8*(8). https://doi.org/10.1101/cshperspect.a005926

Nickel, A. G., Von Hardenberg, A., Hohl, M., Löffler, J. R., Kohlhaas, M., Becker, J., Reil, J. C., Kazakov, A., Bonnekoh, J., Stadelmaier, M., Puhl, S. L., Wagner, M., Bogeski, I., Cortassa, S., Kappl, R., Pasieka, B., Lafontaine, M., Lancaster, C. R. D., Blacker, T. S., … Maack, C. (2015). Reversal of mitochondrial transhydrogenase causes oxidative stress in heart failure. *Cell Metabolism*. https://doi.org/10.1016/j.cmet.2015.07.008

Nickel, A., Kohlhaas, M., & Maack, C. (2014). Mitochondrial reactive oxygen species production and elimination. *J Mol Cell Cardiol*, *73*, 26–33. https://doi.org/10.1016/j.yjmcc.2014.03.011

Nuutinen, E. M. (1984). Subcellular origin of the surface fluorescence of reduced nicotinamide nucleotides in the isolated perfused rat heart. *Basic Research in Cardiology*, *79*(1). https://doi.org/10.1007/BF01935806

Oropeza-Almazán, Y., & Blatter, L. A. (2020). Mitochondrial calcium uniporter complex activation protects against calcium alternans in atrial myocytes. *American Journal of Physiology - Heart and Circulatory Physiology*, *319*(4). https://doi.org/10.1152/AJPHEART.00375.2020

Paillard, M., Tubbs, E., Thiebaut, P. A., Gomez, L., Fauconnier, J., Da Silva, C. C.,

Teixeira, G., Mewton, N., Belaidi, E., Durand, A., Abrial, M., Lacampagne, A., Rieusset, J., & Ovize, M. (2013). Depressing mitochondria-reticulum interactions protects cardiomyocytes from lethal hypoxia-reoxygenation injury. *Circulation*, *128*(14). https://doi.org/10.1161/CIRCULATIONAHA.113.001225

Pallafacchina, G., Zanin, S., & Rizzuto, R. (2021). From the identification to the dissection of the physiological role of the mitochondrial calcium uniporter: An ongoing story. In *Biomolecules* (Vol. 11, Issue 6). https://doi.org/10.3390/biom11060786

Palty, R., Silverman, W. F., Hershfinkel, M., Caporale, T., Sensi, S. L., Parnis, J., Nolte, C., Fishman, D., Shoshan-Barmatz, V., Herrmann, S., Khananshvili, D., & Sekler, I. (2010). NCLX is an essential component of mitochondrial Na+/Ca2+ exchange. *Proceedings of the National Academy of Sciences*, *107*(1), 436–441. https://doi.org/10.1073/pnas.0908099107

Patron, M., Checchetto, V., Raffaello, A., Teardo, E., VecellioReane, D., Mantoan, M., Granatiero, V., Szabò, I., DeStefani, D., & Rizzuto, R. (2014). MICU1 and MICU2 finely tune the mitochondrial Ca2+ uniporter by exerting opposite effects on MCU activity. *Molecular Cell*, *53*(5). https://doi.org/10.1016/j.molcel.2014.01.013

Patron, M., Granatiero, V., Espino, J., Rizzuto, R., & De Stefani, D. (2019). MICU3 is a tissue-specific enhancer of mitochondrial calcium uptake. *Cell Death and Differentiation*, *26*(1). https://doi.org/10.1038/s41418-018-0113-8

Payne, R., Hoff, H., Roskowski, A., & Foskett, J. K. (2017). MICU2 Restricts Spatial Crosstalk between InsP3R and MCU Channels by Regulating Threshold and Gain of MICU1-Mediated Inhibition and Activation of MCU. *Cell Reports*, *21*(11). https://doi.org/10.1016/j.celrep.2017.11.064

Petrungaro, C., Zimmermann, K. M., Küttner, V., Fischer, M., Dengjel, J., Bogeski, I., & Riemer, J. (2015). The Ca2+-dependent release of the Mia40-induced MICU1-MICU2 dimer from MCU regulates mitochondrial Ca2+ uptake. *Cell Metabolism*, *22*(4). https://doi.org/10.1016/j.cmet.2015.08.019

Plummer, B. N., Liu, H., Wan, X., Deschênes, I., & Laurita, K. R. (2015). Targeted antioxidant treatment decreases cardiac alternans associated with chronic myocardial infarction. *Circulation: Arrhythmia and Electrophysiology*, *8*(1). https://doi.org/10.1161/CIRCEP.114.001789

Qiao, X., Jia, S., Ye, J., Fang, X., Zhang, C., Cao, Y., Xu, C., Zhao, L., Zhu, Y., Wang, L., & Zheng, M. (2017). PTPIP51 regulates mouse cardiac ischemia/reperfusion through mediating the mitochondria-SR junction. *Scientific Reports*, *7*. https://doi.org/10.1038/srep45379

Quinlan, C. L., Goncalves, R. L. S., Hey-Mogensen, M., Yadava, N., Bunik, V. I., & Brand, M. D. (2014). The 2-Oxoacid Dehydrogenase Complexes in Mitochondria Can Produce Superoxide/Hydrogen Peroxide at Much Higher Rates Than Complex I. *Journal of Biological Chemistry*, *289*(12), 8312–8325. https://doi.org/10.1074/jbc.M113.545301

Raffaello, A., De Stefani, D., Sabbadin, D., Teardo, E., Merli, G., Picard, A., Checchetto, V., Moro, S., Szabò, I., & Rizzuto, R. (2013). The mitochondrial calcium uniporter is a multimer that can include a dominant-negative pore-forming subunit. *EMBO Journal*, *32*(17). https://doi.org/10.1038/emboj.2013.157

Rahman, F., Kwan, G. F., & Benjamin, E. J. (2014). Global epidemiology of atrial fibrillation. In *Nature Reviews Cardiology* (Vol. 11, Issue 11). https://doi.org/10.1038/nrcardio.2014.118

Randle, P. J. (1981). Phosphorylation–Dephosphorylation Cycles and the Regulation of Fuel Selection in Mammals. In *Current Topics in Cellular Regulation* (Vol. 18, Issue C). https://doi.org/10.1016/B978-0-12-152818-8.50013-X

Rapizzi, E., Pinton, P., Szabadkai, G., Wieckowski, M. R., Vandecasteele, G., Baird, G., Tuft, R. A., Fogarty, K. E., & Rizzuto, R. (2002). Recombinant expression of the voltage-dependent anion channel enhances the transfer of Ca2+ microdomains to mitochondria. *Journal of Cell Biology*, *159*(4), 613–624. https://doi.org/10.1083/jcb.200205091

Reilly, S. N., Jayaram, R., Nahar, K., Antoniades, C., Verheule, S., Channon, K. M., Alp, N. J., Schotten, U., & Casadei, B. (2011). Atrial sources of reactive oxygen species vary with the duration and substrate of atrial fibrillation: implications for the antiarrhythmic effect of statins. *Circulation*, *124*(10), 1107–1117. https://doi.org/10.1161/circulationaha.111.029223

Reinhardt, F., Beneke, K., Pavlidou, N. G., Conradi, L., Reichenspurner, H., Hove-Madsen, L., & Molina, C. E. (2021). Abnormal calcium handling in atrial fibrillation is linked to changes in cyclic amp dependent signaling. *Cells*, *10*(11). https://doi.org/10.3390/cells10113042

Ren, L., Gopireddy, R. R., Perkins, G., Zhang, H., Timofeyev, V., Lyu, Y., Diloretto, D. A., Trinh, P., Sirish, P., Overton, J. L., Xu, W., Grainger, N., Xiang, Y. K., Dedkova, E. N., Zhang, X.-D., Yamoah, E. N., Navedo, M. F., Thai, P. N., & Chiamvimonvat, N. (2022). Disruption of mitochondria-sarcoplasmic reticulum microdomain connectomics contributes to sinus node dysfunction in heart failure. *Proceedings of the National Academy of Sciences of the United States of America*, *119*(36), e2206708119. https://doi.org/10.1073/pnas.2206708119

Rienstra, M., Lubitz, S. A., Mahida, S., Magnani, J. W., Fontes, J. D., Sinner, M. F., Van Gelder, I. C., Ellinor, P. T., & Benjamin, E. J. (2012). Symptoms and functional status of patients with atrial fibrillation: State of the art and future research opportunities. In *Circulation* (Vol. 125, Issue 23). https://doi.org/10.1161/CIRCULATIONAHA.111.069450

Rizzuto, R., Pinton, P., Carrington, W., Fay, F. S., Fogarty, K. E., Lifshitz, L. M., Tuft, R. A., & Pozzan, T. (1998). Close contacts with the endoplasmic reticulum as determinants of mitochondrial Ca2+ responses. *Science*, *280*(5370). https://doi.org/10.1126/science.280.5370.1763

Rodrigo, R., Korantzopoulos, P., Cereceda, M., Asenjo, R., Zamorano, J., Villalabeitia, E., Baeza, C., Aguayo, R., Castillo, R., Carrasco, R., & Gormaz, J. G. (2013). A randomized controlled trial to prevent post-operative atrial fibrillation by antioxidant reinforcement. *Journal of the American College of Cardiology*, *62*(16). https://doi.org/10.1016/j.jacc.2013.07.014

Rossini, M., & Filadi, R. (2020). Sarcoplasmic Reticulum-Mitochondria Kissing in Cardiomyocytes: Ca2+, ATP, and Undisclosed Secrets. In *Frontiers in Cell and Developmental Biology*. https://doi.org/10.3389/fcell.2020.00532

Saks, V., Dzeja, P., Schlattner, U., Vendelin, M., Terzic, A., & Wallimann, T. (2006). Cardiac system bioenergetics: Metabolic basis of the frank-starling law. In *Journal of Physiology* (Vol. 571, Issue 2). https://doi.org/10.1113/jphysiol.2005.101444

Sancak, Y., Markhard, A. L., Kitami, T., Kovács-Bogdán, E., Kamer, K. J., Udeshi, N. D., Carr, S. A., Chaudhuri, D., Clapham, D. E., Li, A. A., Calvo, S. E., Goldberger, O., & Mootha, V. K. (2013). EMRE is an essential component of the mitochondrial calcium uniporter complex. *Science*.

https://doi.org/10.1126/science.1242993

Sander, P., Arduino, D. M., Schweitzer, M. K., Wilting, F., Gudermann, T., Perocchi, F., & Schredelseker, J. (2020). Novel Mitochondrial Ca2+ Uptake Enhancers for the Treatment of Cardiac Arrhythmia. *Biophysical Journal*, *118*(3). https://doi.org/10.1016/j.bpj.2019.11.1492

Sander, P., Feng, M., Schweitzer, M. K., Wilting, F., Gutenthaler, S. M., Arduino, D. M., Fischbach, S., Dreizehnter, L., Moretti, A., Gudermann, T., Perocchi, F., & Schredelseker, J. (2021). Approved drugs ezetimibe and disulfiram enhance mitochondrial Ca2+ uptake and suppress cardiac arrhythmogenesis. *British Journal of Pharmacology*, *178*(22). https://doi.org/10.1111/bph.15630

Sander, P., Gudermann, T., & Schredelseker, J. (2021). A calcium guard in the outer membrane: Is vdac a regulated gatekeeper of mitochondrial calcium uptake? In *International Journal of Molecular Sciences* (Vol. 22, Issue 2). https://doi.org/10.3390/ijms22020946

Schlotthauer, K., & Bers, D. M. (2000). Sarcoplasmic reticulmn Ca2+ release causes myocyte depolarization: Underlying mechanism and threshold for triggered action potentials. *Circulation Research*, *87*(9). https://doi.org/10.1161/01.RES.87.9.774

Schnabel, R. B., Yin, X., Gona, P., Larson, M. G., Beiser, A. S., McManus, D. D., Newton-Cheh, C., Lubitz, S. A., Magnani, J. W., Ellinor, P. T., Seshadri, S., Wolf, P. A., Vasan, R. S., Benjamin, E. J., & Levy, D. (2015). 50 year trends in atrial fibrillation prevalence, incidence, risk factors, and mortality in the Framingham Heart Study: A cohort study. *The Lancet*, *386*(9989). https://doi.org/10.1016/S0140-6736(14)61774-8

Schotten, U., Greiser, M., Benke, D., Buerkel, K., Ehrenteidt, B., Stellbrink, C., Vazquez-Jimenez, J. F., Schoendube, F., Hanrath, P., & Allessie, M. (2002). Atrial fibrillation-induced atrial contractile dysfunction: A tachycardiomyopathy of a different sort. *Cardiovascular Research*, *53*(1). https://doi.org/10.1016/S0008-6363(01)00453-9

Seibertz, F., Reynolds, M., & Voigt, N. (2020). Single-cell optical action potential measurement in human induced pluripotent stem cell-derived cardiomyocytes. *Journal of Visualized Experiments*, *2020*(166). https://doi.org/10.3791/61890

Seidlmayer, L. K., Kuhn, J., Berbner, A., Arias-Loza, P. A., Williams, T., Kaspar, M., Czolbe, M., Kwong, J. Q., Molkentin, J. D., Heinze, K. G., Dedkova, E. N., & Ritter, O. (2016). Inositol 1,4,5-Trisphosphate-mediated sarcoplasmic reticulum-mitochondrial crosstalk influences adenosine triphosphate production via mitochondrial Ca2+ uptake through the mitochondrial ryanodine receptor in cardiac myocytes. *Cardiovascular Research*. https://doi.org/10.1093/cvr/cvw185

Seidlmayer, L. K., Mages, C., Berbner, A., Eder-Negrin, P., Arias-Loza, P. A., Kaspar, M., Song, M., Dorn, G. W., Frantz, S., Maack, C., Gerull, B., & Dedkova, E. N. (2019). Mitofusin 2 is essential for IP3-mediated SR/mitochondria metabolic feedback. In *Frontiers in Physiology*. https://doi.org/10.3389/fphys.2019.00733

Sharma, S., Sharma, G., Hote, M., Devagourou, V., Kesari, V., Arava, S., Airan, B., & Ray, R. (2014). Light and electron microscopic features of surgically excised left atrial appendage in rheumatic heart disease patients with atrial fibrillation and sinus rhythm. *Cardiovasc Pathol*, *23*(6), 319–326. https://doi.org/10.1016/j.carpath.2014.07.008

Sharma, V. K., Ramesh, V., Franzini-Armstrong, C., & Sheu, S. S. (2000). Transport

of Ca2+ from sarcoplasmic reticulum to mitochondria in rat ventricular myocytes. *J Bioenerg Biomembr*, *32*(1), 97–104. https://doi.org/10.1023/a:1005520714221

Shimizu, H., Schredelseker, J., Huang, J., Lu, K., Naghdi, S., Lu, F., Franklin, S., Fiji, H. D. G., Wang, K., Zhu, H., Tian, C., Lin, B., Nakano, H., Ehrlich, A., Nakai, J., Stieg, A. Z., Gimzewski, J. K., Nakano, A., Goldhaber, J. I., … Chen, J. N. (2015). Mitochondrial ca2+ uptake by the voltage-dependent anion channel 2 regulates cardiac rhythmicity. *ELife*, *2015*(4). https://doi.org/10.7554/eLife.04801

Sies, H., & Jones, D. P. (2020). Reactive oxygen species (ROS) as pleiotropic physiological signalling agents. In *Nature Reviews Molecular Cell Biology* (Vol. 21, Issue 7). https://doi.org/10.1038/s41580-020-0230-3

Skasa, M., Jüngling, E., Picht, E., Schöndube, F., & Lückhoff, A. (2001). L-type calcium currents in atrial myocytes from patients with persistent and non-persistent atrial fibrillation. *Basic Research in Cardiology*, *96*(2). https://doi.org/10.1007/s003950170065

Smirnova, E., Shurland, D. L., Ryazantsev, S. N., & Van Der Bliek, A. M. (1998). A human dynamin-related protein controls the distribution of mitochondria. *Journal of Cell Biology*, *143*(2). https://doi.org/10.1083/jcb.143.2.351

Smith, R. M., Visweswaran, R., Talkachova, I., Wothe, J. K., & Tolkacheva, E. G. (2013). Uncoupling the mitochondria facilitates alternans formation in the isolated rabbit heart. *American Journal of Physiology - Heart and Circulatory Physiology*, *305*(1). https://doi.org/10.1152/ajpheart.00915.2012

Sossalla, S., Kallmeyer, B., Wagner, S., Mazur, M., Maurer, U., Toischer, K., Schmitto, J. D., Seipelt, R., Schöndube, F. A., Hasenfuss, G., Belardinelli, L., & Maier, L. S. (2010). Altered Na+ Currents in Atrial Fibrillation. Effects of Ranolazine on Arrhythmias and Contractility in Human Atrial Myocardium. *Journal of the American College of Cardiology*. https://doi.org/10.1016/j.jacc.2009.12.055

Sovari, A. A., & Dudley, S. C. (2012). Antioxidant therapy for atrial fibrillation: lost in translation? *Heart*, *98*(22), 1615–1616. https://doi.org/10.1136/heartjnl-2012-302328

Spinelli, J. B., & Haigis, M. C. (2018). The multifaceted contributions of mitochondria to cellular metabolism. In *Nature Cell Biology* (Vol. 20, Issue 7). https://doi.org/10.1038/s41556-018-0124-1

Staerk, L., Sherer, J. A., Ko, D., Benjamin, E. J., & Helm, R. H. (2017). Atrial Fibrillation: Epidemiology, Pathophysiology, Clinical Outcomes. In *Circulation Research* (Vol. 120, Issue 9). https://doi.org/10.1161/CIRCRESAHA.117.309732

Stanley, W. C., Recchia, F. A., & Lopaschuk, G. D. (2005). Myocardial substrate metabolism in the normal and failing heart. In *Physiological Reviews*. https://doi.org/10.1152/physrev.00006.2004

Stary, V., Puppala, D., Scherrer-Crosbie, M., Dillmann, W. H., & Armoundas, A. A. (2016). SERCA2a upregulation ameliorates cellular alternans induced by metabolic inhibition. *Journal of Applied Physiology*, *120*(8). https://doi.org/10.1152/japplphysiol.00588.2015

Szabadkai, G., Bianchi, K., Várnai, P., De Stefani, D., Wieckowski, M. R., Cavagna, D., Nagy, A. I., Balla, T., & Rizzuto, R. (2006). Chaperone-mediated coupling of endoplasmic reticulum and mitochondrial Ca2+ channels. *Journal of Cell Biology*, *175*(6). https://doi.org/10.1083/jcb.200608073

Szabadkai, G., Simoni, A. M., Bianchi, K., De Stefani, D., Leo, S., Wieckowski, M. R., & Rizzuto, R. (2006). Mitochondrial dynamics and Ca2+ signaling. In *Biochimica et Biophysica Acta - Molecular Cell Research* (Vol. 1763, Issues 5–6). https://doi.org/10.1016/j.bbamcr.2006.04.002

Tameling, C., Stoldt, S., Stephan, T., Naas, J., Jakobs, S., & Munk, A. (2021). Colocalization for super-resolution microscopy via optimal transport. *Nature Computational Science*, *1*(3). https://doi.org/10.1038/s43588-021-00050-x

Thiedemann, K. U., & Ferrans, V. J. (1976). Ultrastructure of sarcoplasmic reticulum in atrial myocardium of patients with mitral valvular disease. *American Journal of Pathology*, *83*(1).

Thiedemann, K. U., & Ferrans, V. J. (1977). Left atrial ultrastructure in mitral valvular disease. *Am J Pathol*, *89*(3), 575–604. https://www.ncbi.nlm.nih.gov/pmc/articles/PMC2032253/pdf/amjpathol00394-0047.pdf

Trollinger, D. R., Cascio, W. E., & Lemasters, J. J. (1997). Selective loading of Rhod 2 into mitochondria shows mitochondrial Ca2+ transients during the contractile cycle in adult rabbit cardiac myocytes. *Biochemical and Biophysical Research Communications*, *236*(3). https://doi.org/10.1006/bbrc.1997.7042

Trollinger, D. R., Cascio, W. E., & Lemasters, J. J. (2000). Mitochondrial calcium transients in adult rabbit cardiac myocytes: Inhibition by ruthenium red and artifacts caused by lysosomal loading of Ca2+-indicating fluorophores. *Biophysical Journal*, *79*(1), 39–50. https://doi.org/10.1016/S0006-3495(00)76272-2

Turrens, J. F., Alexandre, A., & Lehninger, A. L. (1985). Ubisemiquinone is the electron donor for superoxide formation by complex III of heart mitochondria. *Archives of Biochemistry and Biophysics*, *237*(2), 408–414. https://doi.org/10.1016/0003-9861(85)90293-0

Van Wagoner, D. R., Pond, A. L., Lamorgese, M., Rossie, S. S., McCarthy, P. M., & Nerbonne, J. M. (1999). Atrial L-type Ca2+ currents and human atrial fibrillation. *Circulation Research*, *85*(5). https://doi.org/10.1161/01.RES.85.5.428

Voigt, N., Heijman, J., Wang, Q., Chiang, D. Y., Li, N., Karck, M., Wehrens, X. H. T., Nattel, S., & Dobrev, D. (2014). Cellular and molecular mechanisms of atrial arrhythmogenesis in patients with paroxysmal atrial fibrillation. *Circulation*, *129*(2), 145–156. https://doi.org/10.1161/CIRCULATIONAHA.113.006641

Voigt, N., Li, N., Wang, Q., Wang, W., Trafford, A. W., Abu-Taha, I., Sun, Q., Wieland, T., Ravens, U., Nattel, S., Wehrens, X. H. T., & Dobrev, D. (2012). Enhanced sarcoplasmic reticulum Ca2+ leak and increased Na+-Ca2+ exchanger function underlie delayed afterdepolarizations in patients with chronic atrial fibrillation. *Circulation*, *125*(17), 2059–2070. https://doi.org/10.1161/CIRCULATIONAHA.111.067306

Waddell, H. M. M., Zhang, J. Z., Hoeksema, K. J., McLachlan, J. J., McLay, J. C., & Jones, P. P. (2016). Oxidation of RyR2 Has a Biphasic Effect on the Threshold for Store Overload-Induced Calcium Release. *Biophysical Journal*, *110*(11). https://doi.org/10.1016/j.bpj.2016.04.036

Wagner, M., Bertero, E., Nickel, A., Kohlhaas, M., Gibson, G. E., Heggermont, W., Heymans, S., & Maack, C. (2020). Selective NADH communication from α-ketoglutarate dehydrogenase to mitochondrial transhydrogenase prevents reactive oxygen species formation under reducing conditions in the heart. *Basic Research in Cardiology*, *115*(5). https://doi.org/10.1007/s00395-020-0815-1

Wellens, H. J. J., & Gorgels, A. P. (2004). The Electrocardiogram 102 Years after Einthoven. In *Circulation* (Vol. 109, Issue 5). https://doi.org/10.1161/01.CIR.0000117293.30403.8F

Wescott, A. P., Kao, J. P. Y., Lederer, W. J., & Boyman, L. (2019). Voltage-energized calcium-sensitive ATP production by mitochondria. In *Nature Metabolism* (Vol. 1, Issue 10). https://doi.org/10.1038/s42255-019-0126-8

Wiersma, M., van Marion, D. M. S., Wust, R. C. I., Houtkooper, R. H., Zhang, D., Groot, N. M. S., Henning, R. H., & Brundel, B. (2019). Mitochondrial Dysfunction Underlies Cardiomyocyte Remodeling in Experimental and Clinical Atrial Fibrillation. *Cells*, *8*(10). https://doi.org/10.3390/cells8101202

Wijesurendra, R. S., & Casadei, B. (2019). Mechanisms of atrial fibrillation. *Heart*, *105*(24), 1860–1867. https://doi.org/10.1136/heartjnl-2018-314267

Williams, G. S. B., Boyman, L., Chikando, A. C., Khairallah, R. J., & Lederer, W. J. (2013). Mitochondrial calcium uptake. In *Proceedings of the National Academy of Sciences of the United States of America*. https://doi.org/10.1073/pnas.1300410110

Williams, G. S. B., Boyman, L., & Lederer, W. J. (2015). Mitochondrial calcium and the regulation of metabolism in the heart. In *Journal of Molecular and Cellular Cardiology*. https://doi.org/10.1016/j.yjmcc.2014.10.019

Wilting, F., Kopp, R., Gurnev, P. A., Schedel, A., Dupper, N. J., Kwon, O., Nicke, A., Gudermann, T., & Schredelseker, J. (2020). The antiarrhythmic compound efsevin directly modulates voltage-dependent anion channel 2 by binding to its inner wall and enhancing mitochondrial Ca2+ uptake. *British Journal of Pharmacology*, *177*(13). https://doi.org/10.1111/bph.15022

Workman, A. J., Kane, K. A., & Rankin, A. C. (2001). The contribution of ionic currents to changes in refractoriness of human atrial myocytes associated with chronic atrial fibrillation. *Cardiovascular Research*, *52*(2). https://doi.org/10.1016/S0008-6363(01)00380-7

Xie, W., Santulli, G., Reiken, S. R., Yuan, Q., Osborne, B. W., Chen, B. X., & Marks, A. R. (2015). Mitochondrial oxidative stress promotes atrial fibrillation. *Sci Rep*, *5*, 11427. https://doi.org/10.1038/srep11427

Yoon, Y., Krueger, E. W., Oswald, B. J., & McNiven, M. A. (2003). The Mitochondrial Protein hFis1 Regulates Mitochondrial Fission in Mammalian Cells through an Interaction with the Dynamin-Like Protein DLP1. *Molecular and Cellular Biology*, *23*(15). https://doi.org/10.1128/mcb.23.15.5409-5420.2003

Youn, J. Y., Zhang, J., Zhang, Y., Chen, H., Liu, D., Ping, P., Weiss, J. N., & Cai, H. (2013). Oxidative stress in atrial fibrillation: An emerging role of NADPH oxidase. In *Journal of Molecular and Cellular Cardiology* (Vol. 62). https://doi.org/10.1016/j.yjmcc.2013.04.019

Yuan, M., Gong, M., He, J., Xie, B., Zhang, Z., Meng, L., Tse, G., Zhao, Y., Bao, Q., Zhang, Y., Yuan, M., Liu, X., Luo, C., Wang, F., Li, G., & Liu, T. (2022). IP3R1/GRP75/VDAC1 complex mediates endoplasmic reticulum stress-mitochondrial oxidative stress in diabetic atrial remodeling. *Redox Biology*, *52*. https://doi.org/10.1016/j.redox.2022.102289

Zhang, G. Q., Wei, H., Lu, J., Wong, P., & Shim, W. (2013). Identification and Characterization of Calcium Sparks in Cardiomyocytes Derived from Human Induced Pluripotent Stem Cells. *PLoS ONE*, *8*(2). https://doi.org/10.1371/journal.pone.0055266

Zipes, D. P., Jalife, J., & Stevenson, W. G. (2017). Cardiac Electrophysiology: From Cell to Bedside: Seventh Edition. In *Cardiac Electrophysiology: From Cell to*

Bedside: Seventh Edition. Elsevier. https://doi.org/10.1161/01.cir.0000146800.76451.65

8 Supplementary figures

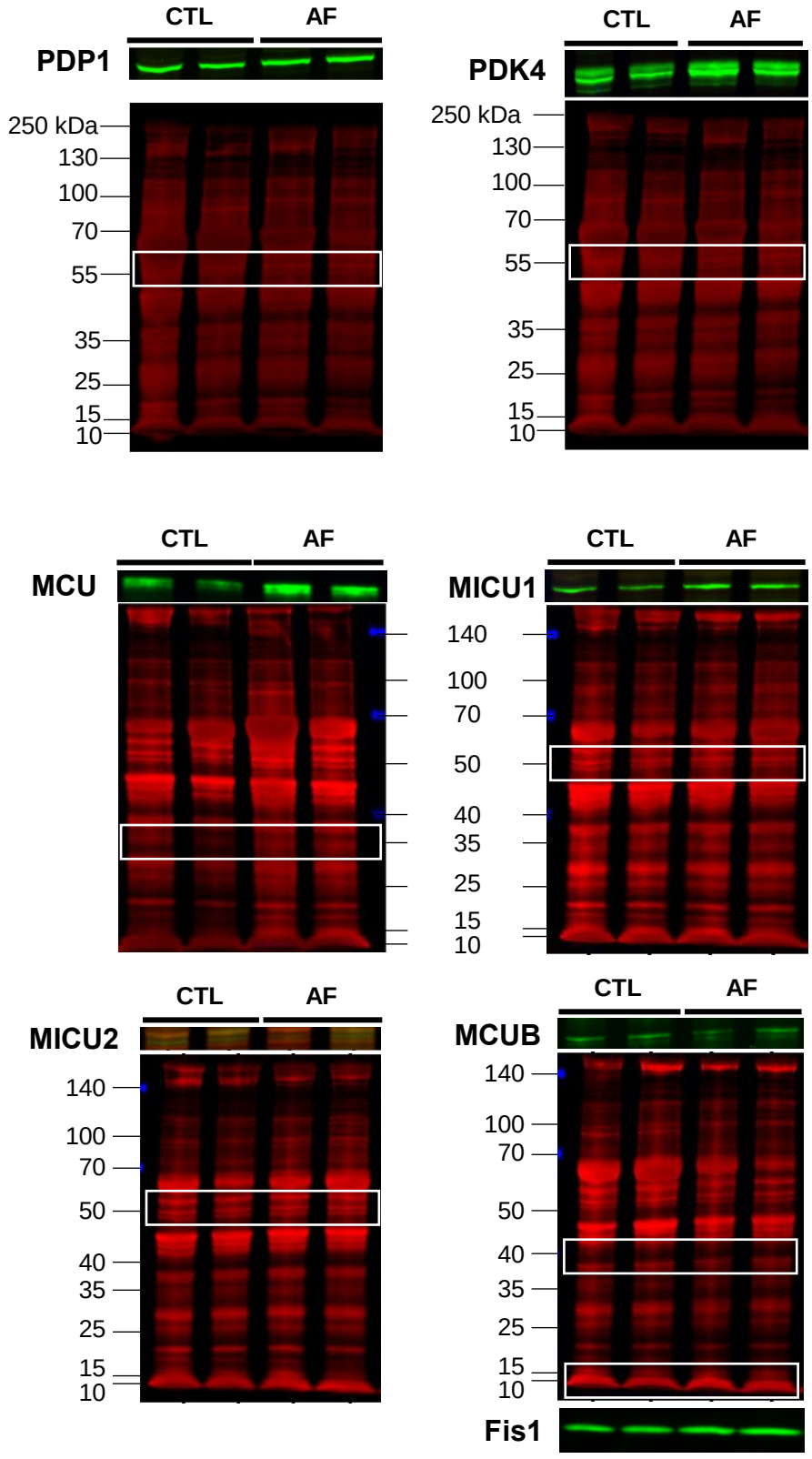

Supplementary Figure 1. Revert™ Total Stain labelled membranes used for normalization of target protein.

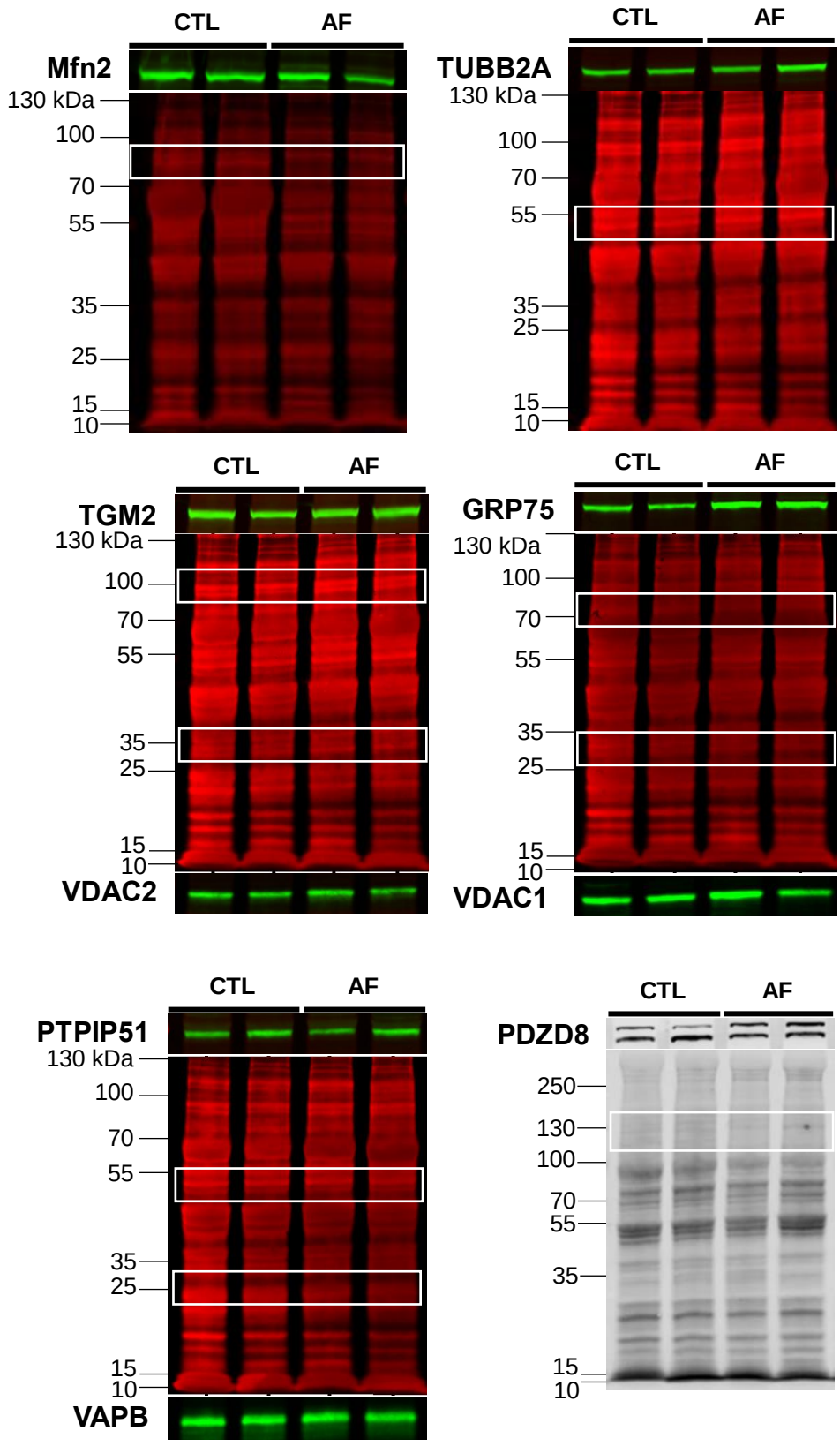

Supplementary Figure 1. Revert™ Total Stain labelled membranes used for normalization of target protein. *Continued from previous page.*